SYNTHESIS OF IRON AND COBALT-BASED SOLID-PHASE CATALYSTS FOR THE REMOVAL OF ANTIBIOTIC PIPEMIDIC ACID FROM WATER BY THE HETEROGENEOUS ELECTRO-FENTON METHOD

Abdoukarim SISOHO

Master's Thesis

Department of Chemistry

Programme in Analytical Chemistry

Supervisor: Prof. Dr. Ali ÖZCAN

Eskişehir

Eskişehir Technical University

Institute of Graduate Programs

September 2022

FINAL APPROVAL FOR THESIS

This thesis titled SYNTHESIS OF IRON AND COBALT-BASED SOLID-PHASE CATALYSTS FOR THE REMOVAL OF ANTIBIOTIC PIPEMIDIC ACID FROM WATER BY THE HETEROGENEOUS ELECTRO-FENTON METHOD has been prepared and submitted by Abdoukarim SISOHO in partial fulfillment of the requirements in “Eskişehir Technical University Directive on Graduate Education and Examination” for the Degree of Master's in Chemistry Department has been examined and approved on 08/09/2022.

Committee Members		Title, Name and Surname	Signature
Member	:	Prof. Dr. Ali ÖZCAN	
Member	:	Assoc. Prof. Dr. Rüsten KEÇİLI	
Member	:	Asst. Prof. Dr. İlker BALCILAR	

Prof. Dr. Murat TANIŞLI

Director of the Institute of Graduate Programs

08/09/2022

SUPERVISOR APPROVAL

Master's student Abdoukarim SISOHO, whom I supervise, has completed this thesis titled SYNTHESIS OF IRON AND COBALT-BASED SOLID-PHASE CATALYSTS FOR THE REMOVAL OF ANTIBIOTIC PIPEMIDIC ACID FROM WATER BY THE HETEROGENEOUS ELECTRO-FENTON METHOD. According to my inspections, the work is scientifically and ethically appropriate for the student to the thesis defense exam.

Supervisor

Prof. Dr. Ali ÖZCAN

ABSTRACT

SYNTHESIS OF IRON AND COBALT-BASED SOLID-PHASE CATALYSTS FOR THE REMOVAL OF ANTIBIOTIC PIPEMIDIC ACID FROM WATER BY THE HETEROGENEOUS ELECTRO-FENTON METHOD

Abdoukarim SISOHO

Department of Chemistry

Programme in Analytical Chemistry

Eskişehir Technical University, Institute of Graduate Programs, September 2022

Supervisor: Prof. Dr. Ali ÖZCAN

In this thesis, the preparation of solid-phase catalysts that can be used in the heterogeneous electro-Fenton removal of pipemidic acid from water was investigated. The study was performed in three main parts. In the first part, the oxidation and mineralization of the model organic pollutant, pipemidic acid, was investigated using the homogeneous electro-Fenton method. In the second stage, the mesoporous silica supported catalysts (Fe_3O_4-mpSiO$_2$ and Co_3O_4-mpSiO$_2$) were prepared and their catalytic activities in the removal of the model organic pollutant were monitored. In the third stage, iron-doped tin dioxide (Fe-d-SnO$_2$) was synthesized and its efficiency in the removal of PPA was also investigated under the same heterogeneous electro-Fenton conditions. The characterization of the prepared solid-phase catalysts were carried out by XRD, SEM, EDX, and BET analyses. Short-chain carboxylic acids and inorganic products formed during the oxidation of pipemidic acid were determined by HPLC and IC analysis, respectively. Moreover, the stability and reusability of the solid-phase catalysts were also investigated. The results indicated that the heterogeneous electroFenton system had certain advantages over the homogeneous electro-Fenton method, such as high oxidation power, low cost, wide working pH range and reusability of the catalysts

Keywords: Pipemidic acid, Electro-Fenton, Hydroxyl radicals, Heterogeneous catalysis, Mesoporous silica.

ÖZET

HETEROJEN ELEKTRO-FENTON YÖNTEMİYLE ANTİBİYOTİK PİPEMİDİKASİTİN SUDAN GİDERİMİ İÇİN DEMİR VE KOBALT TEMELLİ KATI-FAZKATALİZÖRLERİNİN SENTEZLENMESİ

Abdoukarim SISOHO

Kimya Anabilim Dalı

Analitik Kimya Bilim Dalı

Eskişehir Teknik Üniversitesi, Lisansüstü Eğitim Enstitüsü, Eylül 2022

Danışman: Prof. Dr. Ali ÖZCAN

Bu tez çalışmasında, pipemidik asidin (PPA) sudan heterojen elektro-Fenton gideriminde kullanılabilecek katı-faz katalizörlerin hazırlanması araştırılmıştır. Çalışma üç ana aşamadan oluşmaktadır. Birinci aşamada, model organik kirletici olan pipemidik asidin oksidasyonu ve mineralizasyonu homojen elektro-Fenton yöntemi kullanılarak incelenmiştir. Bu aşamada, pipemidik asit gideriminde sistemi etkileyen elektrot tipi, uygulanan akım ve demir konsantrasyonu gibi çalışma parametreleri incelenmiştir. İkinci aşamada, mezogözenekli silika destekli katalizörler (Fe_3O_4-mpSiO_2 ve Co_3O_4-mpSiO_2) hazırlanmış ve model organik kirleticinin giderilmesindeki katalitik aktiviteleri izlenmiştir. Üçüncü aşamada, demir katkılı kalay dioksit (Fe-d-SnO_2) sentezlenmiş ve aynı koşullar altında heterojen elektro-Fenton yöntemiylePPA'nın giderilmesindeki etkinliği araştırılmıştır. Hazırlanan katı-faz katalizörlerin karakterizasyonu XRD, SEM, EDX ve BET analizleri ile gerçekleştirilmiştir. Kısa zincirli karboksilik asitler ve pipemidik asidin oksidasyonu sırasında oluşan inorganik ürünler sırasıyla HPLC ve IC analizi ile belirlenmiştir. Ayrıca, katı fazlı katalizörlerin stabilitesi ve tekrar kullanılabilirliği de araştırılmıştır. Sonuçlar, heterojen elektro-Fenton sisteminin homojen elektro-Fenton yöntemine göre yüksek oksidasyon gücü, düşük maliyetli olması, geniş çalışma pH aralığı ve katalizörlerin yeniden kullanılabilirliği gibi bazı avantajları olduğunu göstermiştir.

Anahtar Sözcükler: Pipemidik asit, Elektro-Fenton, Hidroksil radikalleri, Heterojenkataliz, Mezogözenekli silika.

ACKNOWLEDGEMENTS

I am very much indebted to so many people without whose immense contribution and stewardship this thesis studies would not have been successfully completed. Among these personalities, I wish to first and foremost register my profound appreciation and undiluted gratitude to my supervisor Prof. Dr. Ali ÖZCAN for his unwavering support, steadfastness, mentorship and guidance throughout the course of this thesis. He has showed me exemplary leadership and always been there to put me through whenever I needed him. I would like to also thank Prof. Dr. Ayça Atılır ÖZCAN for voluntarily teaching me the rudiments of HPLC analysis.

Unequivocally, the timely completion of this thesis might have been very difficult without the unflinching support of my colleagues in the laboratory especially at the beginning of the thesis. Cognizant of this, I wish to express my sincere gratitude and appreciation to Zeynep DAŞDELEN for her tireless efforts in the course of this thesis. Also, I wish to recognize the valuable contributions of Harun BAŞ and the entire KL 124 students. Further, I want convey my utmost appreciation to the Board of Directors, management and staff of Medicines Control Agency especially to the Executive Director Mrs. Markieu Janneh-KAIRA for their unreserved support given to me throughout this study. I am equally indebted to Dr. Jenny MUELLA for her continuous support and guidance in this thesis.

Finally, my heartfelt thanks to lovely parents Alieu SISOHO (deceased) and Binta TOURAY for their unreserved support and prayers. Additionally, I want to also express my immeasurable appreciation and gratitude to my sisters Isatou, Mariama and Fatou SISOHO and brothers Lamin CAMARA, Muhammed (deceased) and Ebrima SISOHO for all their endless telephone calls, encouragement and moral support. To my darling wife, Haddy CEESAY words cannot express how grateful I am to you. You have been patient, compassionate, obedient and loyal to me since we got married and by extension throughout my three years stay in Türkiye. I am honored having you as a wife.

Abdoukarim SISOHO

08/09/2022

STATEMENT OF COMPLIANCE WITH ETHICAL PRINCIPLES AND RULES

I hereby truthfully declare that this thesis is an original work prepared by me; that I have behaved in accordance with the scientific ethical principles and rules throughout the stages of preparation, data collection, analysis and presentation of my work; that I have cited the sources of all the data and information that could be obtained within the scope of this study, and included these sources in the references section; and that this study has been scanned for plagiarism with "scientific plagiarism detection program" used by Eskişehir Technical University, and that "it does not have any plagiarism" whatsoever. I also declare that, if a case contrary to my declaration is detected in my work at any time, I hereby express my consent to all the ethical and legal consequences that are involved.

Abdoukarim SISOHO

CONTENTS

Page

LIST OF TABLES

Page

LIST OF FIGURES

GLOSSARY OF SYMBOLS AND ABBREVIATIONS

AOPs	:	Advanced Oxidation Processes
BDD	:	Boron-Doped Diamond
BET	:	Brunauer-Emmett-Teller
CF	:	Carbon Felt
d	:	Doped
EDX	:	Energy Dispersive X-ray
EF	:	Electro-Fenton
HEF	:	Heterogeneous Electro-Fenton
HPLC	:	High Performance Liquid Chromatography
IC	:	Ion Chromatography
M	:	Molar
mA	:	Miliamper
MCE	:	Mineralization Current Efficiency
mM	:	Milimolar
mp	:	Mesoporous
μL	:	Microliter
PPA	:	Pipemidic Acid
Pt	:	Platinum
SEM	:	Scanning Electron Microscope
TOC	:	Total Organic Carbon
XRD		X-Ray Diffraction

1. INTRODUCTION

Water quality has drastically reduced over the last decades mainly due to population growth, urban development, increased industrialization, and unsustainable utilization of natural water resources (Poza-Nogueiras et al., 2018). As a result of this, water pollution has emerged as a major impediment and thus gravely affecting large spectrum of lives and their activities (J. Wang & Tang, 2021b). The pollution of the water bodies may arise from contaminated soil, agricultural runoff, industrial wastewater and leakage of hazardous compounds thereby causing the presence of many contaminated organic compounds in them. The presence of these organic compounds in water bodies can emerge as serious threat to public health owing to the fact that most of them are toxic, endocrine disrupting, mutagenic or potentially carcinogenic to humans, animals and aquatic life in general (Babuponnusami & Muthukumar, 2014).

An antibiotic can be defined as a chemotherapeutic agent that specifically inhibits the proliferation of bacteria by cell destruction or growth inhibition (Rodriguez-Mozaz et al., 2020). Antibiotics are classified into various categories such as penicillins, cephalosporins, macrolides, sulfonamides, tetracyclines, glycopeptides, aminoglycosides, carbapenems and quinolones (Bilal et al., 2019). Among them, quinolones which is sometimes referred to as quinolonecarboxylic acids or 4-quinolones are a group of synthetic antibacterial agents containing a 4-oxo-1,4-dihydroquinoline skeleton and are widely used for the treatment of various infections. The activity of quinolones as antibacterial drugs is mainly due to the effective inhibition of DNA replication. Pipemidic acid (PPA), a 4-quinolone product, is an antibacterial agent used to treat gram-negative urinary tract infections (M. T. Li et al., 2013).

Antibiotics are widely reported as one of the major recalcitrant organic pollutants found in water (Poza-Nogueiras et al., 2021). Approximately 200,000 tons antibiotics are consumed every year (de Souza Santos et al., 2015). The uncontrolled consumption of antibiotics over all the globe results in their discharge and accumulation at low concentrations (usually <10 μg/L) in many aquatic resources including rivers, lakes, sea, and even drinking water (Brillas, 2022). Most of these substances are incompletely metabolized in living organisms due to their chemical stabilities. Therefore, they are mainly excreted in an unaltered form after administration, thereby leading to the accumulation of these substances in water resources and environment (Özcan et al., 2016). The availability of antibiotics and their transformation products in the environment may cause detrimental effects including bacterial resistance and disruption of key cycles critical to aquatic ecology or crop and animal production (Barhoumi et al., 2017).

Since antibiotics are currently regarded as emerging environmental contaminants due to their widespread use and potential ecological risks, their removal from the contaminated water is of utmost importance. Many methods such as physical methods, chemical methods, biological processes, bio-electrochemical system-based methods, and advanced oxidation processes (AOPs) have been examined to remove the pollutants from wastewater. Among them, the AOPs have been considered as the most efficient methods, and have been studied extensively in the removal of recalcitrant organics (B. Zhang et al., 2019) because of their high oxidation ability, relatively low costs and easy applications (Özcan et al., 2017). In these processes, highly reactive intermediates (especially hydroxyl radical, $^{\bullet}OH$ with an oxidation potential of 2.8 V) are generally used to destroy/oxidize non-selectively recalcitrant contaminants until their total mineralization into CO_2, water and inorganic ions (Al-Khafaji & Mohammed, 2019). AOPs can be classified into different categories including photo-chemical, sono-chemical, electro-chemical and Fenton oxidation processes. Among these AOPs, Fenton oxidation is the most commonly investigated process to degrade organic pollutants present in wastewater (Toor et al., 2020) because of its advantages such as low cost, high efficiency, facile control, and the application of environmentally friendly reagents (H_2O_2 and Fe^{2+}) (Lima et al., 2020). Nonetheless, Fenton process are without shortfalls and thus possesses some disadvantages such as consumption of high concentration of Fe^{2+}, production of large amount of Fe sludge which in turn makes the wastewater treatment very exorbitant and thus subsequently demands large quantity of chemicals and human resources. Furthermore, transportation and storage of hydrogen peroxide is very risky and difficult. Also, iron ions will precipitate at higher pH values thus Fenton's reactions are limited to very small pH values (Pushpalatha & Krishna, 2017). In light of the above, researchers have shifted their attention to electrochemical advanced oxidation processes (EAOPs) based on Fenton's reaction as a more efficacious method to remedy the overwhelming challenges**.**

Among the EAOPs, the most widely examined method is the electro-Fenton process. Electro-Fenton method depends heavily on on-site catalytic production of

Fenton's reagent that ultimately generates hydroxyl radicals. These radicals subsequently will react with recalcitrant contaminants in the aqueous systems thereby causing their ultimate destruction (Al-Khafaji & Mohammed, 2019; Pimentel et al., 2008). The electro-Fenton process has the following advantages: (i) better control of the process and avoiding the storing and transportation problems of hydrogen peroxide, (ii) higher degradation rate of organic pollutants because of the continuous regeneration of Fe^{2+} at the cathode, which also minimizes sludge production, (iii) the feasibility of overall mineralization at a relatively low cost if the operation parameters are optimized (Al-Zubaidi & Pak, 2020). However, EF processes also have some disadvantages such as iron sludge production and non-reusability of catalyst (Kalantary et al., 2018). Thus, to overcome the afore-highlighted deficiencies, heterogeneous catalysts have been studied lately. This process is called heterogeneous electro-Fenton (HEF) method.

HEF method has some advantages compared to classical EF process such as higher catalytic efficiency, performance of reaction within a broad range of pH, consumption of low concentration of soluble iron and thus small precipitation of oxyhydroxide componds (Garrido-Ramírez et al., 2016).

Within the scope of this thesis, different heterogeneous catalysts were prepared to use in the heterogeneous electro-Fenton treatment of polluted water with pipemidic acid (PPA). For this purpose, three different catalysts were prepared. These are iron (II, III) oxide-mesoporous silica (Fe_3O_4-mpSiO$_2$), cobalt (II, III) oxide-mesoporous silica (Co_3O_4-mpSiO$_2$) and iron-doped tin dioxide (Fe-d-SnO$_2$). The research was performed in three main steps. Firstly, the oxidation and mineralization of the model organic pollutant, PPA, was investigated using a homogeneous electro-Fenton process. In the second stage, the mesoporous silica supported catalysts (Fe_3O_4-mpSiO$_2$ and Co_3O_4-mpSiO$_2$) were prepared and their catalytic activities in the removal of the model organic pollutant were monitored using the heterogeneous electro-Fenton process. In the third stage, iron-doped tin dioxide (Fe-d-SnO$_2$) was synthesized and its efficiency in the removal of PPA was also investigated under the same heterogeneous electro-Fenton conditions. Thereafter, the two processes-classical electro-Fenton and heterogeneous electro-Fenton were compared.

The major objectives of this thesis are focused on:

- ✓ Investigating the removal of PPA from water by the electro-Fenton method using different electrodes;
- ✓ Investigating the electrochemical oxidation and mineralization kinetics of PPA under different electrode combinations;
- ✓ Investigating the effects of various experimental parameters on the removal of PPA;
- ✓ Synthesis and characterization of different solid-phase catalysts for the heterogeneous electro-Fenton process;
- ✓ Investigating the catalytic performance of the catalysts regarding the influence of the operational parameters on the removal of PPA;
- ✓ Investigating the stability and reusability of the catalysts;
- ✓ Using different chromatographic techniques to detect aliphatic, aromatic, carboxylic acids and inorganic species generated through oxidation of PPA under electro-Fenton conditions;
- ✓ Proposing a plausible reaction mechanism for the destruction of PPA under heterogeneous electro-Fenton conditions.

2. BASIC CONCEPTS

2.1. Advanced Oxidation Processes (AOPs)

Persistent organic pollutants (POPs) are not efficiently taken away from contaminated water sources through traditional water/wastewater treatment processes (M. A. Oturan, 2021). As a result, different studies have been performed to come up with other alternative methods that can effectively curtail the limitations of the traditional wastewater treatment technologies (Bello et al., 2019).

AOPs are very effective and suitable for water treatment that involve the in-situ generation of highly reactive oxidizing agents namely hydroxyl radicals ($^\bullet OH$), ozone (O_3), superoxide radical anions ($^\bullet O_2^-$), and so on. These oxidizing agents will react non-selectively with all kinds of organic pollutants. However, owing the oxidizing nature of $^\bullet OH$, it is considered the most effective in the total mineralization and removal of organic contaminants (Nair et al., 2021; Sopaj et al., 2016). The standard reduction potential of common oxidants is shown in Table 2.1. (Babuponnusami & Muthukumar, 2014).

Table 2.1. *Standard reduction potential of common oxidants*

Oxidant	**Oxidation potential (V)**
Fluorine (F_2)	3.03
Hydroxyl radical ($^\bullet OH$)	2.80
Atomic oxygen (O)	2.42
Ozone (O_3)	2.07
Hydrogen peroxide (H_2O_2)	1.77
Potassium permanganate ($KMnO_4$)	1.67
Chlorine dioxide (ClO_2)	1.5
Hypochlorous acid (HClO)	1.49
Chlorine (Cl_2)	1.36
Oxygen (O_2)	1.23
Bromine (Br_2)	1.09

Hydroxyl radicals ($^{\bullet}OH$) are the second highest oxidizing agent next to fluorine (F_2) with a high redox potential of E^0 ($^{\bullet}OH/H_2O$) = 2.8 V/SHE (Moreira et al., 2017; Pan & Sun, 2021). The generation of $^{\bullet}OH$ can be done through various methods (single oxidants and/or combinations) such as hydrogen peroxide, ozone and UV radiation or combination of hydrogen peroxide with ferrous ions (Fenton's reagent), electrochemical oxidation, supercritical water oxidation sonolysis (ultrasound–US) and various combination of these technologies. Figure 2.1 represents the various AOPs used for the generation of free radicals (Divyapriya et al., 2016).

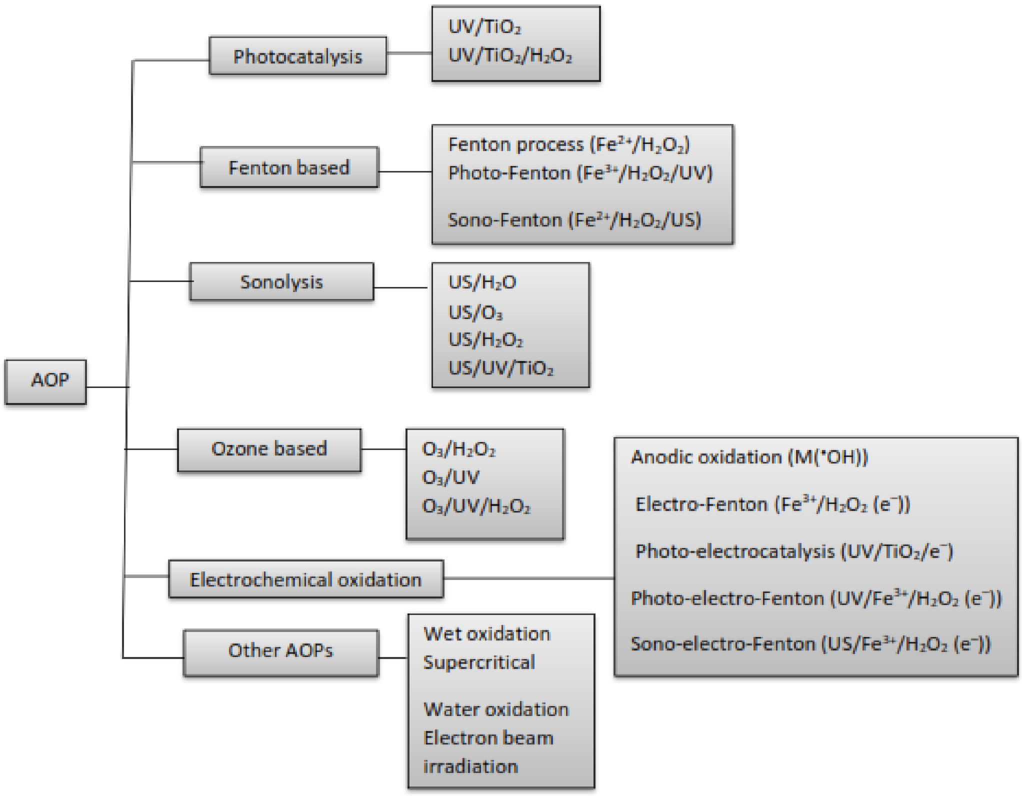

Figure 2.1. *Classification of advanced oxidation processes*

AOPs have many advantages as compared to the conventional treatment methods such as (i) effective against low concentration of pollutants (ii) no chemical or biological sludge production (iii) non-selective (iv) complete mineralization can be achieved.

Among the different AOPs, electrochemical advanced oxidation processes (EAOPs) stands out fascinating in recent years due to their capabilities in the water remediation process (Frontistis et al., 2018).

2.2. Electrochemical Advanced Oxidation Processes

In the recent years, new AOPs depending on the electrochemical technology have been studied thereby leading to the development of the so-called electrochemical advanced oxidation processes (EAOPs) (Al-Khafaji & Mohammed, 2019). EAOPs can be divided into two main categories such as direct electrochemical oxidation methods, widely known as anodic oxidation (AO), and indirect electrochemical oxidation (IEO) methods (Olvera-Vargas et al., 2018). In line with the above information, anodic oxidation is a widely examined EAOP. In this process, pollutants can be oxidized by direct electron transfer reaction from organic pollutants to the electrode surface or the action of highly oxidizing radical species (i.e. hydroxyl radicals) formed on the high O_2-overvoltage anode surface (Özcan, Şahin, Koparal, et al., 2008). For this reason, it can be said that anode material plays very significant role in direct oxidation, thereby determining the catalytic activity, selectivity and current efficiency of the process. On the other hand, electro-oxidation of recalcitrant organic pollutants can be also attained by indirect oxidation via in-situ generation of some active species such as hydrogen peroxide (H_2O_2), hypochlorite (ClO^-) and ozone (O_3). Furthermore, electro-Fenton (EF) is one of the most important processes in indirect oxidation, in which H_2O_2 can be electro-generated by the reduction of oxygen (Eq. (2.16)), and then it can be transformed to a highly powerful $^{\bullet}OH$ in the presence of Fe^{2+} (Eq. (2.17)) (Chao Zhang et al., 2015). These processes have advantages such as high versatility, moderate application condition, limited operative cost, excellent efficiency, suitability for automation and environmentally benign. Moreover, EAOPs based on Fenton's chemistry utilizes hydroxyl radical ($^{\bullet}OH$) generated from Fenton's reaction between in-situ produced or externally added H_2O_2 and Fe^{2+} ions for the removal of organic contaminants (Ganiyu et al., 2018; Ö. Görmez et al., 2021).

2.3. Fenton's Reaction

Fenton's reaction is among the most effective homogeneous AOPs available at room conditions (Kavitha & Palanivelu, 2005; M. A. Oturan, 2021) and it has been largely applied in the treatment of different wastewaters (D. Huang et al., 2017). Fenton process is based on Fenton's reagent which is described as a mixture of hydrogen peroxide and ferrous ion, which ultimately generates hydroxyl radicals (Wu & Wang, 2012). Figure 2.2 shows the generation of hydroxyl radicals in Fenton's reaction.

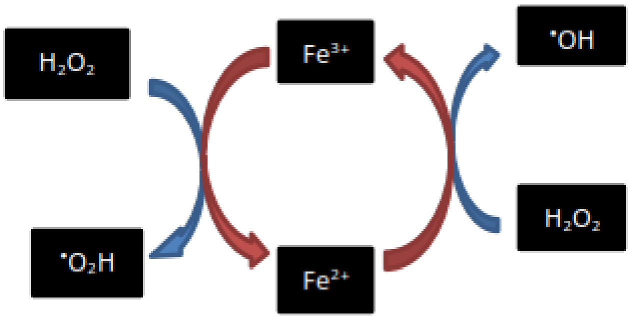

Figure 2.2. *The generation of hydroxide radicals in Fenton's reaction (Divyapriya et al., 2016)*

In 1894, the chemistry of this reagent began when Henry John Horstman Fenton applied it to oxidize tartaric acid (Bulánek et al., 2019). Two mechanisms have been proposed in the oxidation of organic matters by Fenton's reaction. First one is the Haber-Weiss mechanism, which emphasized that active oxide species such as $^{\bullet}OH$ are generated to oxidize organics in Fenton's reaction. On the other hand, Bray and Groin have proposed the mechanism that involved high iron oxide intermediates. According to them, strong oxidizing iron substances (FeO^{2+}, FeO^{3+}) were produced in Fenton reaction, rather than $^{\bullet}OH$. However, with the advent of spectroscopy, it is widely accepted that the formation of $^{\bullet}OH$ initiates the oxidation in Fenton's treatment (Haber & Weiss, 1934).

In the Fenton's reaction, the ferrous and ferric ions are also regarded as coagulants. Due to this reason, the process is considered to carry out both oxidation and coagulation functions in the treatment process. The H_2O_2/Fe^{2+} ratio majorly determine which function is executed. Hence, at a lower H_2O_2/Fe^{2+} ratio the chemical coagulation predominates; on the other hand, chemical oxidation is dominant at higher H_2O_2/Fe^{2+} ratios (J. Li et al., 2012).

Generally, the mechanism of Fenton's reaction below suggests that hydroxyl radicals are produced in accordance with Eq. (2.1) (Gümüş & Akbal, 2016).

$$Fe^{2+} + H_2O_2 \rightarrow Fe(OH)_2 \rightarrow Fe^{3+} + {}^{\bullet}OH + OH^{-} \quad k = 40 - 80\ L.mol^{-1}.s^{-1} \qquad (2.1)$$

Eq. 2.2 is described as a Fenton-like reaction in which the Fe^{3+} produced is further reduced by its reaction with excess H_2O_2 to form Fe^{2+} and hydroperoxyl radicals ($^{\bullet}O_2H$).

It is slower than the Fenton's reaction and the hydroperoxyl radicals may equally attack organic contaminants; however, they are less sensitive than hydroxyl radicals (Babuponnusami & Muthukumar, 2014).

$$Fe^{3+} + H_2O_2 \rightarrow Fe^{2+} + {}^{\bullet}O_2H + H^+ \quad k = 10^{-3}–10^{-2}\ L.mol^{-1}.s^{-1} \quad (2.2)$$

As can be seen in Eq. (2.1), the hydroxyl radical formed by the reaction between Fe^{2+} and H_2O_2 through the homogeneous Fenton's reaction has the ability to destroy organic pollutants non-selectively using different ways such as redox reaction (Eq. (2.3)), dehydrogenation (hydrogen abstraction) reaction (Eq. (2.4)) and electrophilic addition to systems (hydroxylation) (Eq. (2.5)). (Mahtab et al., 2021).

$${}^{\bullet}OH + RX \rightarrow RX^{+\bullet} + OH^- \quad (2.3)$$

$$RH + {}^{\bullet}OH \rightarrow R^{\bullet} + H_2O \quad (2.4)$$

$$RHX + {}^{\bullet}OH \rightarrow RHX\ (OH) \quad (2.5)$$

The Fe^{2+} regeneration (Eq. (2.6) as well as in (2.2), and (2.7)) is kinetically slow compared to its consumption (Eq. (2.1)), thus causing a higher Fe^{2+} requirement than commonly required in catalysts and iron sludge formation (Ribeiro & Nunes, 2021).

$$R^{\bullet} + Fe^{3+} \rightarrow R^+ + Fe^{2+} \quad (2.6)$$

Eq. (2.2) and (2.7) represent the rate limiting steps in the Fenton's reaction since hydrogen peroxide is consumed and ferrous iron is regenerated from ferric ion through these reactions (Babuponnusami & Muthukumar, 2014).

$$Fe^{3+} + {}^{\bullet}O_2H \rightarrow Fe^{2+} + O_2 + H^+ \quad k = (0.3 - 2.1) \times 10^6\ L\cdot mol^{-1}\cdot s^{-1} \quad (2.7)$$

Eq. (2.8) – (2.12) are stated to occur during the Fenton's reaction and they include radical–radical reactions or hydrogen peroxide–radical reaction (Babuponnusami & Muthukumar, 2014). However, according to the literature (Gümüş & Akbal, 2016), these reactions occur as competitive reactions and thus negatively affect the oxidation process.

$${}^{\bullet}OH + {}^{\bullet}O_2H \rightarrow H_2O + O_2 \quad k = 1.4 \times 10^{10}\ L\cdot mol^{-1}\cdot s^{-1} \quad (2.8)$$

$$2{}^{\bullet}O_2H \rightarrow H_2O_2 + O_2 \quad k = (0.1 - 9.7) \times 10^7\ L\cdot mol^{-1}\cdot s^{-1} \quad (2.9)$$

$$2{}^{\bullet}OH \rightarrow H_2O_2 \quad k = (5.0 - 8.0) \times 10^9\ L\cdot mol^{-1}\cdot s^{-1} \quad (2.10)$$

$$^{\bullet}OH + H_2O_2 \rightarrow {}^{\bullet}O_2H + H_2O \qquad k = (1.7 - 4.5) \times 10^7\ L \cdot mol^{-1} \cdot s^{-1} \tag{2.11}$$

$$^{\bullet}O_2H + H_2O_2 \rightarrow {}^{\bullet}OH + H_2O + O_2 \quad k = 3.0\ L \cdot mol^{-1} \cdot s^{-1} \tag{2.12}$$

The above reactions are influenced by operational parameters that eventually affect the efficiency of the Fenton's reaction. Among the operational parameters that directly affect the efficiency of the process are source of iron catalyst, concentrations of iron and hydrogen peroxide and their ratio, initial organic pollutants concentration, pH, temperature, treatment time, nature of the electrodes and current intensity (Mbaye et al., 2022; Toor et al., 2020; M. hui Zhang et al., 2019).

One of the operational parameters that strongly influence the Fenton's reaction is the pH (Cruz et al., 2021; Labiadh et al., 2019). At lower pH values, complex iron species like $[Fe(H_2O)_6]^{2+}$ react with H_2O_2 at slower rates thereby reducing $^{\bullet}OH$ formation. Notwithstanding, at higher pH, iron precipitates as $Fe(OH)_3$. The formed iron precipitates decreases Fe^{3+} in the solution and eventually affects Fe^{2+} regeneration through Fe^{3+} and H_2O_2 reaction. Moreover, H_2O_2 decomposes into O_2 and H_2O in basic medium which also decreases $^{\bullet}OH$ production (Ribeiro et al., 2020; Ribeiro & Nunes, 2021).

There are three general limitations of the Fenton's reaction (Fig 2.3) ; the requirement of a narrow pH range (2.5–4), high cost of chemicals for enhanced pollutants removal and mineralization, and finally large sludge production after the treatment (Mahtab et al., 2021).

Considering the challenges of the Fenton's reaction as discussed above, coming up with a more robust method to overcome the setbacks is imperative. One promising way to resolve these challenges is the combination of Fenton's reaction with electrochemical processes, namely electro-Fenton method.

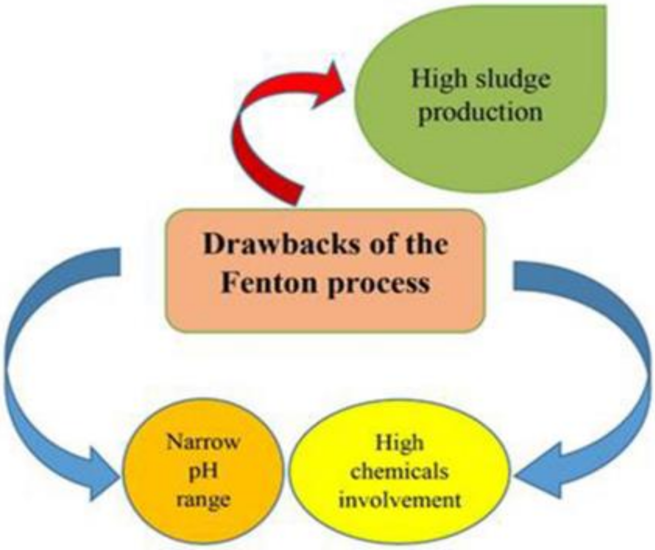

Figure 2.3. *Drawbacks of Fenton process*

2.4. Electro-Fenton (EF) Method

EF is an EAOP that is considered as a suitable alternative to treat highly persistent organic pollutants that are refractory to traditional water treatments (Poza-Nogueiras et al., 2021). This process entails the production of hydroxyl radicals ($^{\bullet}OH$) by using electrochemistry and the Fenton's reaction (Sopaj et al., 2016).

In the EF system, at the cathode, H_2O_2 is produced through the reduction of dissolved oxygen in an acidic environment (Eq. (2.13)) (Jiao et al., 2020; Matyszczak et al., 2020).

$$O_2 + 2H^+ + 2e^- \rightarrow H_2O_2 \qquad (2.13)$$

The $^{\bullet}OH$ is typically considered to be generated by the homogeneous Fenton's reaction (Eq. (2.14)) from the reaction of H_2O_2 and Fe^{2+} in acidic conditions and thereby develops the EF process to treat wastewater (Al-Zubaidi & Pak, 2020).

$$Fe^{2+} + H_2O_2 \rightarrow Fe^{3+} + {}^{\bullet}OH + OH^- \qquad (2.14)$$

Additionally, from the Fenton's reaction , the Fe^{3+} ions formed, are constantly reduced to Fe^{2+} on the cathode surface (Eq. (2.15)), hence, this contributes further to the production of hydroxyl radical (F. Görmez et al., 2019).

$$Fe^{3+} + e^- \rightarrow Fe^{2+} \qquad (2.15)$$

Conversely, a prominent amount of the molecular oxygen that is necessary for the production of H_2O_2 is generated by oxidizing water at the anode in the reactor (2.16). Oxygen can equally be continuously passed through the reaction mixture (Matyszczak et al., 2020).

$$2H_2O \rightarrow 4H^+ + O_2 + 4e^- \qquad (2.16)$$

Figure 2.4 shows the electrocatalytic production of hydroxyl radicals by the electro-Fenton process (M. A. Oturan et al., 2001).

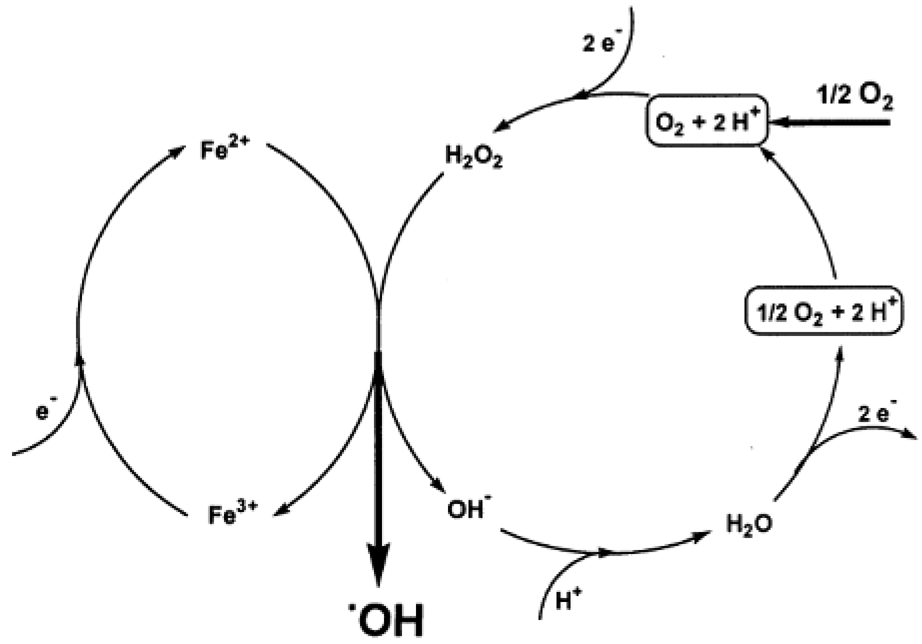

Figure 2.4. *Schematic presentation of the electrocatalytic production of hydroxyl radicals by the electro-Fenton process*

EF process can be divided into different categories depending on Fenton's reagents addition or formation (M. hui Zhang et al., 2019). The typical reaction mechanisms for the different categories of electro-Fenton processes are summarized below.

Category I: Peroxi-coagulation (PC) process: A process in which H_2O_2 and Fe^{2+} are formed in situ via an oxygen sparging cathode and a sacrificial iron anode.

Anode:

$$Fe^0 \rightarrow Fe^{2+} + 2e^- \qquad (2.17)$$

Cathode:

$$O_2 + 2H^+ + 2e^- \rightarrow H_2O_2 \tag{2.18}$$

Moreover, reaction of cathodic H_2O_2 formation in acidic conditions can compete with the reaction of oxygen reduction to water by the following half-reaction:

$$O_2 + 2H^+ + 4e^- \rightarrow 2H_2O \tag{2.19}$$

Category II: Peroxi-electro-coagulation (PEC) process or anodic Fenton treatment (AFT) process: In this process, Fe^{2+} is continuously supplied by a sacrificial iron anode while H_2O_2 is added externally.

Anode:

$$Fe^0 \rightarrow Fe^{2+} + 2e^- \tag{2.20}$$

Cathode:

$$2H_2O + 2e^- \rightarrow H_2 + 2OH^- \tag{2.21}$$

Category III: Electro-Fenton process based on the continuously electro-generation of H_2O_2 on an oxygen sparging cathode while Fe^{2+} is externally added.

Anode:

$$2H_2O \rightarrow 4H^+ + O_2 + 2e^- \tag{2.22}$$

Cathode:

$$O_2 + 2H^+ + 2e^- \rightarrow H_2O_2 \tag{2.23}$$

Category IV: This process is similar to that of category III; however, in this case Fe^{2+} is regenerated through the reduction of Fe^{3+} on the cathode.

Anode:

$$2H_2O \rightarrow 4H^+ + O_2 + 2e^- \tag{2.24}$$

Cathode:

$$Fe^{3+} + e^- \rightarrow Fe^{2+} \tag{2.25}$$

Category V: Fered-Fenton process: Herein both H_2O_2 and Fe^{2+} are externally supplied with in situ regeneration of Fe^{2+} through the reduction of Fe^{3+} at the cathode.

Cathode:

$$Fe^{3+} + e^{-} \rightarrow Fe^{2+} \quad (2.26)$$

The nature of cathode materials strongly determines the efficiency of an EF reaction. An effective cathode material should have characteristics such as high overvoltage for hydrogen evolution reaction (HER), low catalytic activity for H_2O_2 decomposition, high stability and conductivity (Nair et al., 2021).

Carbon-based materials with high catalytic activity are the most prevailing cathodes used in H_2O_2 electro-generation in recent decades (L. Li et al., 2018; Titchou et al., 2021). For example, activated carbon fiber (Lei et al., 2010), graphite felt (W. Zhang et al., 2013) carbon-PTFE air-diffusion electrode (H. Wang & Wang, 2007), carbon sponge (Özcan et al., 2009), graphite (Leng et al., 2019; C. T. Wang et al., 2008), and three-dimensional carbon felt (Panizza & Oturan, 2011) have been used in the literature.

On the other hand, EF processes can also be enhanced through stable anodes with high over-potential for oxygen evolution reaction (OER) that permits the supplementary $^{\bullet}OH$ generation (Nair et al., 2021). There are two types of the anode (active and non-active anodes), which are classified depending on the interaction of the anode material and the adsorbed reactive species. Active anodes are considered to promote the formation of higher states oxides or super-oxides (MO) (Eq. (2.27)). The produced MO mainly oxidizes organic pollutants according to Equation 2.28. On the other hand, their mineralization power is restricted.

$$M(^{\bullet}OH) \rightarrow MO + H^{+} + e^{-} \quad (2.27)$$

$$MO + \text{organic pollutants} \rightarrow M + \text{intermediates} \quad (2.28)$$

In this kind of anode, there is a strong interaction between the radicals and the anode surface. Due to the interaction, the reactions at the surface of the anode are limited. The most common anodes of this type are platinum (Pt) and mixed metal or dimensionally stable anodes (DSA) (Dung et al., 2022). Among these anodes, Pt metal has been widely used in the recent decades owing to its high conductivity and stability. Nonetheless, Pt is considered to have strong interaction with the $^{\bullet}OH$ and this could eventually diminish the availability of $^{\bullet}OH$ for the pollutant degradation (Nair et al., 2021).

In the case of non-active anodes, herein a quite weak interaction between hydroxyl radical ($^{\bullet}OH$) and the anode surface (M) occurs (Eq. (2.29)). The hydroxyl radicals produced can react in the diffusion layer and are able to perform complete mineralization of organics (Eq. (2.30)). The most representative non-active anodes are boron-doped diamond (BDD), tin or lead oxides and sub-stoichiometric titanium oxides (Monteil et al., 2019).

$$M + H_2O \rightarrow M\,(^{\bullet}OH) + H^+ + e^- \quad (2.29)$$

$$M\,(^{\bullet}OH) + \text{organic pollutants} \rightarrow M + CO_2 + H_2O + H^+ + e^- \quad (2.30)$$

Among these anodes, BDD has been recently employed in the EF process owing to its high over-potential for O_2 evolution reaction, large potential window, chemical stability, high corrosion resistance, low background currents, high chemical inertness and long-term response stability (Mbaye et al., 2022). In the 1990s, the BDD thin films have been developed and characterized. Based on the literature, BDD has been used for the first time in electro-oxidation of organics by Comninellis' team and these films showed great capacity in the electrochemical oxidation of organic pollutants (Panizza & Oturan, 2011).

Despite the advantages of classical EF method in the wastewater treatment as mentioned above, there exist some critical limitations like the need of operating at pH 3 for an optimum run and the precipitation of soluble iron species used as catalyst. These drawbacks could be overcome by using heterogeneous catalysts in the electro-Fenton process. The new method is called heterogeneous electro-Fenton method.

2.5. Heterogeneous Electro-Fenton (HEF) Process

EF processes can be operated in different forms depending on the nature of the catalyst. In light of aforementioned, EF process is classified as a homogeneous process when the operations are carried out using a soluble catalyst. On the other hand, it is termed as a heterogeneous process when the soluble catalyst is replaced with a solid catalyst (Q. Li et al., 2021). Considering the problems realized when working with soluble catalysts in the EF process, the development of a more efficient heterogeneous catalyst to be utilized in HEF treatment is of utmost importance. The differences between homogeneous and heterogeneous EF processes are summarized in Table 2.2.

Table 2.2. *The differences between homogeneous and heterogeneous EF processes (Nidheesh & Olvera-vargas, 2017)*

Item	**Homogeneous EF process**	**Heterogeneous EF process**
Solubility of catalyst	Soluble	Insoluble
Physical nature of catalyst during reaction	Liquid	Solid
Optimal operating pH	Acidic, specifically near to 3	Wide range
Reusability of catalyst	Not possible/difficult	Possible
Separation of catalyst from aqueous phase	Difficult	Easy
Reactions	Occurs in liquid phase	Generally occurs on the surface of catalyst

Recently, the development of active heterogeneous catalyst has taken a giant step in order to promote Fenton chemistry (Hammouda et al., 2016). The application of heterogeneous catalysts through the heterogeneous Fenton process has become an efficient approach towards combating the primary shortcomings of the conventional Fenton process (Ghasemi et al., 2019). Figure 2.5 shows the many advantages of heterogeneous catalysis possesses compared to its homogenous counterpart (Biton Seror et al., 2022). Moreover, instead of chemical sources of iron ions, the utilization of heterogeneous catalyst enhances the cost-effectiveness and stability of the Fenton’s reaction in repeated operation (Masoumeh Ghasemi et al., 2019).

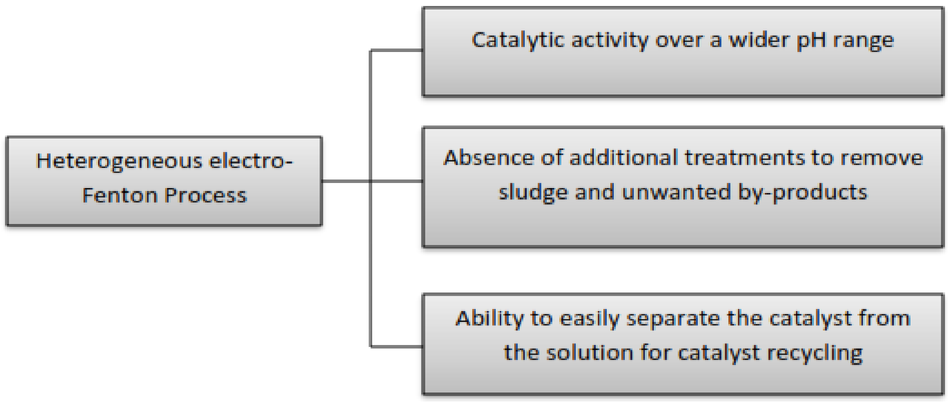

Figure 2.5. *Advantages of heterogeneous EF process over homogeneous EF process*

It is noteworthy to state, acquiring a catalyst that is well-suited for a heterogeneous process would greatly enhance catalytic efficiency and have significant industrial implications. For this reason, several catalysts depending on iron and other metals have been developed and studied for the HEF and HEF-like processes in recent years. These catalysts can be grouped into four major categories namely; iron minerals, metal/ nanoparticles, nanocomposites, and supported catalysts (Ashitha Gopinath et al., 2022). In line of the above information, iron oxides minerals such as pyrite (FeS_2), hematite (Fe_2O_3), goethite (α-FeOOH), and lepidocrocite (γ-FeOOH) have been widely studied in the heterogeneous Fenton-like reactions. Additionally, many different support materials such as activated carbon, zeolites, clays, silicates, layered materials, and graphene oxide have also been used in heterogeneous Fenton processes (Bhawana Jain et al**.,** 2018)**.** Moreover, Fenton-like system containing other transition metals (e.g., Co, Cu and Ni) have also been reported (Liang Liang et al., 2016).

Among the various types of catalysts found in the literature, Fe-containing solid catalysts have been widely used in the heterogeneous electro-Fenton process. Considering their unique properties such as their good biocompatibility, comparatively low toxicity, ready availability and environmentally benign nature as well as the high natural abundance of iron element in the earth's crust, Fe-based catalysts can also be seen reasonably suitable for the HEF processes like Fenton and electro-Fenton processes. In addition to the foregoing, the cost of iron is lower than other transition metals which favor the development of Fe-based catalysts. Also, Fe-based catalysts can be easily synthesized by many straightforward processes (J. Wang & Tang, 2021a).

Among these Fe-based catalysts, magnetic iron oxide nanoparticles (Fe_3O_4 MNPs) have received a great attention among metal oxide NPs. This could be attributed to their special applications, including small size, good stability, easy recovery, low cost and large specific surfaces (Dadashi et al., 2022).

2.5.1. The main features and surface catalytic mechanism of heterogeneous electro-Fenton processes

The catalytic HEF reaction mechanism in the degradation of recalcitrant organic pollutants is described below (Zining Wang et al., 2022).

Surface iron species catalyzes the surface-induced decomposition of electrogenerated H_2O_2. As can be seen in Figure 2.6, ≡describes the surface-bound iron species in the heterogeneous catalyst.

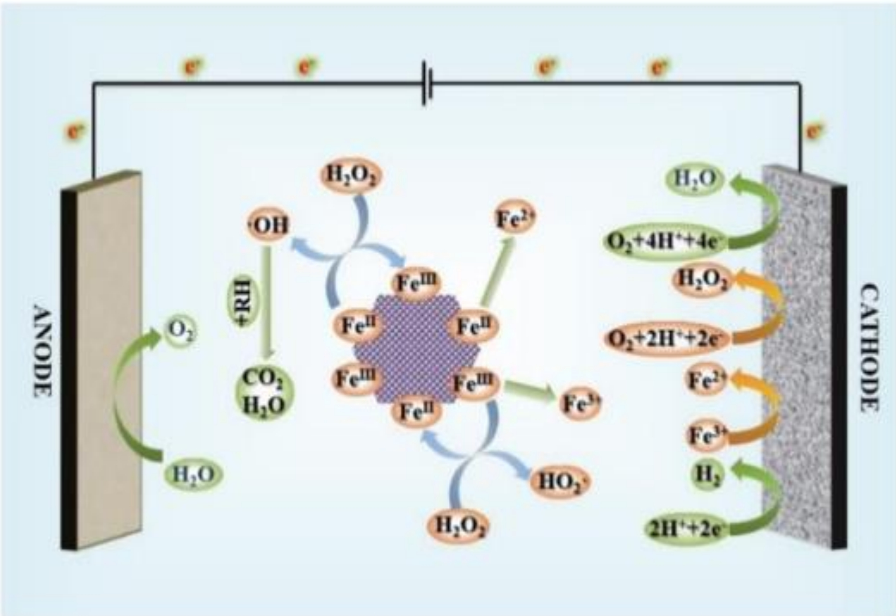

Figure 2.6. *Diagram of degradation mechanism for organic matter by heterogeneous electro-Fenton oxidation.*

At the acidic working pH conditions, the mechanism showing the decomposition of H_2O_2 on the solid catalyst surface is summarized below. In the first stage, $\equiv Fe^{II}$ on the surface of the solid catalyst efficiently decompose H_2O_2 to $^{\bullet}OH$, and at the same time itself oxidizes to $\equiv Fe^{III}$ (Eq. 2.31). Moreover, HEF process may accompany the dissolved Fe^{3+}/Fe^{2+} released from the Fe-functionalized cathodic materials or solid catalysts, the reaction mechanism is similar to the homogeneous EF (Eq.2.32). In the final stage, through $^{\bullet}OH$ attacking, the organic pollutants can be mineralized to H_2O and CO_2 (Eq. 2.33).

$$\equiv Fe^{II} + H_2O_2 \rightarrow \equiv Fe^{III} + {}^{\bullet}OH + OH^{-} \quad (2.31)$$

$$Fe^{2+} + H_2O_2 \rightarrow Fe^{3+} + {}^{\bullet}OH + OH^{-} \quad (2.32)$$

$$^{\bullet}OH + \text{organic pollutants} \rightarrow \text{byproducts} \rightarrow CO_2 + H_2O \quad (2.33)$$

However, Eqs 2.34-2.38 shows the surface catalyzed mechanism for the basic or neutral conditions. In Eqs.2.34 and 2.35, the electrogenerated H_2O_2 binds with the $\equiv Fe^{II}{-}OH$/ $\equiv Fe^{III}{-}OH$ active sites of the iron based catalysts thereby generating a precursor surface complex $\equiv Fe^{II}{-}OH\ (H_2O_2)_{(s)}$/ $\equiv Fe^{III}{-}OH\ (H_2O_2)_{(s)}$

$$\equiv Fe^{II}{-}OH + H_2O_2 \rightarrow \equiv Fe^{II}{-}OH(H_2O_2)_{(s)} \quad (2.34)$$

$$\equiv Fe^{III}{-}OH + H_2O_2 \rightarrow \equiv Fe^{III}{-}OH(H_2O_2)_{(s)} \quad (2.35)$$

Eq. 2.36 shows that $\equiv Fe^{II}{-}OH(H_2O_2)_{(s)}$ in catalysts surface catalyzes the decomposition of adsorbed H_2O_2 into $^{\bullet}OH$ radicals and converted them to $\equiv Fe^{III}{-}OH$ during the reaction.

$$\equiv Fe^{II}{-}OH(H_2O_2)_{(s)} \rightarrow \equiv Fe^{III}{-}OH + OH^{-} + {}^{\bullet}OH \quad (2.36)$$

The surface H_2O_2 complex may transfer into $\equiv Fe^{II}{-}OH(HO_2^{\bullet})_{(s)}$ through a reversible ground-state electron form the ligand to the central atom (Eq. 2.37).

$$\equiv Fe^{III}{-}OH(H_2O_2)_{(s)} \rightarrow \equiv Fe^{II}{-}OH(HO_2^{\bullet})_{(s)} + H^{+} \quad (2.37)$$

In Eq 2.38 the successor complex is activated to $\equiv Fe^{II}{-}OH$

$$\equiv Fe^{II}{-}OH\ (\ HO_2^{\bullet})_{(s)} \leftrightarrow \equiv Fe^{II}{-}OH + HO_2^{\bullet} \quad (2.38)$$

It is important to note that, when the pH value is increased to the basic condition, the reaction rates of Eq. 2.37 can be improved greatly, because the rapid consumption of H^{+} will rapidly change the equilibrium, resulting in the formation of more $\equiv Fe^{II}{-}OH$ species. This cycle will continue to convert electrogenerated H_2O_2 to $^{\bullet}OH$ radicals.

In line with the above information, many authors have reported the use of various types of catalysts for the heterogeneous electro-Fenton treatment of organics and as such their catalytic activities have been summarized in the literature review.

2.5.2. Literature review on heterogeneous electro-Fenton (HEF) process

Classical EF process has strong oxidation ability in wastewater treatment; nonetheless, it still has some critical limitations such as the need of operating at pH 3 for an optimal run and the loss of soluble iron catalyst as hydroxide precipitate. In order to overcome these drawbacks, Fe containing solid catalyst as source of Fe^{2+} ion instead of a soluble iron salt are used (Ammar et al., 2015). Moreover, transition metals and their oxides such as cobalt are used in the production of nanomaterials that are highly effective heterogeneous catalysts for the activation of H_2O_2 which ultimately enhance the production of radicals and oxide ions that degrade organic pollutants via a Fenton-like process (Ding et al., 2021).

In line with the above information, several authors have reported the use of Fe and Co-containing solid substances as heterogeneous catalysts in the degradation of organic pollutants via heterogeneous electro-Fenton processes. Various studies reported in the literature in reference to Fe and Co-containing solid catalysts are summarized in Table 2.3 and 2.4 respectively. Based on the literature analyses, a support material is generally used in the synthesis of iron and cobalt-containing catalysts. For this reason, the use of many different support materials was investigated. In addition; it was observed that iron and cobalt-containing catalysts were synthesized using different methods. In line with the abovementioned, it can be suggested that the effectiveness of the catalyst depends on the support material used. Within the context of this thesis, mesoporous silica nanoparticles ($mpSiO_2$) were used as a support material in order to ensure stability in the structure and enhance the catalytic performance of the synthesized catalysts.

2.6. Mesoporous Silica Nanoparticles ($mpSiO_2$)

Owing to their unique physicochemical properties such as high specific surface area, high pore volume, wide pore dimensions and regular pore structure, mesoporous materials have gained great attention in recent years. These materials have the potentials to be utilized as catalyst supports and adsorbents for chemical, biochemical and environmental applications. In addition, mesoporous supports utilization increases the loading and dispersion of metal components and exhibits good catalyst performance due to their high surface area (Farhadian et al., 2021).

The synthesis of mesoporous silica nanoparticles (MSNs) with controlled particle morphology, size, chemical stability, and porosity have been widely reported in recent years (Tina Joshi et al., 2022). In line with the aforementioned characteristics, MSNs have attracted the attention of researchers for their application in adsorption, polymer filler, optical devices, drug delivery and release, catalysis and anti-reflection coating (Shamim et al., 2022). In addition, MSNs are attractive materials due to some of the advantages such as abundance of the raw material, flexible textural tunability, and ease of surface functionalization (Jia Ding et al., 2021).

Due to these advantages, mpSiO_2 was chosen as a support material in the synthesis of iron (II, III) oxide and cobalt (II, III) oxide nanoparticles as heterogeneous catalysts within the scope of this thesis.

2.7. Iron (II, III) Oxide Nanoparticles

Magnetite (Fe_3O_4) can be described as a mixed-valence iron oxide characterized by unique redox properties. Many methods such as corrosion of iron metal, oxidation of ferrous species, and chemical and biological reduction of ferric species can be utilized to synthesize the Fe_3O_4 nanoparticles (Sun & Lemley, 2011). Fe_3O_4 have been used in many different areas including drug targeting, catalysis, magnetic refrigeration systems, heat transfer applications, cancer therapy, magnetic cell separation, and enzyme immobilization owing to their low toxicity, good biocompatibility, and tunable magnetic properties (Ghanbari et al., 2014). Fe_3O_4 also has some advantages such as the ability to be separated and recycled easily using simple magnets (Thokchom et al., 2017). These characteristics are possible because of the paramagnetic and insoluble nature of the nanoparticles (Nasr-Esfahani et al., 2014). Additionally, Fe_3O_4 is chemically stable due to the electron transfer between Fe^{2+} and Fe^{3+} at octahedral sites (Kim et al., 2016). Also, the nanoparticles are environmentally friendly, less expensive and comparatively non-toxic (Nasr-Esfahani et al., 2014).

As a result of the presented properties, Fe_3O_4 nanoparticles have attracted considerable interest lately in chemistry and material sciences. For instance, Fatemeh Asgharzadeh and co-workers (Asgharzadeh et al., 2019) have prepared Fe_3O_4 nanoparticles as a catalyst in the degradation of pyrene-contaminated soil through enhanced electro kinetic-pseudo-Fenton process. Further, Roshanak Rezaei Kalantary and co-workers (Kalantary et al., 2018) have also synthesized Fe_3O_4 nanoparticles as a heterogeneous catalyst for the degradation of amoxicillin via heterogeneous electro-Fenton process. Additionally, Shalini Rajput and co-workers (Rajput et al., 2016) have developed Fe_3O_4 nanoparticles to be use as a catalyst for the removal of lead (Pb^{2+}) and chromium (Cr^{6+}) from water by batch adsorption experiments. Also, Sheng-Peng Sun and co-workers (Sun & Lemley, 2011) have synthesized a nano-magnetite (Fe_3O_4) as a heterogeneous catalyst for the degradation of p-Nitrophenol (p-NP) via heterogeneous Fenton-like process. Zahra Rahmatinia and co-workers (Rahmatinia & Rahmatinia, 2018) have also synthesized nano-Fe_3O_4 nanoparticles as a heterogeneous catalyst for the degradation of metronidazole via heterogeneous electro-Fenton process. Furthermore, Fengxi Chen and co-workers (Chen et al., 2017) have also synthesized Fe_3O_4 nanoparticles as a heterogeneous catalyst for the degradation of Rhodamine B via heterogeneous Fenton process.

Considering the aforementioned advantages, in this thesis, Fe_3O_4 nanoparticles were chosen as a catalyst to be used in the heterogeneous electro-Fenton removal of pipemidic acid (PPA).

2.8. Cobalt (II, III) Oxide Nanoparticles

Cobalt (II, III) oxide, an inorganic compound with the formula Co_3O_4, is described as a magnetic p-type semiconductor comprising of normal spinel structure wherein Co^{2+} ions are stationed in tetrahedral coordination whereas Co^{3+} ones are occupied in an octahedral coordination (Atique Ullah et al., 2020; Goudarzi & Salavati-Niasari, 2019). Different forms of the oxide such as Co_2O_3, $Co(OH)_2$, CoO, CoO_2 and Co_3O_4 also exist. However, Co_3O_4 is the most stable among the other oxides and as such it has been extensively investigated (Saeed et al., 2018). In addition, characteristics such as specific surface area, crystal size, reducibility, surface oxygen content, morphology, and crystal plane determines the activity of the Co_3O_4 nanoparticles (Z. Liu et al., 2020). Based on the aforementioned, Co_3O_4 is considered a substance with good oxidation activity owing to its high stability and the strong oxygen affinity (Ye et al., 2021).

Moreover, cobalt (II, III) oxide particles have been widely investigated compared to other transition metal oxides owing to their fascinating properties and a wide range of promising applications. It has wide range of applications such as catalysis, energy storage as anodic materials in lithium-ion batteries, and electronic devices (Itteboina & Sau, 2019). Among these applications, Co_3O_4 has been widely applied as a catalytic material with excellence considering its outstanding oxidation capacity which is as a result of its low valence band maximum. In addition, since it is considered as an important magnetic material, it has the potential to incorporate the functions of an external magnetic field in the recovery of materials thereby ultimately reducing the cost of recovery, indicating the great practical application potential (Q. Huang et al., 2017).

Based on the literature, many research have been carried out using cobalt (II, III) oxide nanoparticles as heterogeneous catalyst during the treatment of organic pollutants. For example, Archa Gulati and co-workers (Gulati et al., 2020) have synthesized a magnetic Co_3O_4 NPs for the reduction of para-nitrophenol to para-aminophenol in the presence of $NaBH_4$, as well as for oxidative degradation of the Orange G dye by using an AOP. Further, Cong Wang and co-workers (C. Wang et al., 2020) have synthesized Co_3O_4 nanoparticles for the catalytic oxidation of phenol by persulfate (PS) under alkaline conditions. T. Warang and co-workers (Warang et al., 2013) have synthesized Co_3O_4 nanoparticles as a heterogeneous catalyst for the photocatalytic degradation of methylene blue dye via photo-Fenton reaction in presence of H_2O_2 or oxone oxidants. Also, Wei-Jie Liu and co-workers (W. J. Liu et al., 2021) have fabricated Co_3O_4 nanoparticles for the catalytic oxidation of phenol by monopersulfate (MPS) from water. Yuxian Wang and co-workers (Y. Wang et al., 2015) have synthesized Co_3O_4 nanoparticles for the photochemical degradation of phenol by peroxymonosulfate (PMS). C. Maria Magdalane and co-workers (Magdalane et al., 2019) have synthesized Co_3O_4 nanoparticles for the photocatalytic degradation of hazardous wastewater from the dyeing industry. Further, Oscar M. Rodríguez-Narvaez and co-workers (Rodríguez-Narvaez et al., 2020) have used homogeneous (dissolved cobalt) and heterogeneous (suspended Co_3O_4) for the degradation of acetaminophen (ACT) under a Fenton-like reaction.

Considering the aforementioned advantages, Co_3O_4 nanoparticles were chosen as a catalyst to be used in the mineralization of pipemidic acid (PPA) at HEF conditions.

Within the scope of this thesis, the effectiveness of the synthesized catalysts in the removal of pipemidic acid, an antibiotic of quinolone family, from water was investigated. Thus, in the subsequent subsections the general overview of antibiotics, quinolones, their pollution and problems are discussed.

Table 2.3. *Summary of literature review on Fe-containing catalysts*

Model compound	**Method**	**Catalyst**	**Support**	**Reference**
Aniline	N/A	Goethite (α-FeOOH)	N/A	(Sánchez-Sánchez et al., 2007)
Atrazine	Co-precipitation Wet impregnation Two-step wet impregnation	Iron oxide	Nanostructured allophane clays	(Garrido-Ramírez et al., 2013)
2,4-dichlorophenol (2,4-DCP)	N/A	iron-carbon	Polytetrafluoroethylene (PTFE)	(C. Zhang et al., 2015)
Imidacloprid Chlorpyrifos	Adsorption assays	Fe-containing compound	Y-zeolite Alginaten Y-zeolite	(Iglesias et al., 2015)
Indole	Wet impregnation	Fe-containing compound	Alginate beads	(Hammouda et al., 2016)
Tetracycline	N/A	Chalcopyrite powder	N/A	(Barhoumi et al., 2017)
vanillic acid (VA)	N/A	Natural pyrite	N/A	(Ouiriemmi et al., 2017)
Acid Orange 7 (AO7).	Solvothermal microwave-assisted synthesis	Fe-containing compound	MFI zeolite	(Huong Le et al., 2019)

Table 2.4. *Summary of literature review on Co-containing catalysts*

Model compound	Method	Catalyst	Support	Reference
Diclofenac	Co-precipitation	Co_3O_4	CeO_2	(Xian et al., 2019)
Bisphenol A	One-step microwave-assistant	Co_3O_4-Bi_2O_3	Nickel foam	(Hu et al., 2019)
Ibuprofen (IBU) Trimethoprim (TMP)	Solvothermal	Co_3O_4	BiOI	(Malefane et al., 2020)
Chloramphenicols	Co-precipitation	Co_3O_4	Biochar	(Xu et al., 2020)
4-aminophenylarsonic acid (p-ASA	Two-step hydrothermal in-situ growth	Co_3O_4-La_2CO_5	Rice straw biochar RSBC	(Y. Li et al., 2021)
Levofloxacin (LEV)	Two-step hydrothermal in-situ growth	Co_3O_4	NiO	(Y. Zhang et al., 2021)
Rhodamine R6G dye	Microwave-assisted	Co_3O_4	SBA-15	(Prakash et al., 2022)

2.9. Antibiotics

Antibiotics are considered a class of pharmaceutical active compounds with high rate of prescription and consumption over the globe (Rodriguez-Mozaz et al., 2020). They are mainly used in human and veterinary medicine. It is estimated that over 200,000 tons of antibiotics are consumed every year. Antibiotics are defined as chemotherapeutic agents that used in the treatment and prevention of bacterial infections and have significantly promoted higher health standards. Moreover, they are found to be very useful in livestock production, such as poultry farms and aquaculture to prevent diseases and promote growth (Becker et al., 2016).

Penicillin, the first antibiotic, was discovered by an English Bacteriologist, Sir Alexander Fleming in September 1928. It is reported that from a soil inhabiting fungus Penicillium notatum, he accidentally discovered the antibiotic. Nonetheless, the first discovery and clinical trials were reported and conducted in 1929 and 1940, respectively.

As far as medical discoveries of the twentieth century were concerned, such a discovery was frequently described as one the most outstanding in the scientific community (Ebimieowei & Ibemologi, 2016).

Penicillin was able to stop infectious pathogens such as *Staphylococcus aureus*, a leading cause of death in European hospitals during that period, by inhibiting the cell wall biosynthesis of pathogenic bacteria. Importantly, the growing modern pharmaceutical industry, at around the 1940s and early 1970s, heavily influenced by antibiotic discovery, commercialized over 160 new antibiotics and semi-synthetic derivatives molecules, which consequently became the foundation for the treatment of infectious diseases (Kraemer et al., 2019). Despite the success of antibiotics in the treatment of human and animal diseases, there still exist numerous public health challenges confronting their usage and control. It is important to recognize that most of antibiotics are incompletely metabolized after their consumption and are therefore consequently excreted into the environment in that state. Moreover, due to the non-biodegrdable nature of these compounds, their bioaccumulation in the environment can cause serious problems to both humans and the ecosystem. For this purpose, it is imperative to develop and study a process such as electro-Fenton method using heterogeneous catalysts that will efficiently enhance the removal of these organics from water bodies. In this thesis, pipemidic acid, belonging to an antibiotic quinolone family was chosen as the model organic pollutant to be investigated using an electro-Fenton method.

2.10. Classification of Antibiotics

Classifying antibiotics can be done in many ways. However, the most common classification schemes depend on their molecular structures, mode of action and spectrum of activity. Equally, route of administration (injectable, oral and topical) is considered. Similar pattern of effectiveness, toxicity and allergic-potential side effects is generally manifested by antibiotics within the same structural class. In the light of the above information, antibiotics are grouped into the following classes depending on the chemical or molecular structures (Ebimieowei & Ibemologi, 2016). Figure 2.7 shows the different classes of antibiotics.

In this study, the model organic pollutant, pipemidic acid, is a quinolone antibiotic and as such a well detailed explanation is provided for quinolones and pipemidic acid in the subsequent subsections.

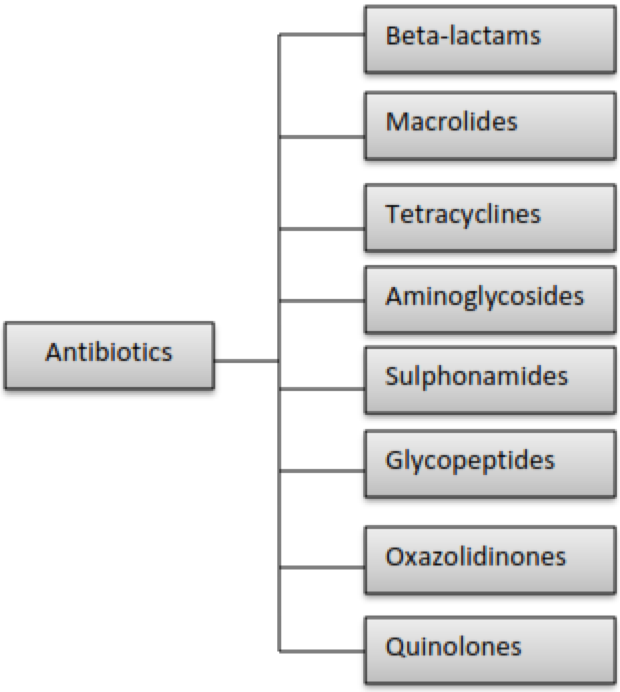

Figure 2.7. *The different classes of antibiotics*

2.10.1. Quinolones

Quinolones, discovered as a by-product in the search for improved synthesis of the anti-malarial chloroquine, are one of the most significant families of antimicrobial agents, widely used to treat bacterial infections (Millanao et al., 2021).

Subsequent to the discovery of chloroquine, nalidixic acid, cinoxacin, rosoxacin, pipemidic acid, piromidic acid and oxolinic acid were also discovered.

Antibiotics classified as quinolones are synthetic broad-spectrum antibacterial drugs used in both human and veterinary medicine. These anti-microbial agents have demonstrated broad–spectrum activity against many pathogenic Gram–negative and Gram–positive bacteria by inhibiting the DNA-gyrase in the bacterial cell (Jia et al., 2012; Pagani & Ibañez, 2019).

Moreover, owing to their strong antibacterial ability, good pharmacokinetic properties, high bioavailability and low price, quinolone antibiotics is extensively applied in the treatment of respiratory and urinary infectious diseases (Zou et al., 2022).

There are many different types of quinolones. Figure 2.8 shows the general structure of quinolone antibiotics (M. zhi Zhang et al., 2022). As can be seen, different functional groups are represented at various positions within the structure. For example, at position one, three and four, nitrogen, carboxylic acid and oxygen are represented, respectively. Also, halogens are represented by ‘X’ and ‘R’ could be hydrogen (H) or other groups. The introduction of other functional groups to the general structure led to the diversification of the quinolones and its subsequent arrangement into various groups.

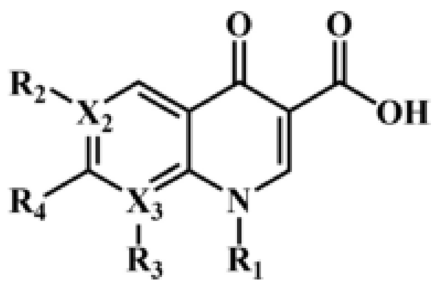

Figure 2.8. *General Structure of Quinolones*

2.10.2. Classification of quinolones

Classifying quinolones correctly is considered a very cumbersome task owing to their varied properties. However, relative to their antibacterial activity and spectrum, four broad groups are recognized as can be seen in table below (Table 2.5) (Ball, 2000): First-generation quinolones are described as compounds with a narrow antibacterial activity directed mainly against Gram-negative organisms, excluding *Pseudomonas* species. Soon after, nalidixic acid was clinically introduced; however, it was observed that its intake has led to quick development of resistance among many organisms thereby diminishing its effectiveness. For this reason, investigations to discover analogues with improved properties were carried out (Pham et al., 2019). They are predominantly used for the treatment of urinary infections ((Ball, 2000). Within the scope of this thesis, the removal of pipemidic acid (PPA), a first-generation quinolone, from water was studied in detail.

Table 2.5. *Classification of quinolone antibiotics*

First-generation	Second-generation	Third-generation	Fourth-generation

Cinoxacin	Ciprofloxacin	Garenoxacin	Gemifloxacin
Flumequine	Enoxacin	Gatifloxacin	Delafloxacin
Nalidixic acid	Norfloxacin	Levofloxacin	Moxifloxacin
Oxolinic acid	Ofloxacin	Sparfloxacin	Nemonoxacin
Pipemidic acid	Pazufloxacin	Tosufloxacin	Sitafloxacin
Piromidic acid	Pefloxacin		Trovafloxacin
Rosoxacin	Prulifloxacin		WCK 771
	Rufloxacin		Zabofloxacin

2.10.3. Pipemidic acid

PPA (8-ethyl-5,8-dihydro-5-oxo-2- (1-piperazinyl)-pyrido[2,3-d]pyrimidine-6-carboxylic acid), belongs to the groups of compounds known as quinolones (Szymańska et al., 2006). As an antibacterial agent, it is used in the treatment of gram-negative urinary tract infections (Efthimiadou et al., 2007) and it severely damages DNA in the absence of an exogenous metabolizing system (M. T. Li et al., 2013; Sha et al., 2011). The capability of PPA to penetrate the bacterial cell wall has been observed to increase due to the introduction of a piperazinyl side chain at the general structure of quinolone antibiotics thereby improving its activity. Moreover, PPA has shown efficiency against some organisms resistant to piromidic or nalidixic acids (Szymańska et al., 2006). The physicochemical properties and structure of PPA are shown in Table 2.6.

Table 2.6. *Physicochemical properties of PPA*

Molecular structure	

	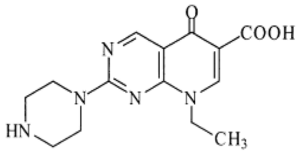
Molecular name	8-ethyl-5,8-dihydro-5-oxo-2-(1-piperazinyl)pyrido(2,3-d)pyrimidine-6-carboxylic acid
Common name	Pipemidic acid
Molecular formula	$C_{14}H_{17}N_5O_3$
Molecular weight	303.32
Solubility(mg/mL)	0.322 mg/mL at 25°C
Melting point	251-255°C
Boiling point	717°C
Flash point	>110°(230°F)
Density	1.1931 g/cm^3

2.11. Antibiotic Pollution in the Environment

In the treatment of human and animal diseases, antibiotics have manifested enormous importance (Jiaxiang Liang et al., 2022). As a consequence, discharges from households, hospitals, pharmaceutical companies, wastewater treatment plants (WWTPs), aquaculture and livestock farms have enabled the release of substantial amounts of antibiotics into the environment (Anh et al., 2021). A schematic flow of antibiotic pollution is shown in Figure 2.9.

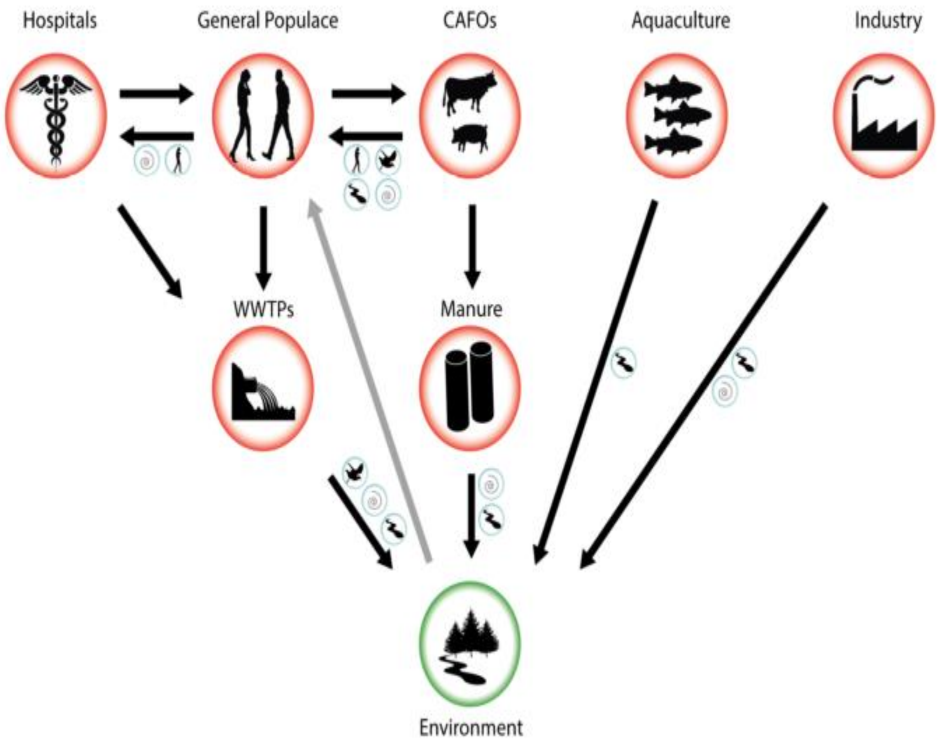

Figure 2.9. *Schematic flow of antibiotic resistance bacteria (ARBs) and antibiotic resistance genes (ARGs) from hotspots of evolution and transmission (red circles) to the environment (green circle). Blue circles indicate possible vectors that may aid transmission between specific environments including air, surface waters, humans, and other animal vectors. Black arrows indicate known flows of ARBs and ARGs; grey arrow indicates a possible transmission route from a contaminated environment back to the general populace (Kraemer et al., 2019)*

Notwithstanding, the consumption of antibiotics has grown steadily over the globe owing to an augmentation of antibiotic use in human medicine and in other sectors of commercial activity. Also, due to intensive farming, the use of antibiotics has increased in aquaculture, the fastest-growing food sector worldwide. Moreover, antibiotic molecules are increasingly available in terrestrial, freshwater, and marine environments. This is as a result of poor regulation of antibiotic pollution at both local and international levels (Kraemer et al., 2019).

The swift proliferation and emergence of antibiotic-resistant bacteria (ARB) and antibiotic resistant genes (ARGs) is triggered by the overuse and misuse of antibiotics. This consequently culminates in the reduction of their therapeutic potential against human and animal pathogens (Qiao et al., 2018).

Diseases such as methicillin-resistant Staphylococcus aureus (MRSA), vancomycin-resistant Enterococcus (VRE), multi-drug resistant Mycobacterium tuberculosis (MDR TB), and carbapenem-resistant Enterobacteriaceae (CRE) gut bacteria are caused by ARBs that can ultimately lead to pneumonia, skin infections, endocarditis and toxic shock syndrome. In addition, the UK Government has reported that infections due to antimicrobial resistance may lead to an increase in deaths by 2050 (Hazra et al., 2022).

Presently, the birth of microbial pathogens having the ability to resist antibiotics treatments is considered as part of the most threatening public health menace. Therefore, antibiotics were selected as the water pollutants in this thesis.

The literature analysis showed that different studies have been conducted for the detection of PPA in water bodies. For example, Ai Jia and co-workers (Jia et al., 2012) have conducted a research on the occurrence and fate of nineteen quinolone and fluoroquinolone antibiotics in a municipal sewage treatment plant (STP). Out of the 19 model antibiotics, ten compounds among them PPA were detected in wastewater samples. Based on the analysis, a concentration of 86 ±17 ng/L was detected in the STP. In addition, Sara Rodriguez-Mozaz and co-workers (Rodriguez-Mozaz et al., 2020) have carried out a study to monitor the impact of antibiotic residues on the aquatic environment from the European wastewater treatment plants. During this study, 53 antibiotics from the seven different European countries were monitored. Out of the 53 antibiotics studied, 17 including PPA were detected at least once in the final effluent of the WWTPs. According to the analysis report; the highest concentration of 117.6 ng/L of PPA was observed in wastewaters obtained from Portugal.

Considering the above, the presence of PPA as an organic pollutant in the various water sources is a concern and thus its complete remediation is highly necessary. In this thesis, PPA was chosen as the model organic pollutant and the efficiency of the synthesized catalysts was tested in the complete mineralization of PPA from water.

3. MATERIALS AND METHODS

3.1.1. Chemicals

The list below shows the chemicals used during the experiments (Table 3.1).

Table 3.1. *Chemicals used in the experiments*

Chemical name	Brand	Chemical name	Brand
Pipemidic acid,98%	Alfa Aesar	Methanol, ≥99.8%	Sigma-Aldrich
$Fe_2(SO_4)_3.5H_2O$, 97%	Sigma-Aldrich	4-Hydroxybenzoic Acid	Acros Organics
$Fe(NO_3)_3.9H_2O$, 99+%	Acros Organics	Glycine	Fluka
Cetyltrimethylammonium bromide (CTAB)	Aldrich	$Co(NO_3)_2.6H_2O$	Sigma-Aldrich
Na_2SO_4, ≥99.0%	Sigma-Aldrich	Methanesulphonic Acid, ≥99.5%	ROTH
H_2SO_4, 97%	Fluka	Sodium carbonate	Aldrich
Acetic acid, 100%	Riedel-De Haen	Tetraethyl orthosilicate (TEOS)	Aldrich
NH_4NO_3, 99%	Carlo Erba	Ethanol	Carlo Erba
$SnCl_2.2H_2O$	Merck	Benzoquinone	Fluka

3.1.2. Homogeneous electro-Fenton experiments

The electro-Fenton experiments were conducted at room temperature in a 0.175 L undivided cylindrical glass cell which has a diameter of 5 cm equipped with two electrodes (Fig 3.1). The working electrode was a piece of carbon-felt (10 × 5 × 0.5 cm). It is placed on the inner wall of the cell covering the totality of the internal perimeter. The counter electrode was a cylindrical Pt gauze or a BDD film placed on the center of the cell. Prior to the electrochemical experiment, compressed air was bubbled through the aqueous solutions, which were agitated continuously by a magnetic stirrer maintained at 500 rpm (IKAMAG, RCT). A determined amount of iron (III) sulphate pentahydrate was introduced into the solution before the beginning of electrolysis. The current and the amount of charge passed through the solution were measured and displayed continuously throughout electrolysis by using a DC power supply (Triple Power Supply, HM8040-3) (Figure 3.2). Before the beginning of each electro-Fenton reaction, the pH of initial solutions was set at 3 by the addition of aqueous H_2SO_4 (1 M). The pH values were measured by a pH glass electrode (OHAUS, STARTER, 3000) calibrated with standard buffers which have pH values of 4, 7 and 10. Also, the ionic strength was maintained constant by the addition of 50 mM Na_2SO_4. The different types of electrodes used in the electrochemical experiments are depicted in Figure 3.3.

Figure 3.1. *Undivided cylindrical glass cell used during the electro-Fenton experiments*

Figure 3.2. *DC power supply used in the electro-Fenton experiments*

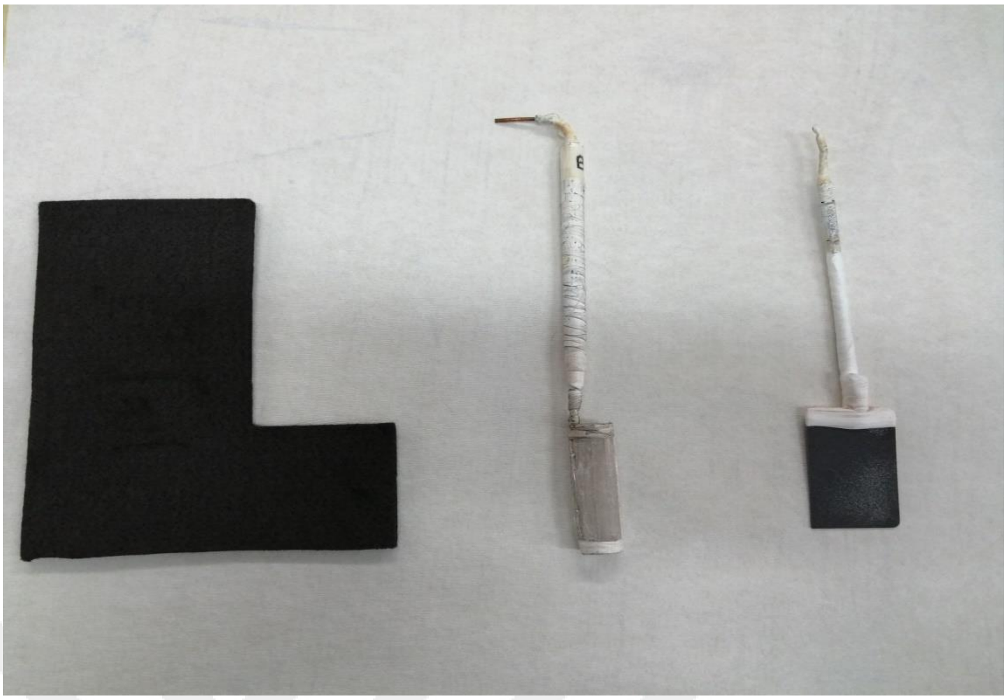

Figure 3.3. *Electrodes used in the electro-Fenton experiments*

3.1.2. High performance liquid chromatography (HPLC) analysis

The degradation of PPA was monitored by HPLC analysis using an Agilent 1100 system coupled with a Diode Array Detector (DAD) and an auto-sampler (Fig 3.4). In this process, a reversed phase Inertsil ODS-3 (5-µm, 4.6-mm x 250-mm) column was used in the experiments. The column temperature was maintained at 35 °C and 10 µL was used as the injection volume. In the determination of PPA, a gradient elution system was used in the experiments. A mixture of 90% water and 10% methanol was defined as eluent A. Eluent B contains 10% water and 90% methanol. The analytical conditions used in the HPLC analysis are shown in Table 3.2.

Figure 3.4. *HPLC analysis system used in the experiments*

Table 3.2. *Analytical conditions used in the HPLC analysis*

Time (min)	Eluent B (%)	Flow rate (mL/ min)	Wavelength (nm)
0.00	10.0	0.8	275
2.00	10.0		
10.00	50.0		
11.00	50.0		
16.00	10.0		
21.00	10.0		

Competition kinetics method was employed to determine the rate constant of the reaction between the hydroxyl radicals and PPA. In this thesis, 4-Hydroxybenzoic Acid (4-HBA) was used as a reference organic compound. HPLC analysis was performed to monitor the initial and electrolyzed samples containing equal concentrations of 4-HBA and PPA. The chromatographic parameters such as injection volume, flow rate and eluents used initially remained unchanged. The analytical conditions used in the experiments were given in Table 3.3.

Table 3.3. *HPLC analysis conditions used to determine the concentrations of 4-HBA and PPA*

Time (min)	Eluent B (%)	Flow rate (mL/ min)	Wavelength (nm)
0.00	10.0	0.8	254
2.00	10.0		
10.00	50.0		
15.00	50.0		
22.00	10.0		
25.00	10.0		

3.14. Determination of carboxylic acids

The evolution of the short-chain carboxylic acids as the final organic by-products of the degradation of PPA was followed by the same HPLC system equipped with a

Supelcogel H (Ø=30 cm X 7.8 mm) column. The column temperature was maintained at 30 °C and 20 µL was used as the injection volume. Additionally, the mobile phase was 4 mM H_2SO_4 with a flow rate of 0.5 mL/ min and the detection was performed at 210 nm.

3.1.5. Determination of inorganic ions

An ion chromatography (Dionex ICS-1100) analysis system (Fig 3.5) fitted with an electrical conductivity detector was used to quantify the concentrations of ammonium(NH_4^+) and nitrate (NO_3^-) ions released during the electrolyzes of the target organic pollutant, PPA. A cationic (IonPac® CS12A-Dionex) and an anionic (IonPac ®AS9-HC-Dionex) exchanger columns were used to attain the concentrations of cations and anions, respectively. The volume of injections was 25 µL. The mobile phase was 20 mM methanesulphonic acid with a flow rate of 0.8 mL/min in the cation analysis. On the other hand, 10 mM sodium carbonate with a flow rate of 1.50 mL/min was used as a mobile phase in the anion analysis. Prior to the analyses of the initial and electrolyzed samples, calibration curves were acquired by using the pure standards of the related ions.

Figure 3.5. *Ion chromatography system used in the experiments*

3.1.6. Monitoring of total organic carbon (TOC) values

A Shimadzu TOC-L analyzer (Fig.3.6) equipped with a non-dispersive infrared detector (NDIR) was used to evaluate the values of the TOC for the initial and electrolyzed samples. Prior to each analysis, dried air was continuously supplied as the carrier gas. Calibration of the analyzer was performed with potassium hydrogen phthalate and sodium hydrogen carbonate standards for total carbon (TC) and inorganic carbon (IC), respectively. The difference between TC and IC analysis gives TOC data of the sample. For total carbon (TC) and inorganic carbon (IC) determination, 50 μL and 800 μL of sample was injected into the system, respectively.

Figure 3.6. *TOC analysis system used in the experiments*

3.1.7. Mineralization current efficiency

The oxidation of PPA by the EF process ultimately leads to its mineralization. The total mineralization of PPA was described according to Equation 3.1.

$$C_{14}H_{17}N_5O_3 + 25H_2O \rightarrow 14CO_2 + 5NH_4^+ + 47H^+ + 52e^- \qquad (3.1)$$

The MCE for treated solutions at a given treatment time t (h) was calculated from the equation below (Eq. (3.2)) (N. Oturan et al., 2011):

$$\mathrm{MCE} = \frac{\mathrm{nFVs}\Delta(\mathrm{TOC})_{\mathrm{exp}}}{4.32\times 10^7\ \mathrm{mIt}} \times 100 \qquad (3.2)$$

n: the number of electrons consumed per PPA molecule (= 52)

F: the Faraday constant (= 96,487 C mol^{-1})

V_s: the solution volume (L)

$\Delta\ (TOC)_{exp}$: the experimental TOC decay (mg L^{-1})

4.32×10^7: the conversion factor to homogenize units (= 3600 s h^{-1} × 12,000 mg of C mol^{-1})

m: the number of carbon atoms of PPA (= 14)

I: the applied current (A)

3.2. Removal of Pipemidic Acid from Water by Heterogeneous Electro-Fenton Process

In the second phase of the thesis, three different solid-phase catalysts namely Fe_3O_4-mpSiO_2, Co_3O_4-mpSiO_2 and Fe-d-SnO_2 were synthesized and characterized to use in the electro-Fenton process. Various methods such as XRD, SEM, EDX and BET were employed in the characterization process of the synthesized catalysts.

3.2.1. Synthesis of the catalysts

Within the context of this thesis, the following catalysts were synthesized Fe_3O_4-mpSiO_2, Co_3O_4-mpSiO_2 and Fe-d-SnO_2. However, prior to the synthesis of the silica supported iron (II, III) oxide and cobalt (II, III) oxide, mesoporous silica nanoparticles (MSNs) were prepared firstly.

3.2.1.1. Synthesis of mesoporous silica nanoparticles (mpSiO_2)

MSNs were synthesized by a sol-gel/emulsion method according to a previously reported study (Zhao et al., 2017). Briefly, 220 mL of de-ionized water and 104 mL of anhydrous ethanol were mixed initially. Then, to the mixed solution, 4 mL of TEOS and 0.64 g of CTAB were added under a magnetic stirring speed of 700 rpm and stirred for 15 min. Subsequently, 4 mL of ammonium hydroxide was added and the mixture was allowed to react for about 3 h. The observed white precipitates were washed and isolated by a vacuum filter set-up using de-ionized water, dried at 60°C under a vacuum of 600 mbar and later grounded to fine powder. Afterwards, the fine powders were calcined at 550°C for 5 h to remove the residual surfactant.

3.2.1.2. Synthesis of Fe_3O_4-mpSiO_2 and Co_3O_4-mpSiO_2

Firstly, 2.5 mmol of $Fe(NO_3)_2.9H_2O$ (or $Co(NO_3)_2.6H_2O$) and 1.25 mmol of glycine ($C_2H_5NO_2$) were dissolved in 50 mL of de-ionized water and kept under continuous magnetic stirring for a few minutes to ensure complete dissolution. Afterwards, 200 mg of the synthesized mpSiO_2 were added to the reaction mixture. The above reaction mixture was heated on a hot plate maintained at 250°C to induce vaporization. The viscous gel formed was calcined at 400°C for about 3 h and subsequently milled into fine powder.

3.2.1.3. Synthesis of Fe-d-SnO_2 catalyst

Fe-d-SnO_2 was synthesized by a sol-gel method according to a previously reported study (Zhao et al., 2017). Initially, 1.25 g $SnCl_2.2H_2O$ and 1.0 g $Fe(NO_3).9H_2O$ were dissolved by de-ionized water in a 25 mL and 10 mL volumetric flask, respectively. Afterwards, both solutions were mixed in a 100 mL round bottom flask. Then, a dilute NH_4OH solution was added to the reaction mixture under a constant magnetic stirring in a drop-wise fashion until the pH value reached 9.0. The mixture was allowed to react for about three hours. After the reaction, the precipitates were washed by a vacuum filter set-up using de-ionized water, dried at 100°C under a vacuum of 600 mbar for 6 h, and calcined at 500°C for 3 h.

3.2.2. Characterization of catalysts

3.2.2.1. X-ray diffraction analyses

X-Ray diffraction (XRD) technique makes use of x-ray radiation on crystalline organic and inorganic samples. The diffraction of these rays into different patterns is determined by the position, arrangement, and size of the constituents of the crystal. Furthermore, XRD is primarily used for the characterization of material properties like crystal structure, crystallite size, and strain.

A BRUKER D8 ADVANCE X-ray diffractometer (Fig 3.7) was used to conduct the XRD measurements. Data were collected in the angular region of $2\theta = 15–90°$ in a step-scanning mode, with a step length of 0.02°. Nanoparticles such as mpSiO_2, Fe_3O_4, Co_3O_4, Fe_3O_4-mpSiO_2, Co_3O_4-mpSiO_2 and Fe-d-SnO_2 were characterized using the XRD analyzer.

Figure 3.7. *XRD system used in the experiments*

3.2.2.2. Scanning electron microscope analyses

The scanning electron microscope (SEM) utilizes the focusing of a beam of high-energy electrons to produce many different signals at the surface of solid specimens. The signals that are generated as a result of electron-sample interactions provide information about the sample such as external morphology (texture), chemical composition, and crystalline structure and orientation of materials making up the sample.

A ZEISS ULTRA plus SEM instrument (Fig 3.8) was used for the analyses of the synthesized catalysts. A gold coating process was applied to increase the surface conductivity of the samples before the measurements. Nanoparticles such as $mpSiO_2$, Fe_3O_4, Co_3O_4, Fe_3O_4-$mpSiO_2$, Co_3O_4-$mpSiO_2$ and Fe-d-SnO_2 were characterized using the SEM analyzer.

Figure 3.8. *SEM system used in the experiments*

3.2.3. Heterogeneous electro-Fenton experiments

In the heterogeneous electro-Fenton experiments, the same electrochemical system described in subsection 3.2.1 was used by replacing the soluble iron salt with solid-phase catalysts.

4. RESULTS AND DISCUSSIONS

In this thesis, the preparation and characterization of solid-phase catalysts have been aimed for the heterogeneous electro-Fenton treatment of pipemidic acid, a widely used antibiotic. The research was separated in three different main stages. In the first stage, the oxidation and mineralization of the model organic pollutant, pipemidic acid (PPA), was investigated using a homogeneous electro-Fenton process. In the second stage, the mesoporous silica supported catalysts (Fe_3O_4-mpSiO_2 and Co_3O_4-mpSiO_2) were prepared and their catalytic activities in the heterogeneous electro-Fenton removal of PPA were monitored and subsequently compared. In the third stage, iron-doped tin dioxide (Fe-d-SnO_2) was synthesized and its efficiency in the removal of PPA was also investigated under the same heterogeneous electro-Fenton conditions. Thereafter, the two processes- homogeneous electro-Fenton and heterogeneous electro-Fenton in the removal of PPA were compared.

4.1. Investigation of the Removal of Pipemidic Acid using the Homogeneous Electro-Fenton Method

At the first stage of the thesis, the efficiency of the homogeneous EF system on the removal of PPA was carefully studied. The EF process which entails the production of hydroxyl radicals ($^{\bullet}OH$) was observed to destroy PPA and subsequently transformed it into less harmful compounds such as short chain carboxylic acids with their further mineralization into CO_2 and H_2O. The effects of the operation parameters such as type of electrode, applied current and iron concentration on the degradation and mineralization of PPA were monitored by HPLC and TOC analysis. Ion-exclusion chromatography and ion-exchange chromatography analysis were used to determine the released carboxylic acids and inorganics ions, respectively.

4.1.1. Investigation of the effectiveness of different electrodes in the electro-Fenton process

In the EF system, different electrode materials can be used for the production of hydroxyl radicals. The degradation rates of the organic pollutants can be influenced by the type of electrodes utilized as cathode and anode in the experiment. In this thesis, carbon felt (CF), platinum (Pt) and boron-doped diamond (BDD) electrodes in different anode/cathode combinations were employed to study the removal behavior of PPA. As can be seen in Figure 4.1, the concentration of PPA has gradually decreased for both

BDD/CF and Pt/CF electrode combinations. Also, the disappearance of PPA by BDD/CF electrode combination was observed to take place within the first 15 min of the electrolysis time. On the other hand, the disappearance of PPA in the case of Pt/CF electrode combination took 30 min before complete oxidation was achieved. For this reason, it can be said that the rate of destruction was faster in BDD/CF than Pt/CF electrode combination throughout the electrolysis. The degradation rate of PPA was slower and took longer electrolysis time when a Pt/CF electrode combination and this could be explained as Pt is considered to have strong interaction with the $^{\bullet}OH$ and this might eventually decrease the availability of $^{\bullet}OH$ for the pollutant degradation (Nair et al., 2021). The fast rate of degradation in BDD/CF electrode combination on the other hand can be attributed to the different sources of hydroxyl radical production during the treatment. Firstly, $^{\bullet}OH$ were produced from the Fenton's reaction (Eq. (2.1)). Secondly, $^{\bullet}OH$ was also produced from the oxidation of water on the BDD anode surface according to Eq. (4.1). Cumulatively, these sources contributed to the increase in the degradation of PPA (Özcan et al., 2016).

$$BDD + H_2O \rightarrow {}^{\bullet}OH + OH^- + e^- \qquad (4.1)$$

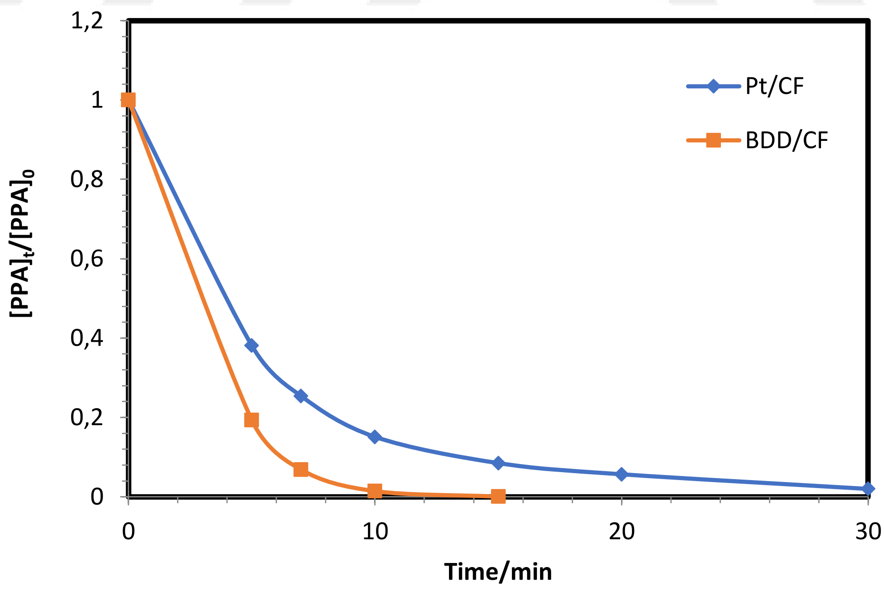

Figure 4.1. *Time-course of the concentration of PPA during the electro-Fenton treatment of PPA using different electrode combinations. $[PPA]_0$: 0.25 mM, $[Fe^{3+}]_0$: 0.1 mM, $[Na_2SO_4]_0$: 0.05 M, I: 100 mA, pH: 3.0, V: 0.175 L*

The TOC values during the oxidation of PPA using different electrode combinations were depicted in Figure 4.2. As can be seen, the concentration of PPA present in the solutions for both electrode combinations decreased as electrolysis time increased. However, after 30 min of the experiment, the amount of PPA in the reaction solution was very high for Pt/CF as well as BDD/CF electrode combinations corresponding to a TOC removal of 34.76% and 47.13%, respectively. Nonetheless, as time progressed, the concentration of PPA in the solution has greatly decreased. For example, after 3 h of the electrochemical experiment, TOC removal values reached 67.41% and 86.55% for Pt/CF and BDD/CF electrode combinations, respectively. Moreover, at the end of the electrolysis, 78.41% and 95.49% mineralization for Pt/CF and BDD/CF electrode combinations, respectively, was yielded showing a significant decrease in the amount of organic pollutant present in the reaction solution. With this amounts of mineralization of PPA from the solution, it can be suggested that there was interaction between the organic species available within the PPA structure and the $^{\bullet}OH$ which subsequently transformed them into CO_2 and H_2O. It can be further stated that the BDD/CF electrode combination had achieved higher rate of mineralization as compared to Pt/CF electrode combination.

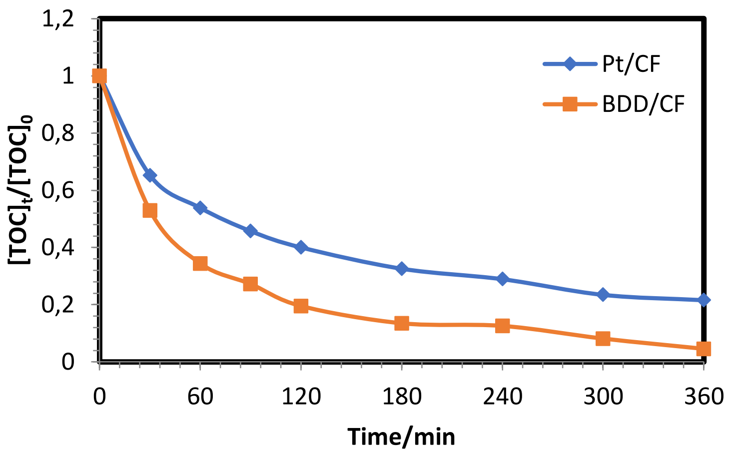

Figure 4.2. *Time-course of the TOC values during the electro-Fenton treatment of PPA using different electrodes combinations. $[PPA]_0$: 0.25 mM, $[Fe^{3+}]_0$: 0.1 mM, $[Na_2SO_4]_0$: 0.05 M, I: 100 mA, pH: 3.0, V: 0.175 L*

4.1.2. Optimization of the applied current intensity

One of the most significant operational parameters in determining the effectiveness of an EF process is the applied current intensity. In this study, experiments were performed under the following conditions: 0.25 mM PPA, 0.1 mM Fe^{3+} and current intensities of 25, 50, 100 and 300 mA. As it can be observed in Figure 4.3, the results indicate that as the current intensity increases from 25 mA to 300 mA during the electrolysis, the rate of disappearance of PPA also increases. This fast rate of disappearance in association with the increase in the current intensities could be as a result of an increase of H_2O_2 production and an increase of the regeneration rate of Fe^{2+} at the cathode, leading to a higher amount of hydroxyl radicals produced (Annabi et al., 2016).

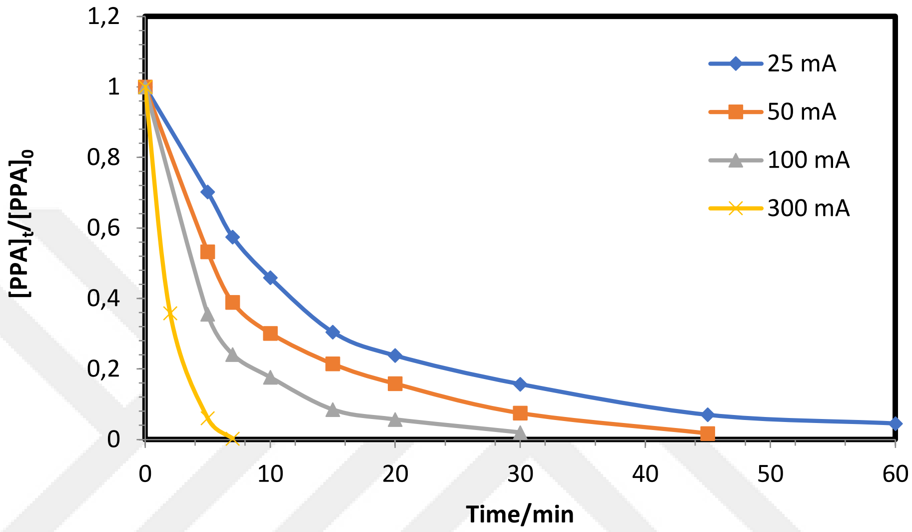

Figure 4.3. *Time-course of the concentration of PPA during the electro-Fenton treatment at different applied current intensities. $[PPA]_0$: 0.25 mM, $[Fe^{3+}]_0$: 0.1 mM, $[Na_2SO_4]_0$: 0.05 M, Pt/CF, pH: 3.0, V: 0.175 L*

As can be seen in Figure 4.4, there was a reduction in the initial TOC values as time progressed during the electrolysis. However, TOC removal values of 18.36%, 34.76% and 47.25% for 50, 100 and 300 mA were achieved after 30 min of the electrolysis. These results imply that not much mineralization was obtained at this particular time of electrolysis, however, as the electrolysis time increased the rate of mineralization also increased. After 180 min of electrolysis, mineralization values of 52.57%, 67.41% and 73.81% were achieved for 50, 100 and 300 mA, respectively. From these results, it can be deduced that substantial decrease in the amount of PPA from the reaction medium was made. In addition, after 360 min of electrolysis, a significant reduction in the amount of PPA from the solution was shown as can be seen from the TOC removal values consisting of 64.81%, 76.79% and 83.72% for 50, 100 and 300 mA, respectively. The obtained results show that as the current intensity increases from 50mA to 300mA, the rate of PPA removal during the electrolysis increased accordingly. Further, it was observed that the highest rate of mineralization when a 300mA was used in the experiments.

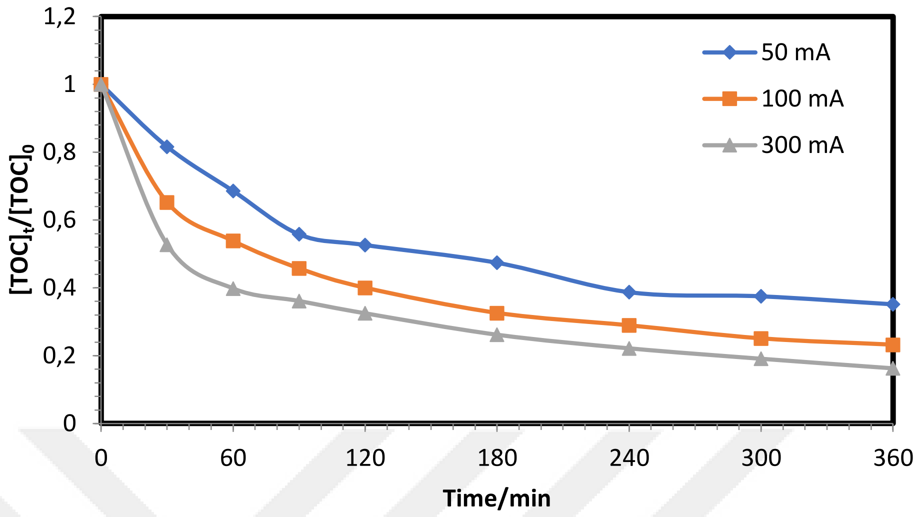

Figure 4.4. *Time-course of the TOC values of PPA during the electro-Fenton treatment at different applied current intensities. $[PPA]_0$: 0.25 mM, $[Fe^{3+}]_0$: 0.1 mM, $[Na_2SO_4]_0$: 0.05 M, Pt/CF, pH: 3.0, V: 0.175 L*

So, it could be concluded that in monitoring the effect of applied current intensities for the oxidation and mineralization of PPA followed by HPLC and TOC, respectively, the best results was obtained when 300mA was used in the experiments.

The MCE values for the different applied current intensities are presented in Figure 4.5. As can be seen, the MCE values decrease with increase in applied current intensities. Moreover, the MCE values were observed to be within the range of 17.39% and 42.02% after the first 30 min of electrolysis indicating that 50 mA has the highest MCE values at this particular time. It was further observed that as time of electrolysis increased the values of MCE decreased with increase in applied current values accordingly. For instance, after 180 mins of electrolysis, MCE values of 20.05%, 12.05% and 4.53% for 50, 100 and 300 mA, respectively were obtained. Moreover, after 360 min of electrolysis, a significant decrease was shown as can be seen from the MCE values of 12.36%, 6.86% and 2.575% for 50, 100 and 300 mA, respectively. From the data above, it can be said that 300mA produced the lowest MCE (%) value as compared to 50mA. This foregoing condition can be explained as follows: the energy that increases with increase in the current intensity in the system is spent by parasitic reactions that do not contribute to the production of the hydroxyl radicals.

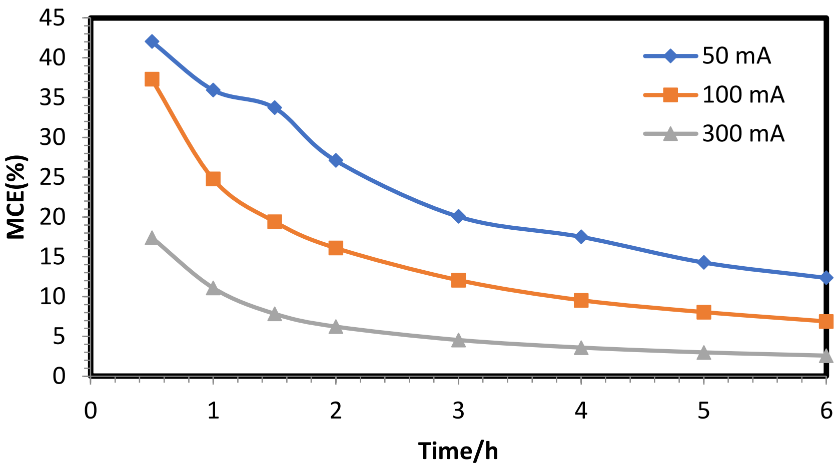

Figure 4.5. *Time-course of MCE (%) values of PPA during the electro-Fenton treatment at different applied current intensities. $[PPA]_0$: 0.25 mM, $[Fe^{3+}]_0$: 0.1 mM, $[Na_2SO_4]_0$: 0.05 M, Pt/CF, pH: 3.0, V: 0.175 L*

4.1.3. Optimization of the iron concentration

In this study, the effect of the concentration of Fe^{3+} on the removal of the model organic pollutant was monitored at constant current intensity of 50 mA. The Fe^{3+}concentrations used in the study includes 0.025 mM, 0.05 mM , 0.1 mM and 0.2 mM. As can be seen in Figure 4.5, the iron concentrations gave very close results in the oxidation of PPA during the first 45 min of electrolysis. Notwithstanding, 0.1 mM is observed to provided much faster rate of removal with shorter electrolysis time as compared to other iron concentrations.

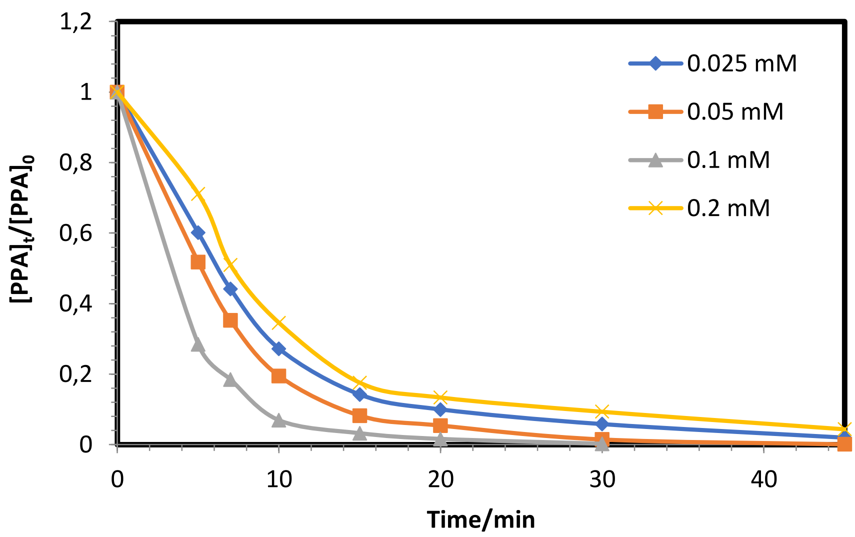

Figure 4.6. *Time-course of the concentration of PPA during the electro-Fenton treatment at different iron*

concentrations. [PPA]₀: 0.25 mM, [Na₂SO₄]₀: 0.05 M, I: 50 mA, Pt/CF, pH: 3.0, V: 0.175 L

The mineralization during the electrolysis of PPA was followed by TOC analyses (Fig 4.6). The results appear very similar to that the one produced by the HPLC analyses (Fig 4.5). As can be seen, the rate of mineralization has increased with an increase in the amount of iron concentration. Also, the rate of mineralization of PPA was observed to increase as time progressed. Mineralization values of 7.23%, 15.51%, 29.02% and 21.65% for 0.025 mM, 0.05 mM, 0.1 mM and 0.2 mM, respectively were achieved after 30 min of the experiment showing that insufficient amounts of PPA were removed from the reaction medium but with increase in electrolysis time, a decrease in the amount of PPA in the solution was observed. For example, after 180 min of electrolysis, TOC removal values of 53.82%, 60.24%, 66.28% and 49.21% for 0.025 mM, 0.05 mM , 0.1 mM and 0.2 mM, respectively was achieved indicating an increase in the removal of PPA from the solution. Similarly, more reduction in the amount of PPA was observed to occur at the end of the experiment with mineralization values of 66.92%, 72.94%, 81.56% and 63.29% corresponding to 0.025 mM, 0.05 mM, 0.1 mM and 0.2 mM, respectively. As can be seen, the rate of mineralization was highest when a 0.1 mM was used in the experiments. On the other hand, the rate of removal had somehow decreased with increase in iron concentration especially in the case of 0.2 mM. This reduction can be attributed to reaction between Fe^{2+} and the hydroxyl radicals in the system as shown in Eq. 4.2 thereby ultimately reducing the oxidation power of the system (Özcan et al., 2009).

$$Fe^{2+} + {}^{\bullet}OH \rightarrow Fe^{3+} + OH^{-} \qquad (4.2)$$

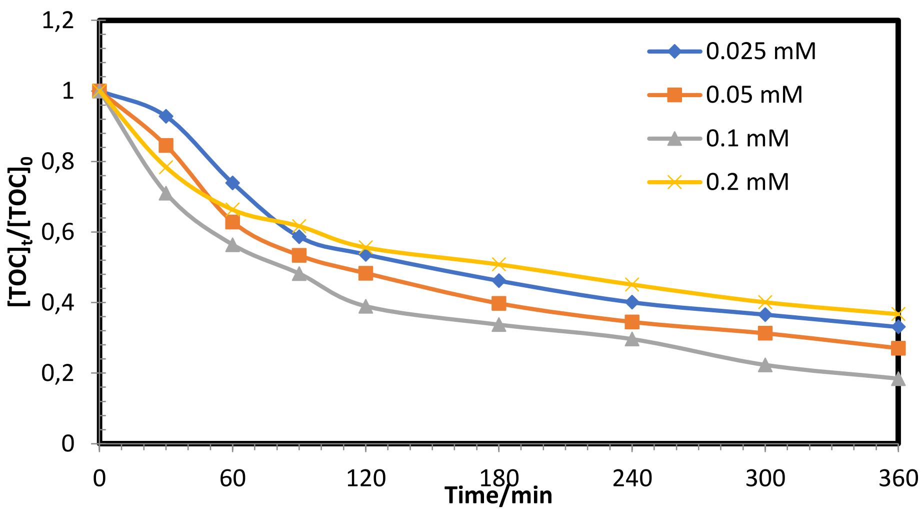

Figure 4.7. *Time-course of the TOC values of PPA during the electro-Fenton treatment at different iron*

concentrations. [PPA] $_0$: 0.25 mM, [Na_2SO_4]$_0$: 0.05 M, I: 50 mA, Pt/CF, pH: 3.0, V: 0.175 L

As far the above results are concerned regarding HPLC and TOC analyses, it can be concluded that 0.1 mM gave the most outstanding result in the removal of PPA. For this reason, 0.1 mM of Fe^{3+} was considered the optimum concentration and used in the subsequent experiments.

4.1.5. Investigation of Kinetics of Oxidation Reaction of Pipemidic Acid by Hydroxyl Radicals

At a certain current intensity, H_2O_2 and Fe^{2+} are continuously generated during the EF process. This generation of the Fenton's reagent makes sure that after certain time, the amount of hydroxyl radical produced reaches its maximum value. For this reason, when the current value is kept constant during the electrolysis, the amount of $^{\bullet}OH$ radical that will react with PPA is also constant.

The rate constants of the reactions between PPA and $^{\bullet}OH$ radicals was determined by competition kinetics method. Among the reference materials, 4-hydroxybenzoic acid (4-HBA) at 25°C, $k_{4\text{-HBA}}$ 2.1×10^9 $M^{-1}s^{-1}$ was chosen during this study. To determine the rate constant, equal concentrations of 4-HBA and PPA were firstly electrolyzed by the electro-Fenton process and subsequently analyzed by the HPLC. During the analyzes, the changes in 4-HBA and PPA concentrations were monitored and the graphs of In([PPA]$_0$/[PPA]) and In([4-HBA]$_0$/[4HBA]) were plotted against time (Fig 4.8).

The degradation rate of an organic pollutant (OP) using a galvanostatic condition can be represented as (Eq.4.3):

$$\frac{-d[OP]}{dt} = k[OH^{\bullet}][OP] \tag{4.3}$$

Since $^{\bullet}OH$ are continuously produced and destroyed at a constant rate indicating a steady state concentration in the bulk solution, the above rate of reaction can be further simplified as (Eq. 4.4):

$$\frac{-d[OP]}{dt} = k_{app}[OP] \tag{4.4}$$

Herein, k_{app} indicates the apparent rate constant, $k_{app} = k\,[^{\bullet}OH]$, k being the absolute rate constant (Nair et al., 2021). HPLC was employed to determine the pseudo first order kinetics of both standard ($k_{app,S}$) and pollutants ($k_{app,OP}$) as shown in Figure 4.8.

The absolute rate constant of an organic pollutant ($k_{abs,OP}$) was then further calculated using the following equation (Eq. (4.5)) (Nair et al., 2021; Özcan et al., 2016):

$$k_{abs,OP} = k_{abs,S} \times \frac{k_{app,OP}}{k_{app,S}} \tag{4.5}$$

Herein, the organic pollutant is PPA and the standard is 4-HBA, thus inserting into the equation above gives (Eq. (4.6)):

$$k_{abs,PPA} = k_{abs,4\text{-}HBA} \times \frac{k_{app,PPA}}{k_{app,4-HBA}} \tag{4.6}$$

Using this equation, second-order rate constant was found to be $(1.18 \pm 0.03)\ x10^{9}$ $M^{-1}s^{-1}$.

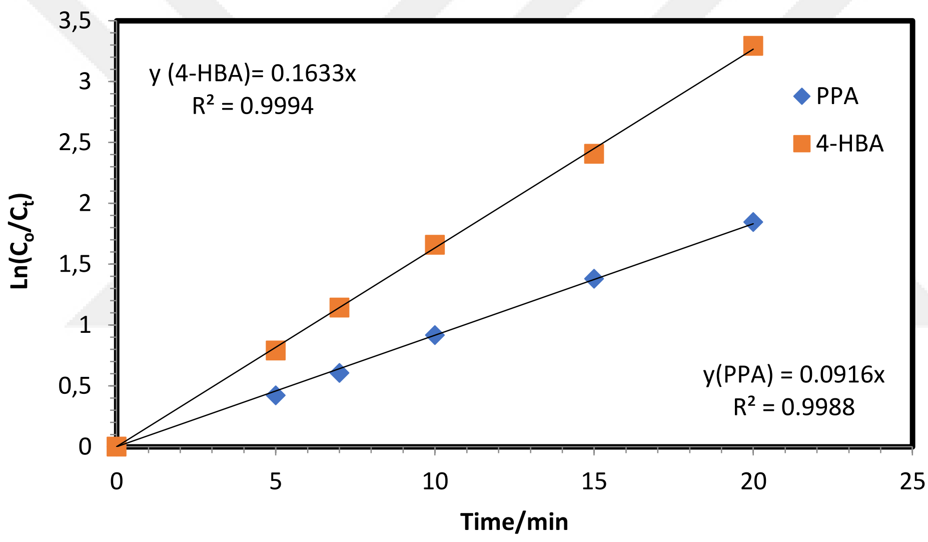

Figure 4.8. *Time-course of In ([PPA]$_0$/ [PPA]) and In ([4-HBA]$_0$/ [4HBA]) of PPA during the electro-Fenton treatment. [PPA]$_0$: 0.25 mM, [4-HBA]$_0$: 0.25 mM, [Fe^{3+}]$_0$: 0.1 mM, [Na_2SO_4]$_0$: 0.05 M, I: 50 mA, Pt/CF, pH: 3.0, V: 0.175 L*

4.2. Removal of Pipemidic Acid from Water by Heterogeneous Electro-Fenton (HEF) Method

In this part of the thesis, the research was focused on the synthesis, characterization and thereafter examining the efficiency of the solid-phase catalysts (Fe_3O_4-mpSiO_2, Co_3O_4-mpSiO_2 and Fe-d-SnO_2) on the removal of PPA by the HEF method. The synthesized catalysts were characterized using different methods. In the HEF method, Pt/CF electrode combination was used to explore the efficiencies of the catalysts properly. The effects of the operation parameters such as applied current, mass of catalysts and initial pH values were monitored by TOC analyses sequentially. In addition, HPLC was utilized in monitoring the concentrations of PPA during the electrolysis. Ion-exclusion chromatography and ion-exchange chromatography analysis were used to determine the released carboxylic acids and inorganics ions, respectively. The reusability and stability of the synthesized catalysts were also investigated.

4.2.1. Characterization of the catalysts

Characterization of the synthesized catalysts (Fe_3O_4-mpSiO_2, Co_3O_4-mpSiO_2 and Fe-d-SnO_2) was made by X-Ray Diffraction (XRD), Scanning Electron Microscopy (SEM), Energy Dispersive X-ray (EDX) and Brunauer, Emmett, Teller (BET) methods.

4.2.1.1. XRD analyses

Within the scope of the thesis, XRD analyses were carried out to determine the crystal structures of the synthesized catalysts and as such the results for each of the catalysts are described in detail below.

As seen in Figure 4.9, no crystal peaks were observed in the XRD pattern of mpSiO_2 sample. Considering the aforementioned, it can be suggested that mpSiO_2 is amorphous in nature (Jabbar et al., 2021). Moreover, a broad characteristic peak located between 2θ values of 17.96° and 38.77° was observed corresponding to the amorphous structure of silica. A similar result showing a broad characteristic peak pattern of mpSiO_2 is found in the literature (Feng et al., 2021). This result verifies that the mpSiO_2 was synthesized successfully.

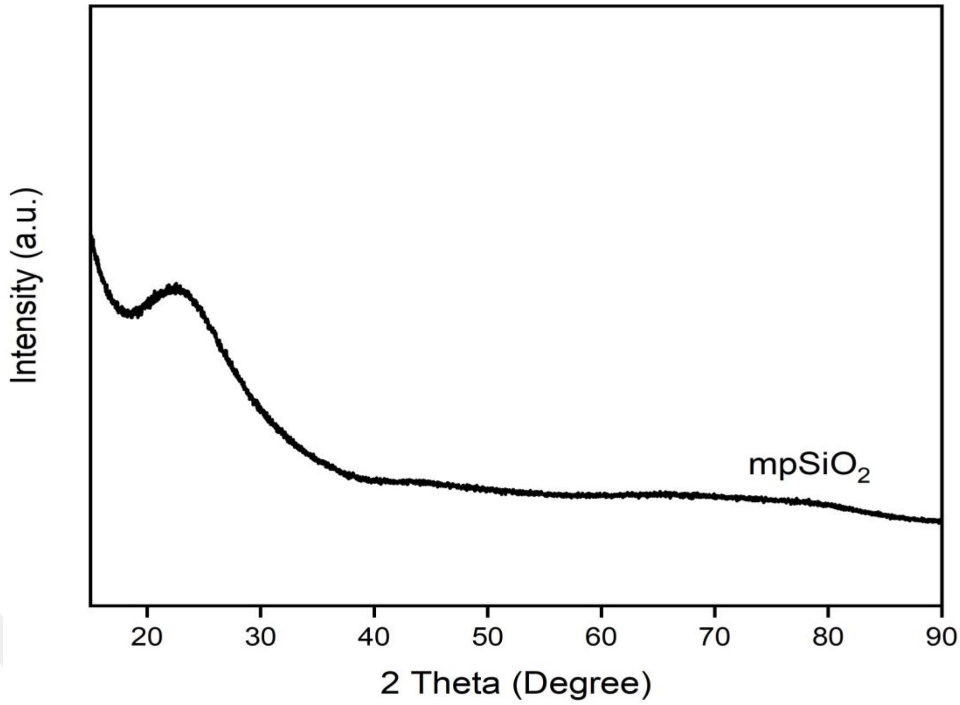

Figure 4.9. *XRD pattern of* $mpSiO_2$

The composition and structure of Fe_3O_4 and Fe_3O_4-$mpSiO_2$ samples were characterized with XRD and shown in Figure 4.10. As for the pure Fe_3O_4, a number of sharp diffraction peaks were found at 2θ = 24.33°, 33.34°, 35.83°, 41.10°, 49.59°, 54.26°, 57.86°, 62.69°, 64.11° and 72.29°. These peaks match closely with JCPDS No: 19-0629 (Cai et al., 2021). These intense peaks produced are an indication that the prepared nanoparticles are indeed strongly crystalline in nature which in turn emphasizes the typical pattern of Fe_3O_4 (Hammouda et al., 2015). Almost the same diffraction peaks were observed in the XRD pattern of Fe_3O_4-$mpSiO_2$, indicating the successful synthesis of Fe_3O_4 on $mpSiO_2$.

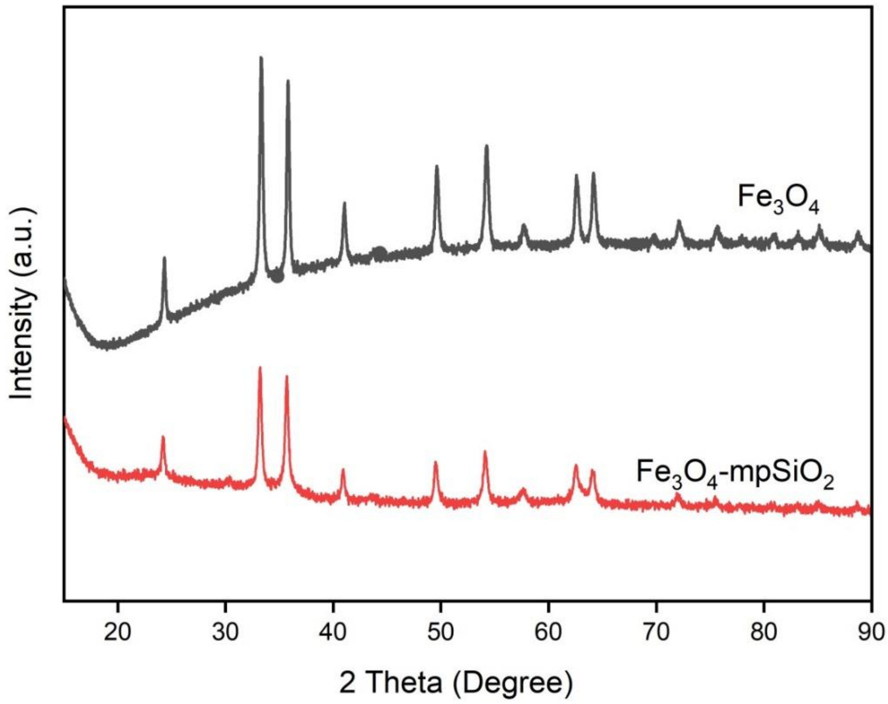

Figure 4.10. *XRD patterns of Fe_3O_4 and Fe_3O_4-mpSiO$_2$*

The XRD patterns of Co_3O_4 and Co_3O_4-mpSiO$_2$ samples are shown in Figure 4.11. A number of diffraction peaks were found in the pure Co_3O_4 sample at $2\theta = 19.09°$, 31.41°, 36.86°, 38.63°, 45.00°, 55.84°, 59.48°and 65.36°. All Co_3O_4 peaks show good agreement with JCPDS card No: 073- 1701 file (Agarwal et al., 2017). Also, similar results were obtained in the study conducted by Qiujing Yang and co-workers (Yang et al., 2008), Pradeep Shukla and co-workers (Shukla et al., 2011) as well as Ramakrishna Itteboina and co-workers (Itteboina & Sau, 2019). The patterns are attributed to the presence of spinel cobalt (II, III) oxide (Co_3O_4) (Jaafarzadeh et al., 2017). The presence of the same diffraction peaks in the case of Co_3O_4-mpSiO$_2$ revealed the formation of Co_3O_4 on the surface of mpSiO$_2$.

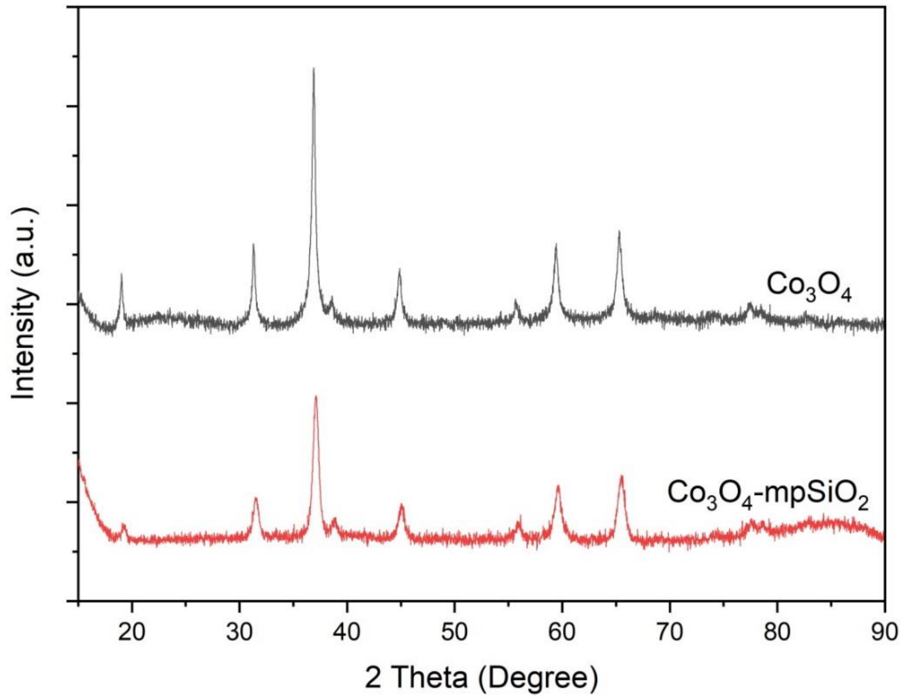

Figure 4.11. *XRD patterns of Co_3O_4 and Co_3O_4-mpSiO$_2$*

The XRD pattern of Fe-d-SnO$_2$ nanoparticles is depicted in Figure 4.12. In this figure, some intense diffraction peaks can be seen to occur at 2θ =26.64°, 34.10°, 37.89° and 52.20°. Similar diffraction patterns are found in the literature (Agarwal et al., 2017; Rezaei et al., 2021) corresponding to JCPDS file No. 41-1445 indicating the successful synthesis of iron doped tin dioxide.

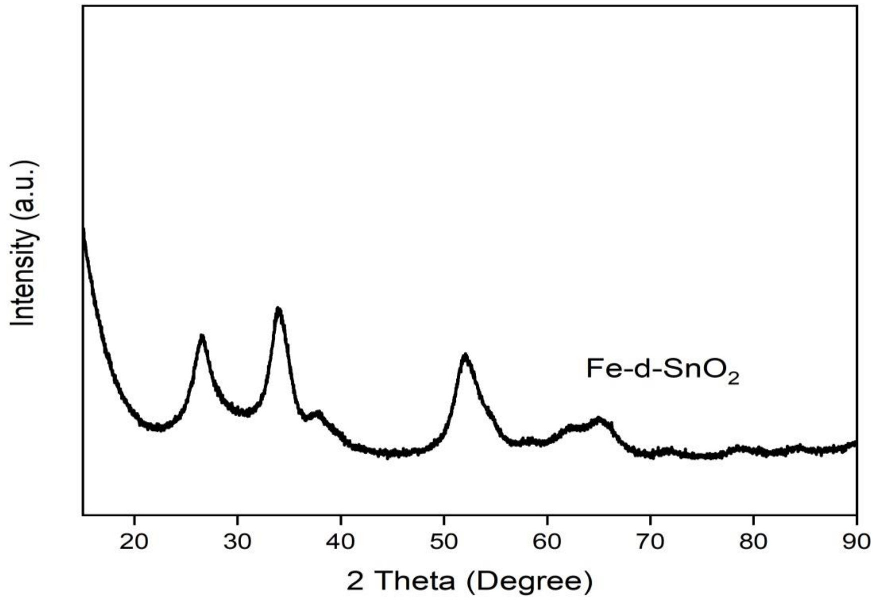

Figure 4.12. *XRD pattern of Fe-d-SnO_2*

4.2.1.2. SEM analyses

In this thesis, SEM analyses were performed to determine the morphological formation of the synthesized catalysts. In light of the above, a well detailed explanation for each catalyst is provided below.

The SEM images of mpSiO_2, Fe_3O_4 and Fe_3O_4-mpSiO_2 nanoparticles are shown in Figure 4.13, Figure 4.14 and Figure 4-15, respectively.

In Figure 4.13, the mpSiO_2 nanoparticles were remarkably well-dispersed and composed of many smaller convex spherical particles. The mpSiO_2 nanoparticles displayed an average size of about 300 nm with a standard deviation of ± 43 nm.

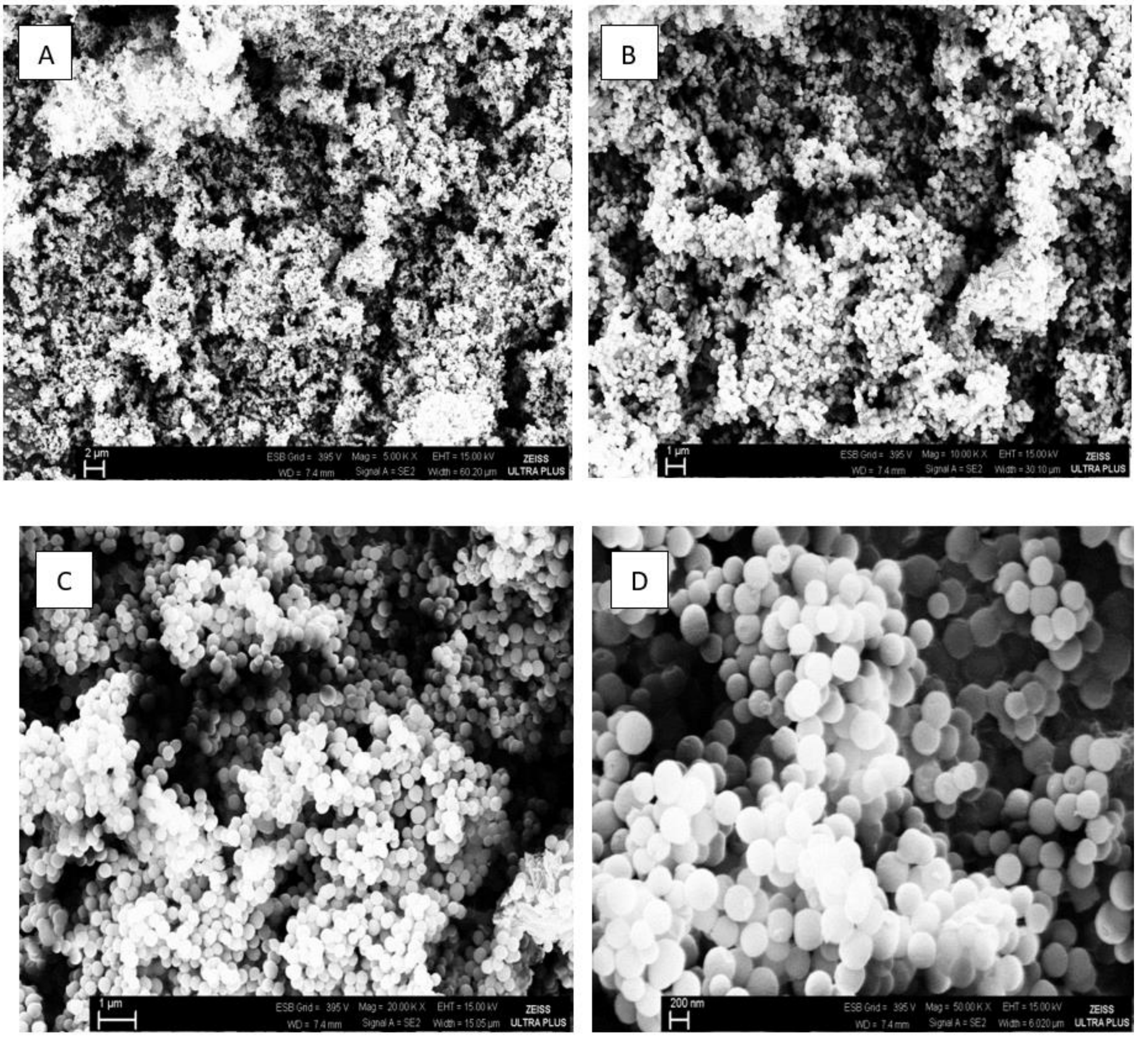

Figure 4.13. *SEM images of mpSiO$_2$; A) 5000X B) 10000X C) 20000 D) 50000X*

The SEM images of Fe_3O_4 nanoparticles are provided in Figure 4.14. As can be seen, the image shows well-compacted agglomeration of Fe_3O_4 nanoparticles with some self-oriented flower geometry with a diameter of about 297 nm. The presence of these large agglomerates could be attributed to the large particle size of the nanoparticles leading to small surface area as can be seen from the BET analysis results (Table 4.1).

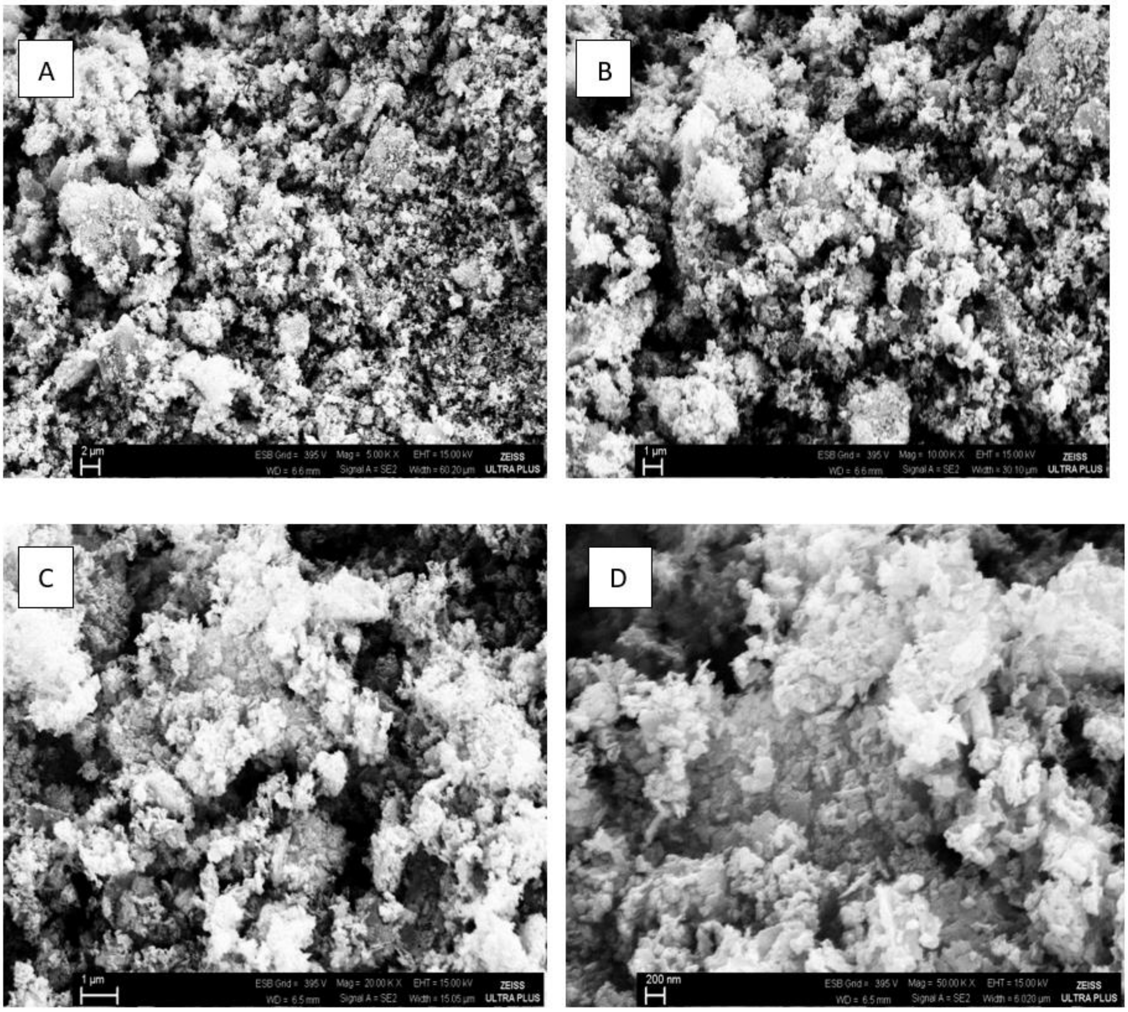

Figure 4.14. *SEM images of Fe_3O_4; A) 5000X B) 10000X C) 20000X D) 50000X*

Figure 4.15 shows the SEM images of Fe_3O_4-mpSiO_2 nanoparticles. It can be observed that the nanoparticles had a smooth surface, which suggested that a layer of Fe_3O_4 NPs was successfully coated on the surface of the naked mpSiO_2, producing somehow loosely aggregated Fe_3O_4-mpSiO_2 NPs with particle size between 250 and 435 nm. The presence of low aggregates in these nanoparticles can be said to occur because of the coating of the bare Fe_3O_4 on the surface of mpSiO_2 which eventually increased the surface area of the nanocomposite.

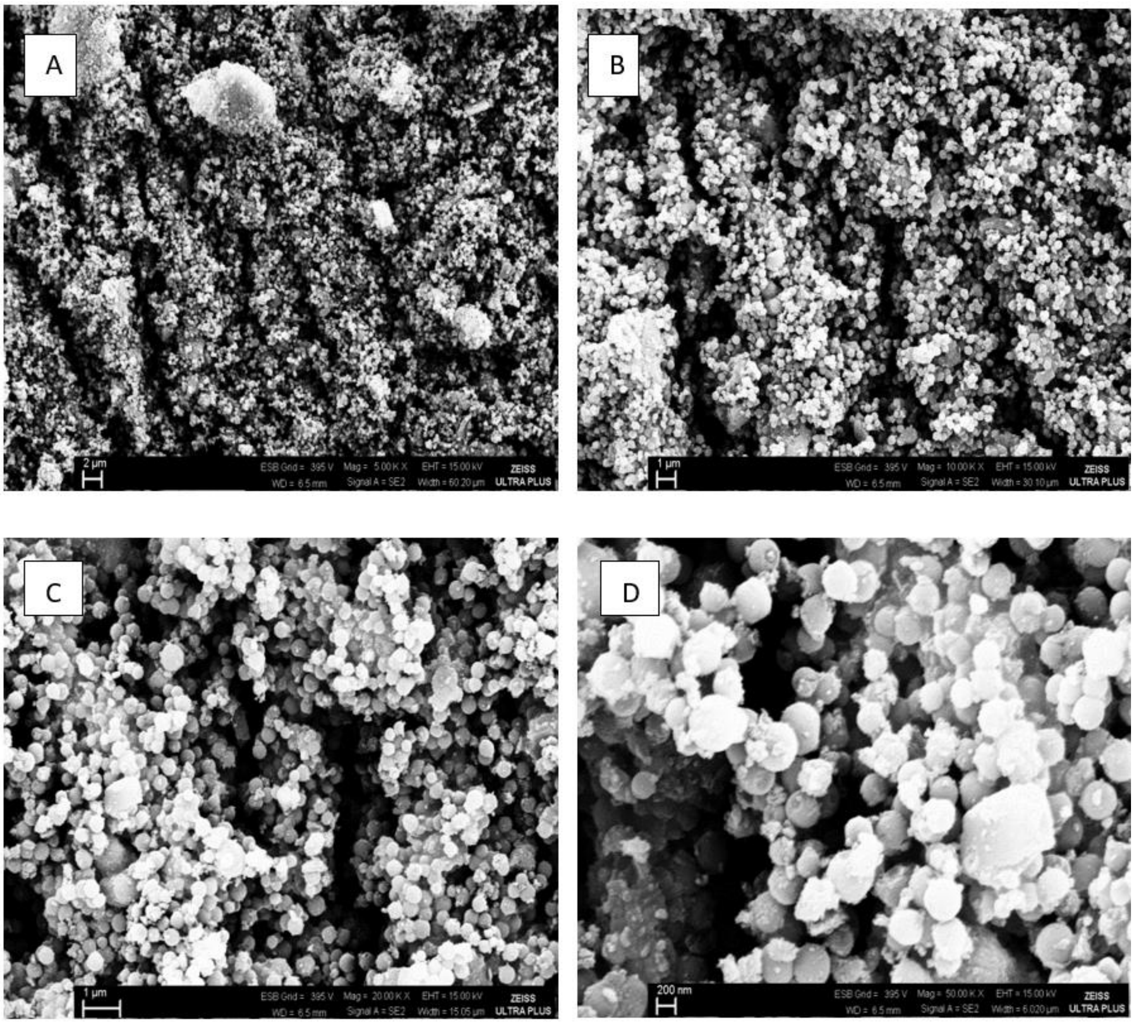

Figure 4.15. *SEM images of Fe_3O_4-mpSiO$_2$; A) 5000X B) 10000X C) 20000X D) 50000X*

The SEM images of Co_3O_4 and Co_3O_4-mpSiO$_2$ nanoparticles are shown in Figure 4.16 and Figure 4.17, respectively.

As shown in Figure 4.16, the image shows well-dispersed aggregates of Co_3O_4 nanoparticles with some sponge-like shape with a mean particle size of ~250 nm.

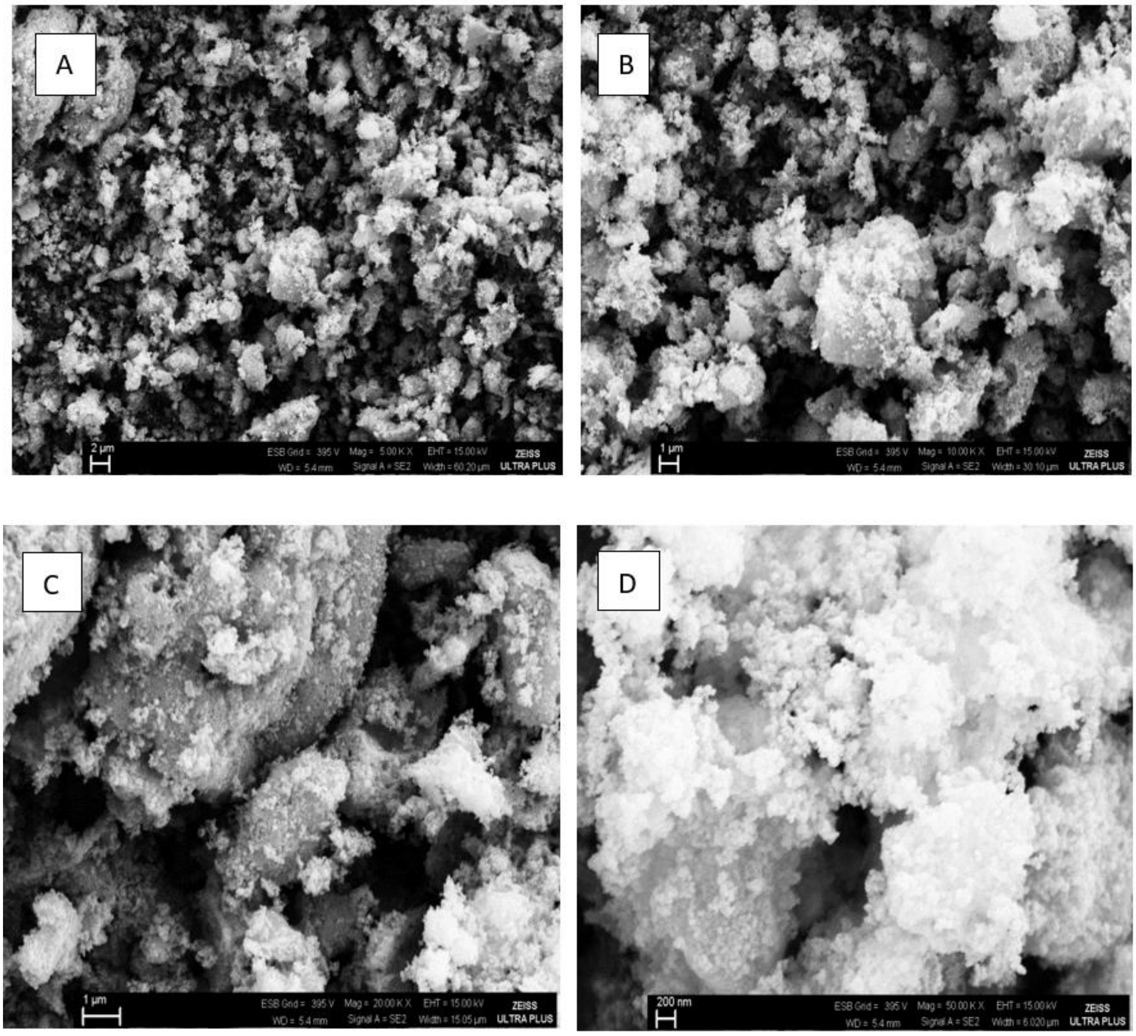

Figure 4.16. *SEM images of Co_3O_4; A) 5000X B) 10000X C) 20000X D) 50000X*

The SEM images of Co_3O_4-mpSiO_2 are provided in Figure 4.17. As can be seen, the micrographs show a similar morphology as in Figure 4.15 in which the nanoparticles had a smooth surface, which indicates that on the surface of the naked mpSiO_2 a layer of Co_3O_4 NPs was successfully coated. Moreover, the coating of Co_3O_4 NPs on the surface of the mpSiO_2 had significantly reduced the formation of agglomerates of Co_3O_4-mpSiO_2 NPs as compared to bare Co_3O_4 NPs. The Co_3O_4-mpSiO_2 NPs have a particle size of about 200-420 nm.

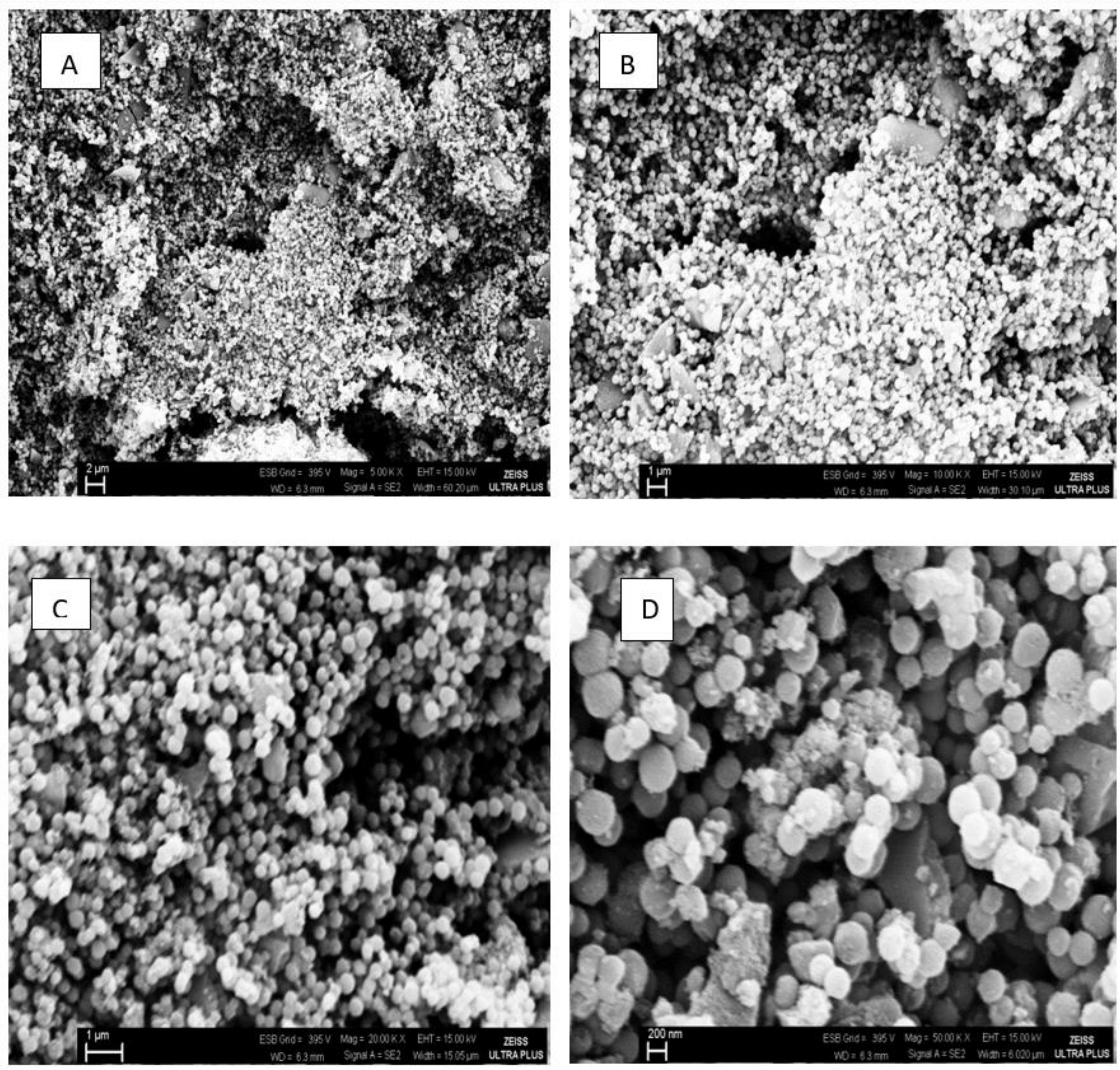

Figure 4.17. *SEM images of Co_3O_4-mpSiO$_2$; A) 5000X B) 10000X C) 20000X D) 50000X*

The SEM micrographs of Fe-d-SnO_2 are depicted in Figure 4.18. Mixtures of many shapes are observed, some of which are relatively undefined while others appeared somehow spherical in shape. Furthermore, aggregation of small spherical nanoparticles has also been observed. The incorporation of Fe in SnO_2 matrix has enhanced the agglomeration which is caused by *van der wall* forces as reported (Duhan et al., 2020).

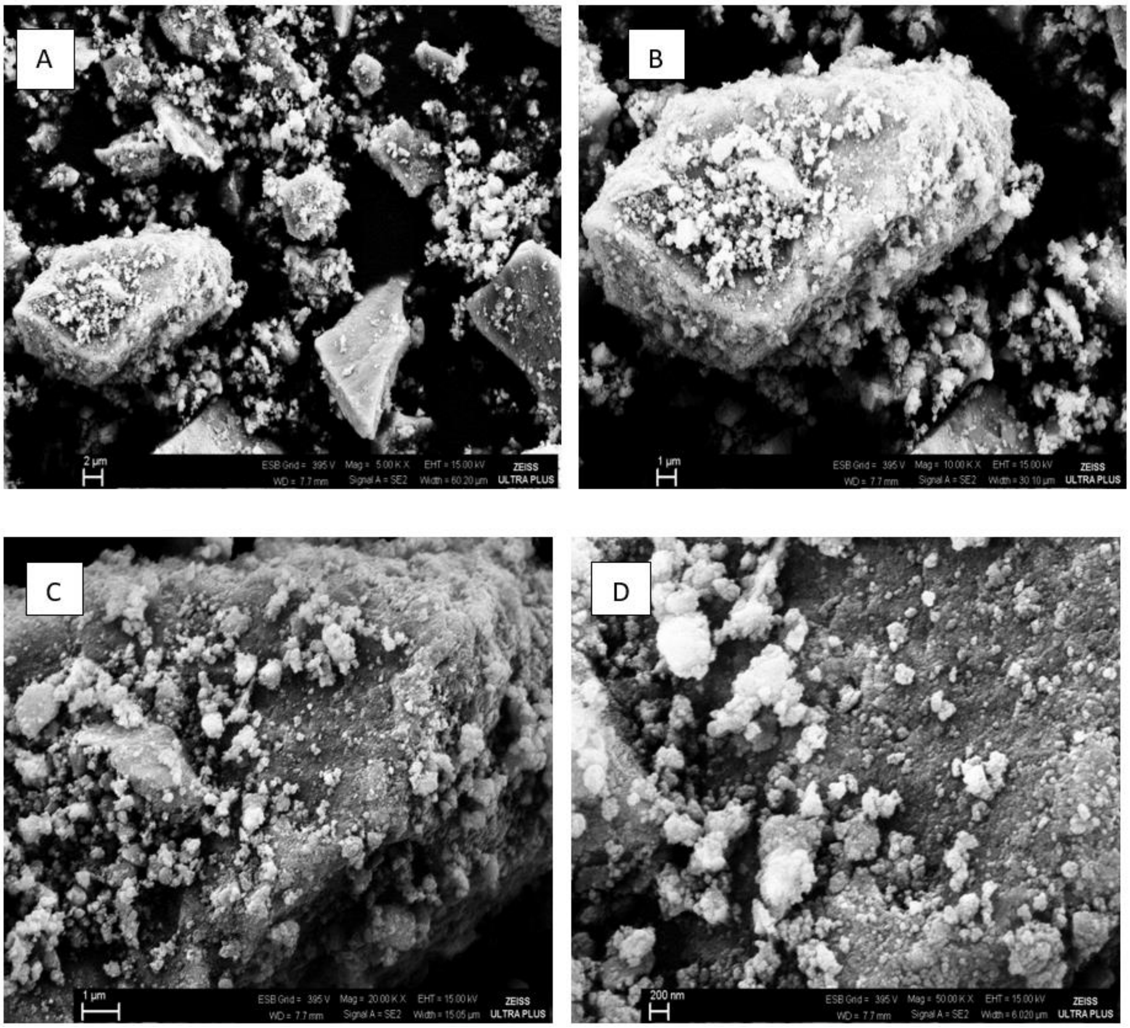

Figure 4.18. *SEM images of Fe-d- SnO_2; A) 5000X B) 10000X C) 20000X D) 50000X*

4.2.1.3. EDX analyses

EDX analyses were carried out to determine the elemental composition of the prepared solid-phase catalysts. In this regard, a well-detailed description for each of the prepared solid-phase catalysts is provided below.

The energy dispersive X-ray mapping images of the Fe_3O_4-mpSiO_2 are shown in Figure 4.19. The prepared nanocomposite catalyst consisted of only Fe, O, and Si elements. Moreover, the determination of the iron and silicon composition in the nanocomposite also proved the successful preparation of the catalyst.

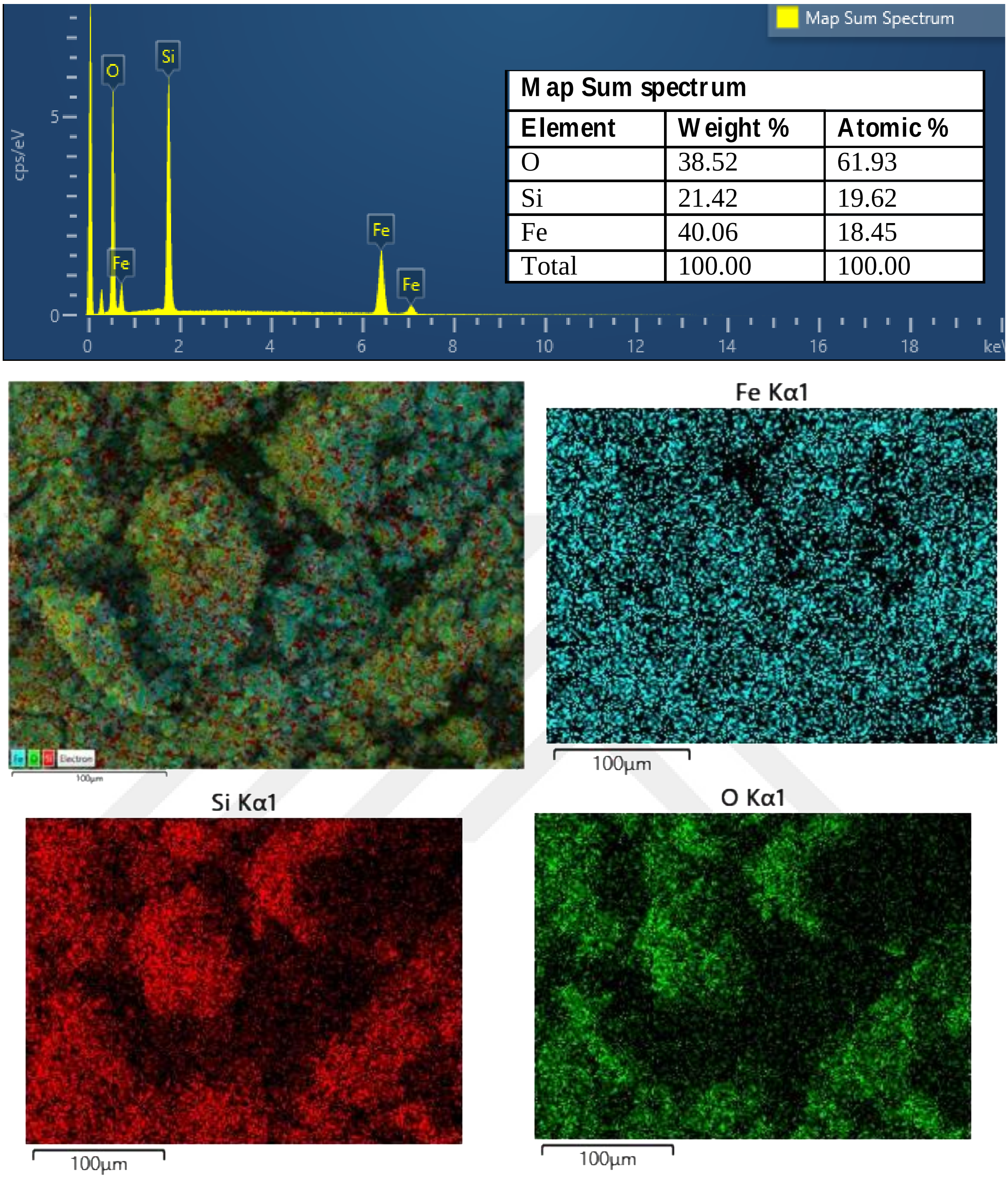

Figure 4.19. *Energy dispersive X-ray (EDX) spectra of Fe_3O_4-mpSiO$_2$*

Elemental analysis for chemical purity of the Co_3O_4-mpSiO$_2$ sample was taken by energy dispersive X-ray spectroscopy analysis to confirm the chemical composition of the prepared solid-phase catalyst (Fig. 4.20). EDX shows that the final product includes Co, O, and Si. Therefore, the X-ray microanalysis result demonstrated that nanoparticles were successfully synthesized by the facile method used during the preparation.

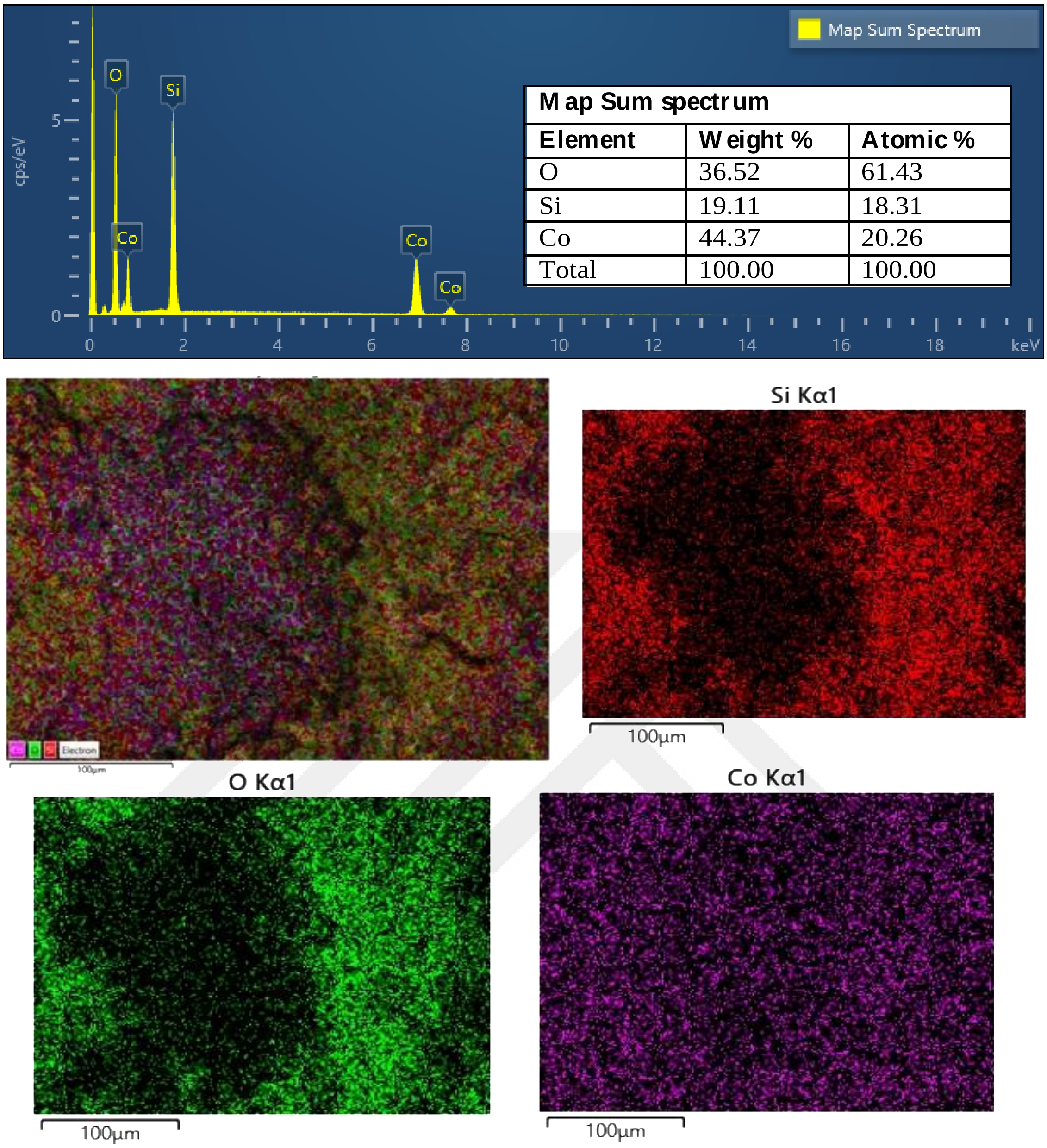

Figure 4.20. *Energy dispersive X-ray (EDX) spectra of Co_3O_4-mpSiO$_2$*

EDX analysis was also carried out for Fe-d-SnO_2 samples and presented as shown in Figure 4.21**.** The EDX spectrum reveals the presence of elements such as Fe, O and Sn in accordance with the chemical composition of the as-prepared catalyst. Therefore, the X-ray microanalysis and X-ray diffraction pattern results showed that nanoparticles were successfully synthesized by the sol-gel method.

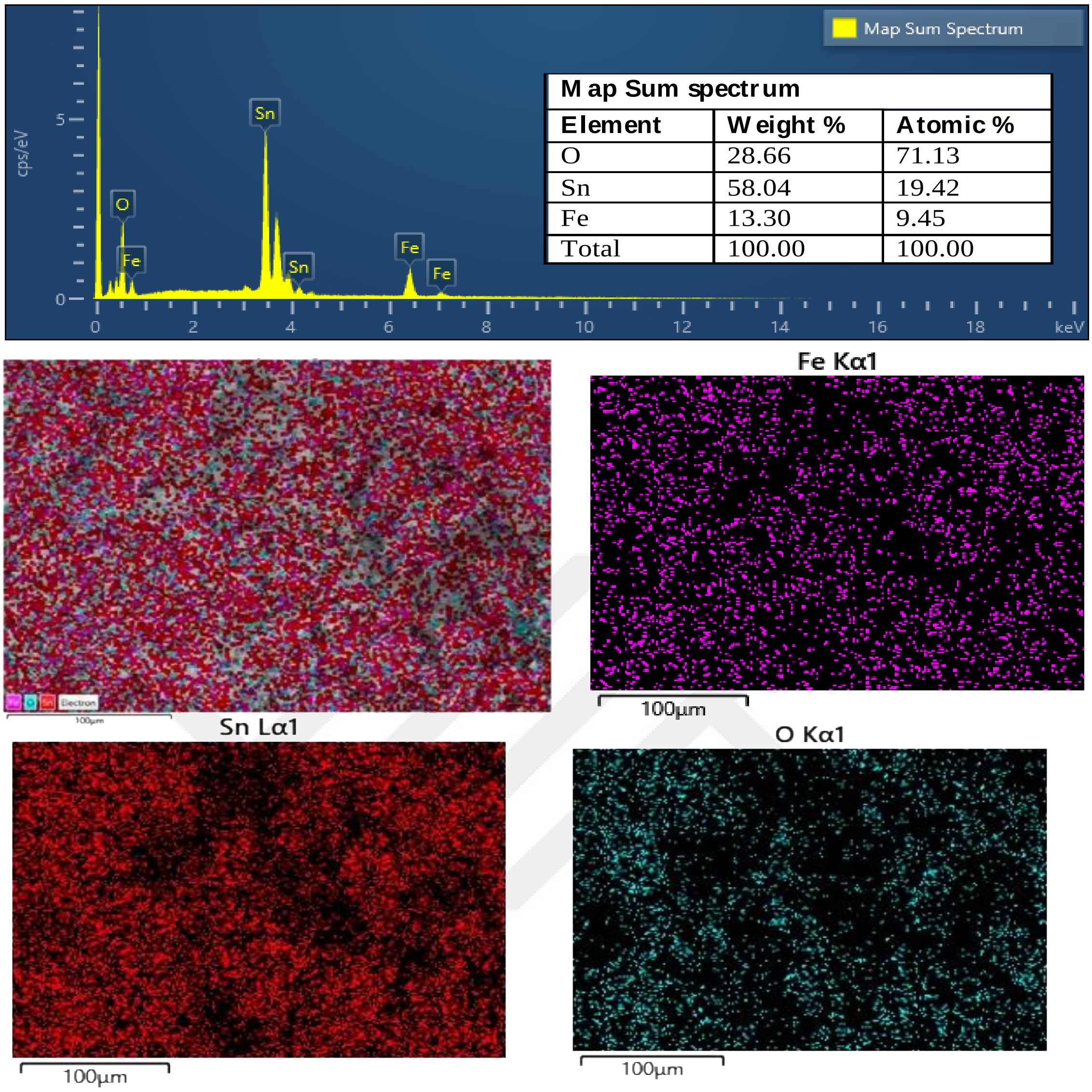

Figure 4.21. *Energy dispersive X-ray (EDX) spectra of Fe-d-SnO_2*

4.2.1.4. BET analyses

BET analyses were carried out to determine the surface areas of the developed solid-phase catalysts. In the light of this, a well-detailed description for each of the prepared solid-phase catalysts is provided below.

The BET analysis of $mpSiO_2$, Fe_3O_4, Co_3O_4, Fe_3O_4-$mpSiO_2$, Co_3O_4-$mpSiO_2$ and Fe-d-SnO_2 nanoparticles are presented in Table 4.1.

The surface area of Fe_3O_4-$mpSiO_2$ (or Co_3O_4-$mpSiO_2$) nanoparticles was 501.13m^2/g (or 427.92m^2/g), about seventeen times larger than that of the bare Fe_3O_4 (or Co_3O_4) nanoparticles (29.33m^2/g) or (or 24.71m^2/g). This reduction in particle size as in the case of Fe_3O_4-$mpSiO_2$ (or Co_3O_4-$mpSiO_2$) could be attributed to the presence of mesoporous silica. The presence of these micro-mesopores could benefit the pre-concentration of pollutants around Fe_3O_4-mpSiO_2 (or Co_3O_4-mpSiO_2) nanoparticles and eventually enhance PPA degradation during the electro-Fenton process. As shown in Table 4.1, the surface area of Fe-d-SnO_2 catalyst was calculated to be 91.55m^2/g. It is important to emphasize that in this thesis, the surface area of SnO_2 was not calculated; however, the observed high surface area of Fe-d-SnO_2 might be due to the reduced particle sizes of SnO_2 caused by Fe doping (Xiaoli Zhao et al., 2017).

Table 4.1. *BET surface area of the studied catalysts*

Catalyst	**BET surface area / (m^2 g^{-1})**
mpSiO_2	789.37
Fe_3O_4	29.33
Co_3O_4	24.71
Fe_3O_4-mpSiO_2	501.13
Co_3O_4-mpSiO_2	427.93
Fe-d-SnO_2	91.55

4.2.2. Heterogeneous electro-Fenton removal of pipemidic acid

The activities of the synthesized catalysts were tested in the same conditions used in the electro-Fenton treatment of PPA by replacing soluble iron catalyst with the solid-phase catalysts. For this purpose, electrolyzes were performed in the presence of different amount of each catalyst and the TOC changes were monitored as a function of time. The results were given in Figure 4.22, Figure 4.23 and Figure 4.24 for Fe_3O_4-mpSiO_2, Co_3O_4-mpSiO_2 and Fe-d-SnO_2, respectively. The results indicated that the rate of mineralization increased with the increase in the concentration of catalyst in the reaction medium for all the catalysts. A similar pattern of mineralization was also observed for all the catalysts.

In Figure 4.22, the effect of the amount of Fe_3O_4-mpSiO_2 on the removal of PPA from the reaction solution is provided. It is observed that as time passed the amount of PPA in the solution decreases accordingly. Notwithstanding, after 30 min of the electrolysis, the amount of PPA still remained high for all the different Fe_3O_4-mpSiO_2 concentrations with a TOC removal of 25.49%, 31.34%, 40.05% and 44.14% for 0.571 g/L, 1.143 g/L, 1.714 g/L and 2.286 g/L catalysts, respectively. Moreover, the rate of mineralization had improved as the electrolysis time increased. After 180 min of the experiment, a reduction in the amount of PPA was observed as shown from the mineralization values of 63.55%, 67.84%, 74.80 and 79.18% for 0.571 g/L, 1.143 g/L, 1.714 g/L and 2.286 g/L, respectively. Similarly, the amount of rate of mineralization has increased significantly at the end of the electrolysis with TOC removal values of 76.37%, 79.85%, 84.59% and 94.04% for 0.571 g/L, 1.143 g/L, 1.714 g/L and 2.286 g/L, respectively. In accordance with the results provided, the highest rate of mineralization was achieved when a 2.286 g/L was used in the experiment.

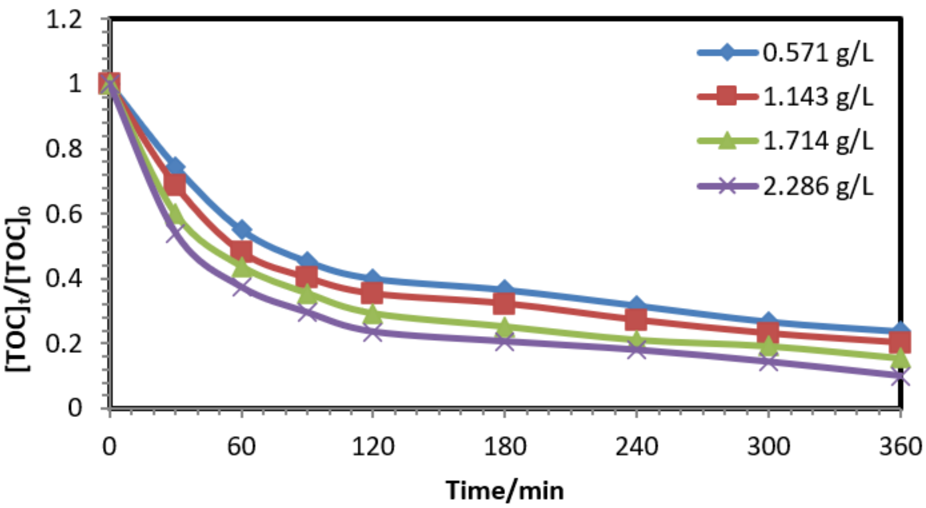

Figure 4.22. *The effect of concentrations of Fe_3O_4-mpSiO$_2$ on the mineralization of PPA during the HEF treatment. [PPA]$_0$: 0.25 mM, [Na_2SO_4]$_0$: 0.05 M, I: 100 mA, Pt/CF, pH: 3.0, V: 0.175 L*

In the case of Co_3O_4-mpSiO$_2$ (Fig 4.23), the rate of mineralization also increased with increase in the amount of catalyst concentration. Herein as well, not enough amount of PPA has decreased after 30 min of the experiment. However, as the experiment continued, a decrease in the amount of the organic pollutant was observed. This foregoing statement is supported by the amount of TOC removals values achieved after 180 min of electrolysis. At the end of this electrolysis time, mineralization values of 43.58%, 51.28%, 56.71% and 64.33% for 0.571 g/L, 1.143 g/L, 1.714 g/L and 2.286 g/L, respectively were yielded. Furthermore, after 360 min of electrolysis, a substantial amount of PPA was degraded as indicated by TOC removal values of 66.28%, 72.03%, 75.41% and 80.58% for 0.571 g/L, 1.143 g/L, 1.714 g/L and 2.286 g/L, respectively. Here too, the highest amount of PPA removal was obtained when a 2.286 g/L was used in the experiment.

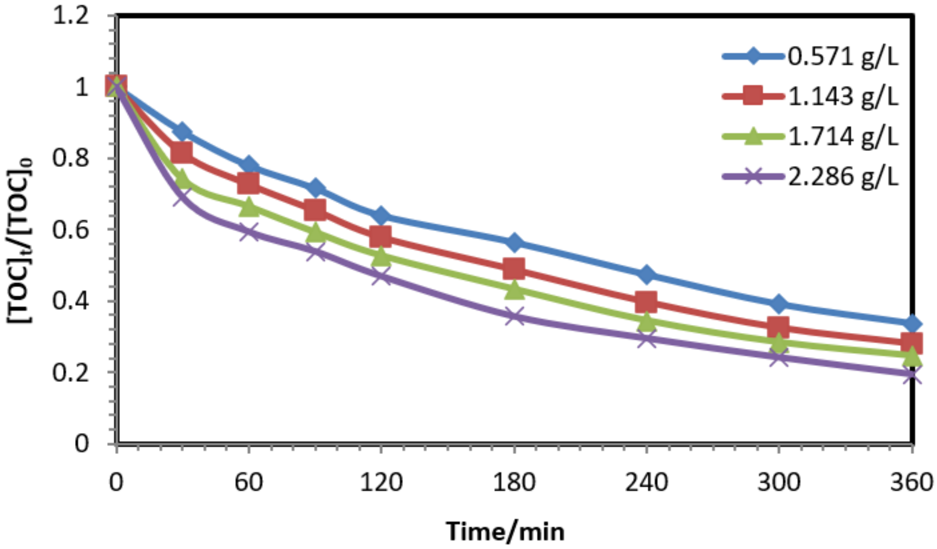

Figure 4.23. *The effect of concentrations of Co_3O_4-mpSiO$_2$ on the mineralization of PPA during the HEF treatment. [PPA]$_0$: 0.25 mM, [Na_2SO_4]$_0$: 0.05 M, I: 100 mA, Pt/CF, pH: 3.0, V: 0.175 L*

The results of the effect of Fe-d-SnO_2 concentration on the removal of PPA from the experiment solution are provided in Figure 4.24. The removal of PPA from the solution was observed to be very minimal during the first 30 min of electrolysis indicating the presence of large amount of the organic pollutant in the solution. At this time of electrolysis, a TOC removal of 28.84%, 22.15%, 27.83% and 35.70% for 0.571 g/L, 1.143 g/L, 1.714 g/L and 2.286 g/L, respectively were obtained. However, as time progressed, the presence of PPA in the solution has decreased. For example, after 180 min of electrolysis, mineralization values of 58.76%, 62.41%, 67.55% and 73.82% for 0.571 g/L, 1.143 g/L, 1.714 g/L and 2.286 g/L, respectively were achieved showing an increase in the rate of PPA mineralization from the solution. Moreover, after 360 min of electrolysis, a remarkable removal of PPA was achieved as indicated by the TOC removal values of 71.33%, 74.96%, 81.51% and 88.84% for 0.571 g/L, 1.143 g/L, 1.714 g/L and 2.286 g/L, respectively. In line with the above results, the highest rate of mineralization was achieved when a 2.286 g/L was used in the electrolysis.

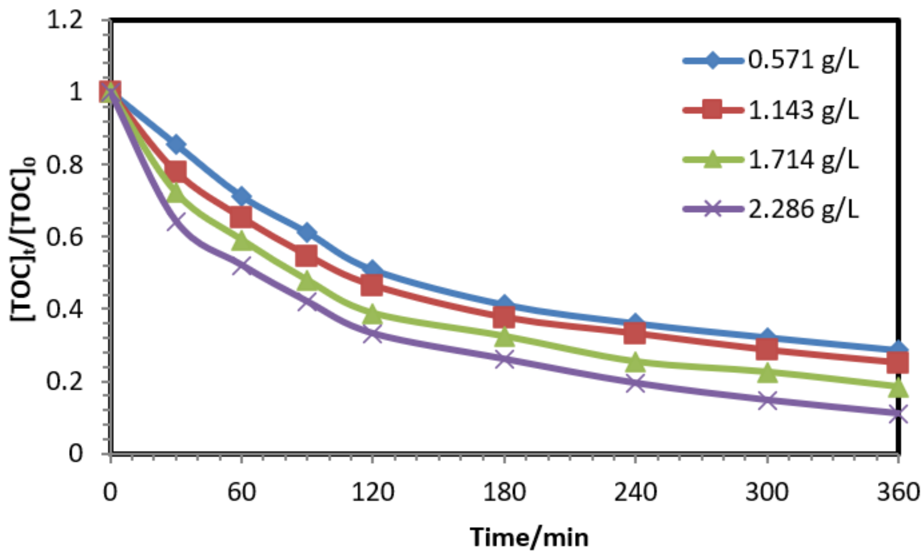

Figure 4.24. *The effect of concentrations of Fe-d-SnO_2 on the mineralization of PPA during the HEF treatment. $[PPA]_0$: 0.25 mM, $[Na_2SO_4]_0$: 0.05 M, I: 100 mA, Pt/CF, pH: 3.0, V: 0.175 L*

Considering the above results, it can be concluded that at the end of 360 min electrolysis, the highest rate of mineralization was achieved when a Fe_3O_4-mpSiO_2 catalyst was used in the experiment. It can be further stated that for all the synthesized solid-phase catalysts, the highest amount of TOC removals were achieved when 2.286 g/L was used in the experiments.

The results of the MCE values of the different concentrations of Fe_3O_4-mpSiO_2 are provided in Figure 4.25. As can be seen, at the end of 30 min electrolysis, MCE values of 24.24%, 28.76%, 34.53% and 42.26% for 0.571 g/L, 1.143 g/L, 1.714 g/L and 2.286 g/L, respectively were obtained indicating that the highest MCE value was attained when a 2.286 g/L was used in the experiment. However, it was observed that the MCE values decreased with time for all the Fe_3O_4-mpSiO_2 concentrations. For instances, after 180 min of electrolysis, the MCE values obtained are as follows: 9.78%, 10.38%, 11.56% and 13.18% for 0.571 g/L, 1.143 g/L, 1.714 g/L and 2.286 g/L, respectively. However, at the end of electrolysis, MCE values such as 5.96%, 6.11%, 6.54% and 7.47% for 0.571 g/L, 1.143 g/L, 1.714 g/L and 2.286 g/L, respectively. From the above results, it is observed that the lowest MCE value was obtained when a 0.571 g/L was used in the experiments. Therefore, it can be said that MCE values increased with increase in the concentration of the catalyst.

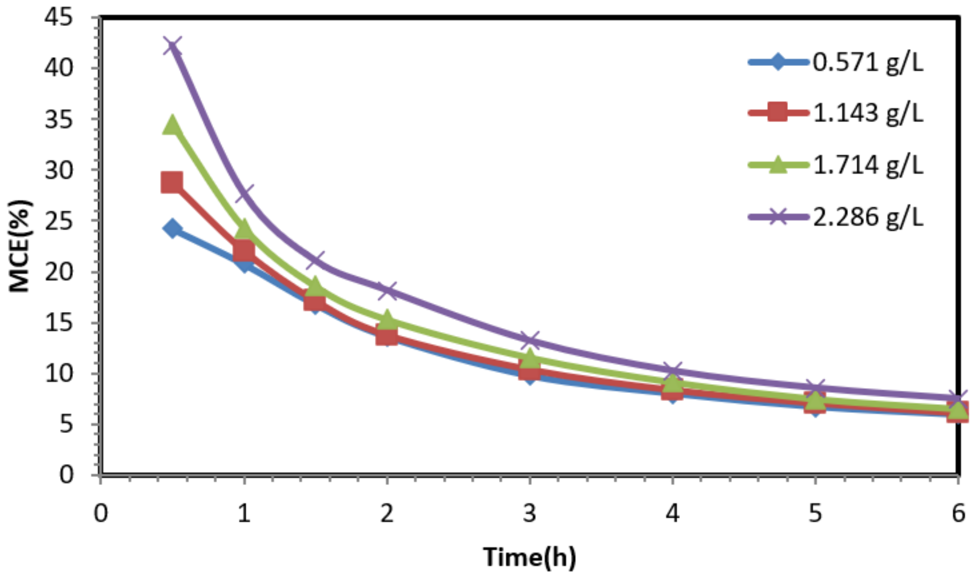

Figure 4.25. *MCE (%) values of PPA solution using different concentrations of Fe_3O_4-mpSiO_2 calculated by using the data given in Figure 4.22. $[PPA]_0$: 0.25 mM, $[Na_2SO_4]_0$: 0.05 M, I: 100 mA, Pt/CF, pH: 3.0, V: 0.175 L*

Figure 4.26 shows the MCE values of the different amounts of Co_3O_4-mpSiO_2 used during HEF treatment of PPA from reaction solution. MCE values including 9.05%, 20.28%, 24.68% and 30.64% for 0.571 g/L, 1.143 g/L, 1.714 g/L and 2.286 g/L, respectively were achieved in the first half an hour of the electrolysis showing that the highest MCE values was obtained when a 2.286 g/L was used in the experiment. As the electrolysis time increased, a decrease in MCE values as compared to the above values was observed. After 180 min of electrolysis, for example, the concentrations 0.571 g/L, 1.143 g/L, 1.714 g/L and 2.286 g/L had the following MCE values 6.09%, 9.29%, 7.53% and 10.63%, respectively. After the completion of the experiments, MCE values such as 6.07%, 6.43%, 6.47% and 6.66% were obtained for 0.571 g/L, 1.143 g/L, 1.714 g/L and 2.286 g/L, respectively. Here too, the lowest MCE value was achieved when 0.571 g/L was used in the experiment.

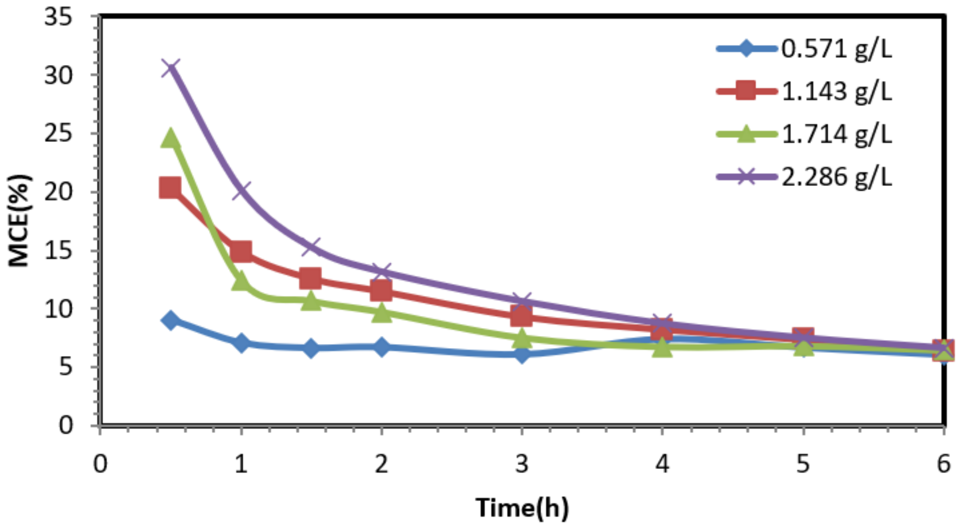

Figure 4.26. *MCE (%) values of PPA solution using different concentrations of Co_3O_4-mpSiO$_2$ calculated by using the data given in Figure 4.23. [PPA]$_0$: 0.25 mM, [Na_2SO_4]$_0$: 0.05 M, I: 100 mA, Pt/CF, pH: 3.0, V: 0.175 L*

The results showing the MCE values of the different concentrations of Fe-d-SnO_2 are illustrated in Figure 4.27. As can be seen, after 30 min of the electrochemical experiment, MCE values of 16.04%, 23.78%, 26.00% and 33.33% were achieved for 0.571 g/L, 1.143 g/L, 1.714 g/L and 2.286 g/L, respectively which indicates that the highest MCE value was attained when a 2.286 g/L was used in the experiment. On the other hand, it is also observed as the experimental time lengthens the MCE values decreased for all the Fe-d-SnO_2 concentrations. After 180 min of electrolysis, the MCE values obtained were as follows: 10.81%, 11.17%, 10.52% and 11.49% for 0.571 g/L, 1.143 g/L, 1.714 g/L and 2.286 g/L, respectively. At the end of electrolysis, MCE values such as 6.56%, 6.71%, 6.59% and 6.91% for 0.571 g/L, 1.143 g/L, 1.714 g/L and 2.286 g/L, respectively.

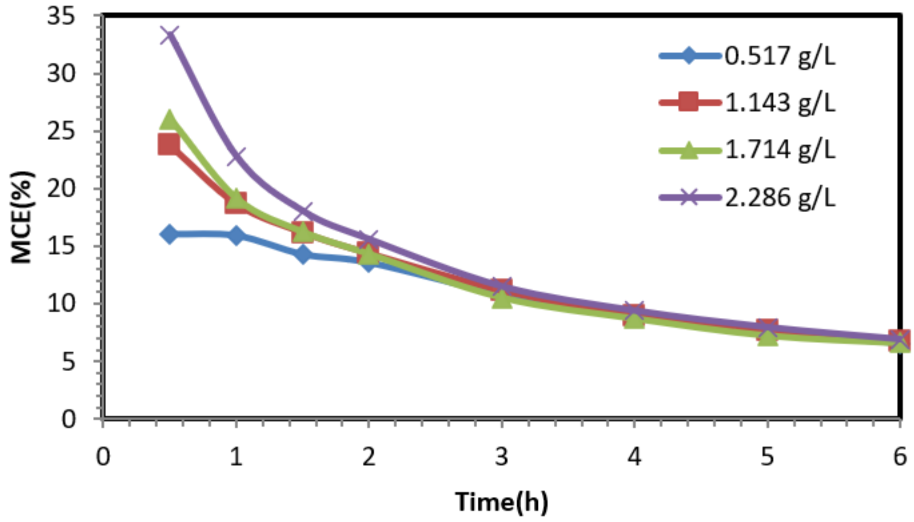

Figure 4.27. *MCE (%) values of PPA solution using different concentrations of Fe-d-SnO_2 calculated by using the data given in Figure 4.24. $[PPA]_0$: 0.25 mM, $[Na_2SO_4]_0$: 0.05 M, I: 100 mA, Pt/CF, pH: 3.0, V: 0.175 L*

In conclusion, it was observed that MCE values increased with increase in the amount of catalyst. Moreover, it was observed that for the catalysts, the highest MCE values of were obtained when Fe_3O_4-mpSiO_2 and 2.286 g/L were used in the experiments.

4.2.3. Optimization of the applied current intensity

It is noteworthy to state that the concentration of $^{\bullet}OH$ radical depends on the applied current intensity. Therefore, in this thesis, the effect of applied current intensities on the degradation rate of PPA was studied by using the applied current intensities of 50, 100 and 300mA.

As can be seen in Figure 4.28, the rate of mineralization is dependent on the applied current intensity. For this reason, as the amount of applied current increases the rate of mineralization increases accordingly. With the TOC removal values of 16.40%, 25.49% and 35.96% for 50, 100 and 300 mA, respectively, it was observed that ample amount of PPA remained non-destroyed during first 30 min of electrolysis. Nonetheless, as the electrolysis time extends, for instance, after 180 min, a decrease in the amount of PPA present in the solution was shown in the corresponding to TOC removal values of 53.78%, 63.55% and 73.52% for 50, 100 and 300 mA, respectively. At the end of the 360 min of the electrolysis, the amount of TOC removals are as follows 63.72%, 76.37%, 87.04% representing 50 mA, 100 mA, and 300 mA, respectively. According to the results presented above, the highest rate of mineralization was achieved when a 300 mA was used in the experiments. Also, it was observed that the rate of mineralization increased with increase in the applied current intensity. This result is in conformity with the literature (Ammar et al., 2015). Similar behaviors were observed for Co_3O_4-mpSiO$_2$ (Fig 4.29) and Fe-d-SnO$_2$ (Fig 4.30).

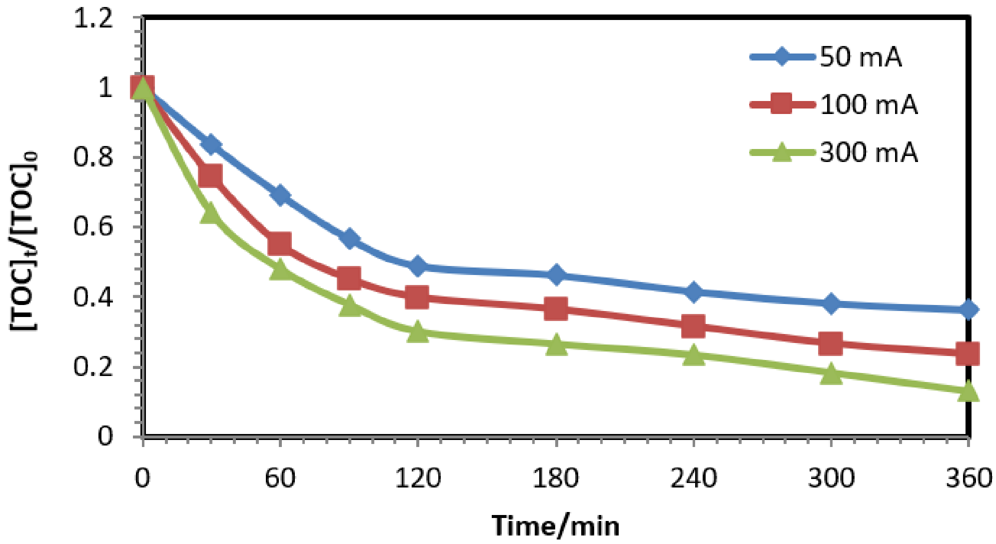

Figure 4.28. *The effect of applied current on the mineralization of PPA during the HEF treatment using Fe_3O_4-mpSiO$_2$. [PPA]$_0$: 0.25 mM, m(Fe_3O_4-mpSiO$_2$): 0.571 g/L, [Na_2SO_4]$_0$: 0.05 M, Pt/CF, pH: 3.0, V: 0.175 L*

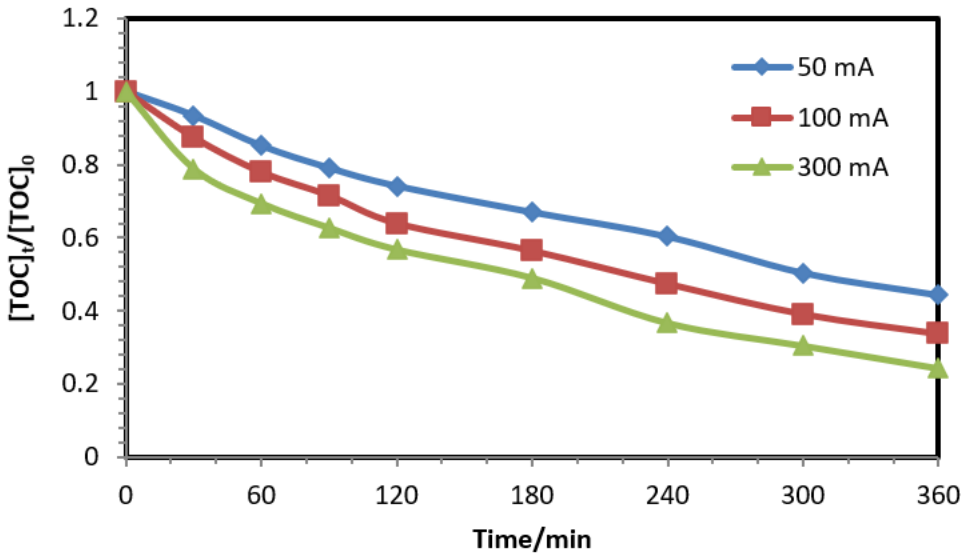

Figure 4.29. *The effect of applied current on the mineralization of PPA during the HEF treatment using Co_3O_4-mpSiO$_2$. [PPA]$_0$: 0.25 mM, m(Co_3O_4-mpSiO$_2$): 0.571 g/L, [Na_2SO_4]$_0$: 0.05 M, Pt/CF, pH: 3.0, V: 0.175 L*

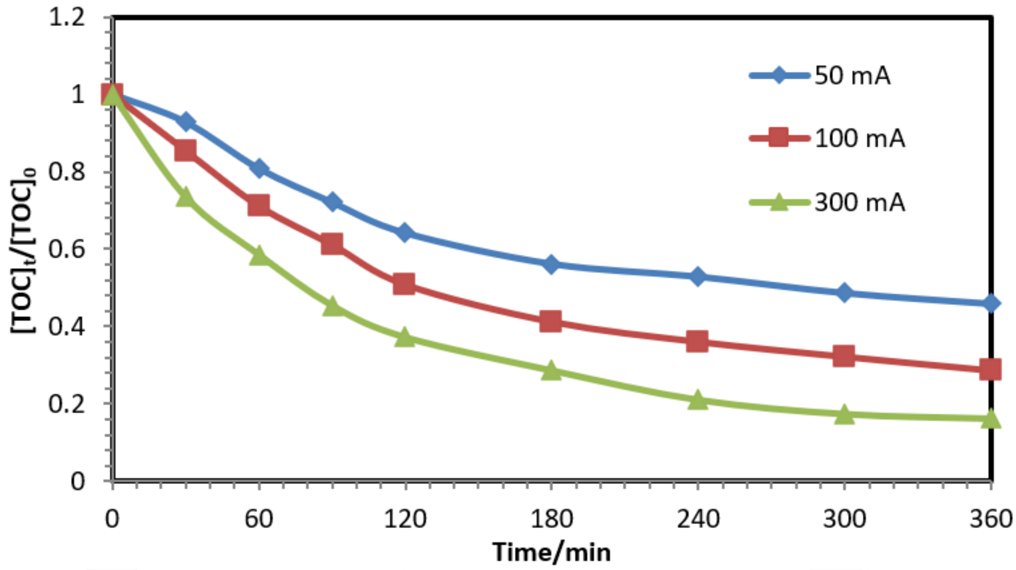

Figure 4.30. *The effect of applied current on the mineralization of PPA during the HEF treatment using Fe-d-SnO$_2$.[PPA]$_0$: 0.25 mM, m(Fe-d-SnO$_2$): 0.571 g/L, [Na$_2$SO$_4$]$_0$: 0.05 M, Pt/CF, pH: 3.0, V: 0.175 L*

In conclusion, it can be said that the highest rate of mineralization among the prepared solid-phase catalysts was achieved when Fe_3O_4-mpSiO$_2$ was used in the experiments. Comparing this catalyst with the other synthesized solid-phase catalysts, it is observed that at the end of the 360 min electrolysis it has achieved mineralization value of 87.04% as compared to 75.71% and 83.83% for Co_3O_4-mpSiO$_2$ and Fe-d-SnO$_2$, respectively. On the other hand, the catalytic activity of Fe-d-SnO$_2$ was also seen to be better than that of Co_3O_4-mpSiO$_2$. Thus, it can be viewed that Co_3O_4-mpSiO$_2$ has the lowest rate of mineralization. This poor catalytic performance of Co_3O_4-mpSiO$_2$ may be attributed to different catalytic activities of Co^{2+} and Fe^{2+} found in the catalysts structures (Yang et al., 2008). It was further observed that the rate of mineralization increased with increase in applied current intensity. The reason for this condition could be as a result of an increase of H_2O_2 production and an increase of the regeneration rate of Fe^{2+} at the cathode, leading to a higher amount of hydroxyl radicals produced (Annabi et al., 2016). In line with the above information, it can be said that 300 mA was the optimum applied current intensity in the experiments.

The MCE values of the different applied current intensities of Fe_3O_4-mpSiO$_2$ are provided in the Figure 4.31. As can be observed, MCE values decreased with increase in applied current intensities. After 30 min, MCE values of 33.07%, 24.24% and 10.99% for 50 mA, 100 mA, and 300 mA, respectively. After 180 min, MCE values of 18.07%, 10.07% and 3.75% for 50 mA, 100 mA, and 300 mA, respectively were obtained. Moreover, significant reduction in the MCE values was observed after 360 min of electrolysis. The data obtained indicated that the MCE values decreased with increase in applied current values. The reason for this situation can be explained as the energy of the system that increase with increase in applied current values consequently lead to a prominent increase in the amount of parasitic reactions. A similar trend was observed during the homogeneous electro-Fenton treatment of PPA. Similar behaviors were also observed with the Co_3O_4-mpSiO_2 (Fig 4.32) and Fe-d-SnO_2 (Fig 4.33).

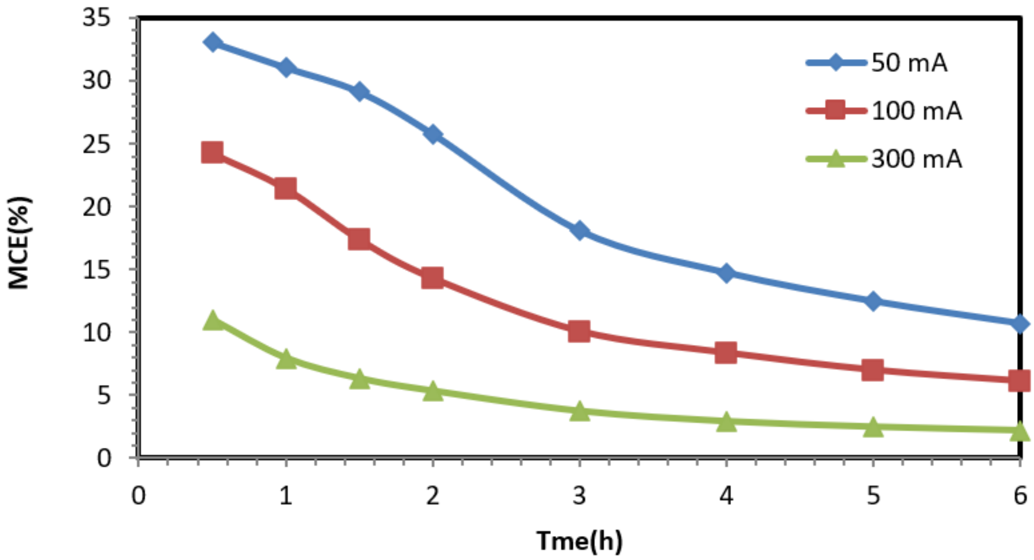

Figure 4.31. *MCE (%) values of PPA solution using different current intensities of Fe_3O_4-mpSiO_2 calculated by using the data given in Figure 4.28. $[PPA]_0$: 0.25 mM, m(Fe_3O_4-mpSiO_2): 0.571 g/L, $[Na_2SO_4]_0$: 0.05 M, Pt/CF, pH: 3.0, V: 0.175 L*

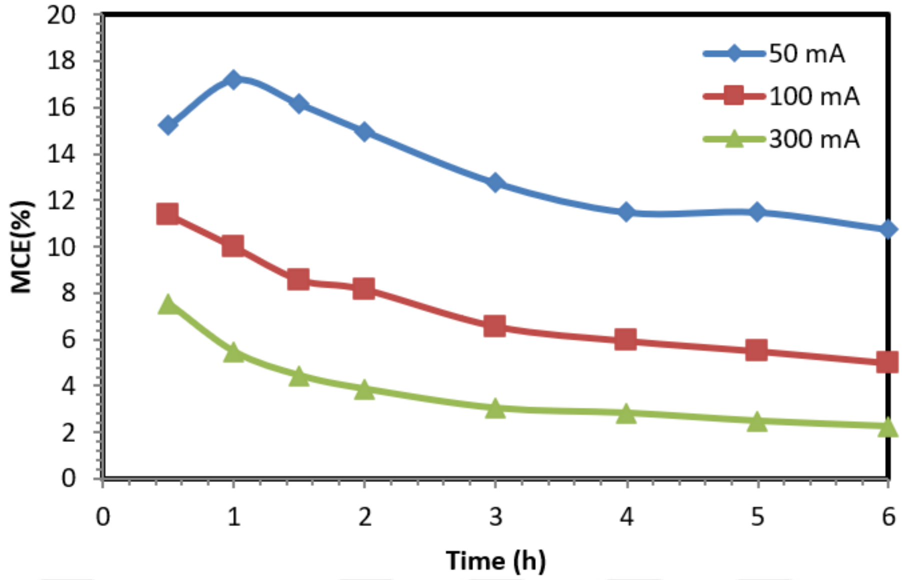

Figure 4.32. *MCE (%) values of PPA solution using different current intensities of Co_3O_4-mpSiO$_2$ calculated by using the data given in Figure 4.29. $[PPA]_0$: 0.25 mM, m(Co_3O_4-mpSiO$_2$): 0.571 g/L, $[Na_2SO_4]_0$: 0.05 M, Pt/CF, pH: 3.0, V: 0.175 L*

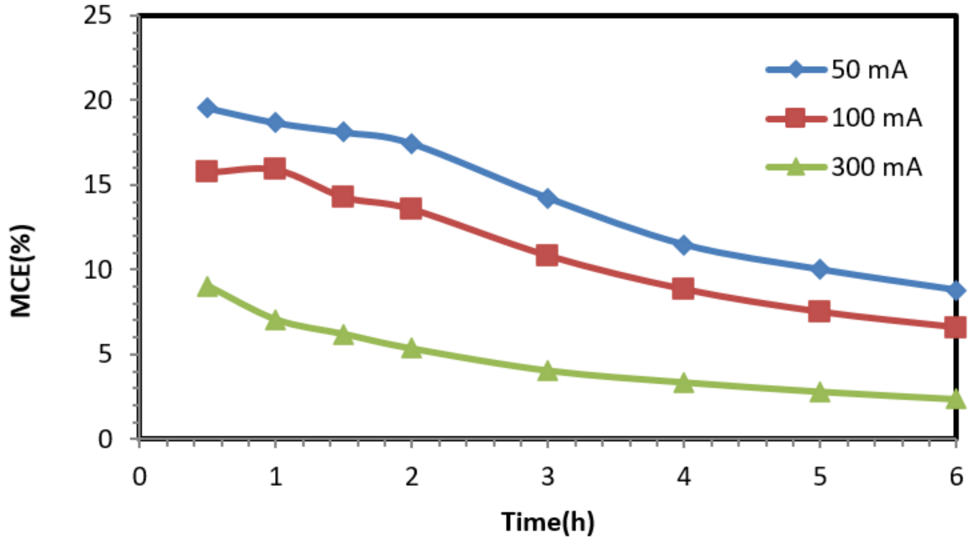

Figure 4.33. *MCE (%) values of PPA solution using different current intensities of Fe-d-SnO$_2$ calculated by using the data given in Figure 4.30. $[PPA]_0$: 0.25 mM, m(Fe-d-SnO$_2$): 0.571 g/L, $[Na_2SO_4]_0$: 0.05 M, Pt/CF, pH: 3.0, V: 0.175 L*

Considering the results above, the lowest MCE value was obtained when Fe_3O_4-mpSiO$_2$ was used in the experiment indicating that the highest rate of mineralization was achieved with the aforementioned catalyst as compared to Co_3O_4-mpSiO$_2$ and Fe-d-SnO$_2$. Additionally, it can be concluded that the highest rate of mineralization for all the catalyst was achieved when 300mA was used in the experiment.

4.2.4. Investigation of the effectiveness of the initial pH values in the removal of PPA

In this thesis, the effectiveness of the initial pH values is one of the parameters tested in the removal of PPA from water using a HEF treatment which was followed by a TOC analysis. The experiments were performed without any pH adjustment at their natural pH values. The initial pH values were measured as 6.39, 6.41 and 6.76 for the PPA solution containing 0.1 g of Fe_3O_4-mpSiO_2, Co_3O_4-mpSiO_2 and Fe-d-SnO_2, respectively. The TOC removal values for these solutions were shown in Figure 4.34, Figure 4.35 and Figure 4.36, respectively. The experiments were also performed at optimal pH value (3.0) of Fenton's reaction.

The effect of initial pH 6.39 and pH 3.0 on the removal of PPA using Fe_3O_4-mpSiO_2 is shown in Figure 4.34. As can be seen, the rate of mineralization of PPA increased with increase in electrolysis time. However, the TOC removal values of 12.07% and 25.49% for initial pH 6.39 and pH 3.0, respectively shows that the concentration of PPA substance in the reaction solution has not sufficiently destroyed after 30 min of electrolysis which implies that high content of PPA was still present in the solution. On the other hand, a decrease in the concentration of PPA was observed after 180 min of electrolysis with mineralization values of 50.27% and 63.55% for initial pH 6.39 and pH 3.0, respectively indicating an increase in the rate of mineralization of PPA. Moreover, the amount of PPA removal from the reaction solution was observed at the end of 360 min electrolysis with TOC removals of 67.13% and 76.37% for initial pH 6.39 and pH 3.0, respectively. While higher rate of mineralization was achieved when the optimal pH (3.0) was used in the experiment, the mineralization rate of PPA without any pH adjustment was also prominent showing the power of HET treatment. The Co_3O_4-mpSiO_2 (Fig 4.35) and Fe-d-SnO_2 (Fig 4.36) also showed similar trends.

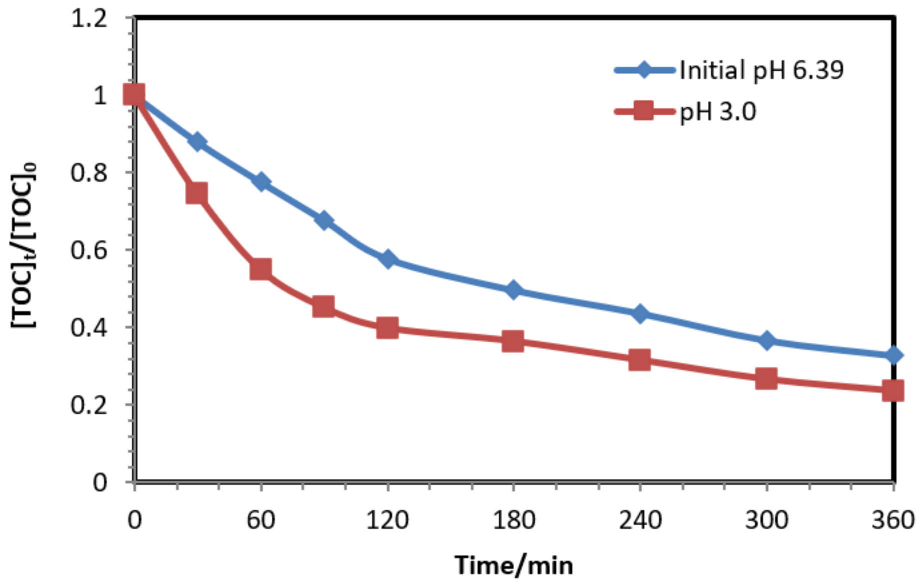

Figure 4.34. *The effect of pH on the removal of PPA during the HEF treatment using Fe_3O_4-mpSiO$_2$. [PPA]$_0$: 0.25 mM, m(Fe_3O_4-mpSiO$_2$): 0.571 g/L, [Na_2SO_4]$_0$: 0.05 M, I: 100 mA, Pt/CF, V: 0.175 L*

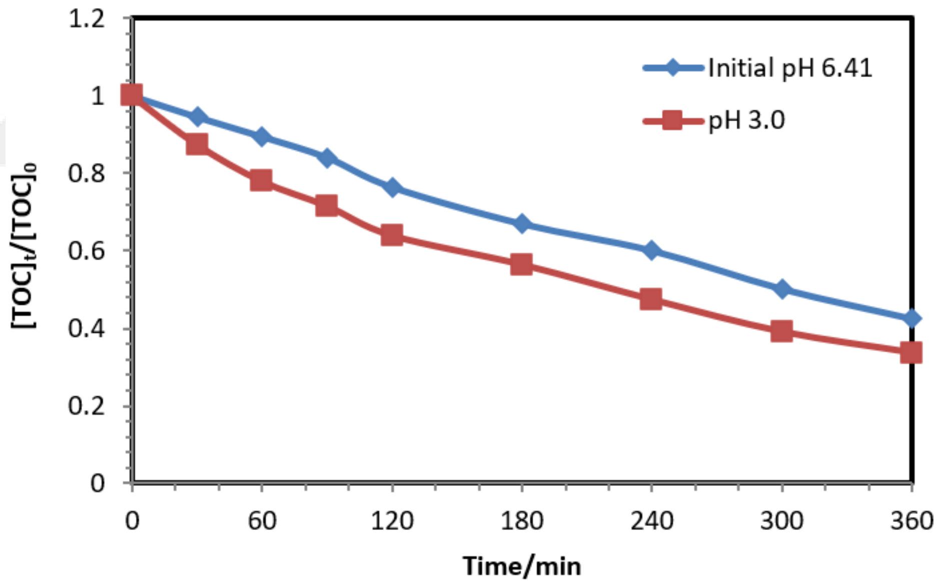

Figure 4.35. *The effect of pH on the removal of PPA during the HEF treatment using Co_3O_4-mpSiO$_2$. [PPA]$_0$: 0.25 mM, m(Co_3O_4-mpSiO$_2$): 0.571 g/L, [Na_2SO_4]$_0$: 0.05 M, I: 100 mA, Pt/CF, V: 0.175 L*

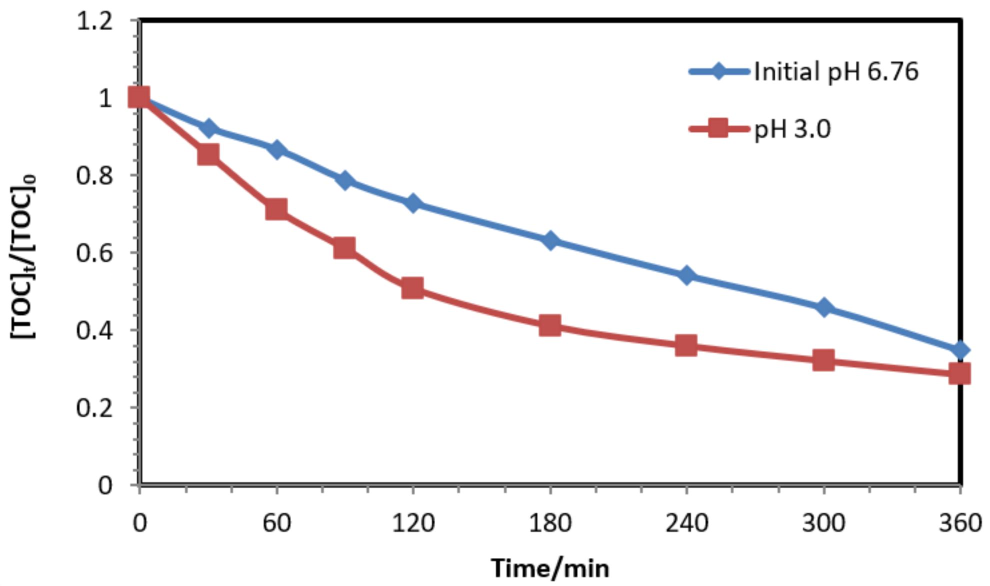

Figure 4.36. *The effect of pH on the removal of PPA during the HEF treatment using Fe-d-SnO$_2$. [PPA]$_0$:0.25 mM, m(Fe-d-SnO$_2$): 0.571 g/L, [Na$_2$SO$_4$]$_0$: 0.05 M, I: 100 mA, Pt/CF, V: 0.175 L*

Considering the data presented above, it can be said that the highest amount of PPA removal from the experimental solutions among the three investigated initial pH values was achieved when the initial pH 6.39 of Fe_3O_4-mpSiO$_2$ was used in the experiment.

4.2.5. Investigation of the stability and reusability of the synthesized catalysts

Reusability and maintaining stability is one of the most important characteristics of a HEF catalyst. The reusability and stability of the synthesized solid-phase catalysts were evaluated in the mineralization of PPA from water. For each solid-phase catalyst, four consecutive runs were performed in the oxidative degradation process. After each run, the electrolyzed catalysts were collected by simple filtration, washed with de-ionized water, heated in an oven and subsequently calcined at different temperatures depending on the catalyst used.

The TOC removal values of Fe_3O_4-mpSiO$_2$, Co_3O_4-mpSiO$_2$ and Fe-d-SnO$_2$ are presented in Figure 4.37, Figure 4.38 and Figure 4.39, respectively. After the first, second, third and fourth runs, the TOC removal values of 76.37%, 76.19%, 76.08% and 75.94%, were observed at the end of the 360 min electrolysis for Fe_3O_4-mpSiO$_2$. These results are in very close agreement with those found in the literature (Ghani Ur Rehman et al., 2021). Considering the mineralization values obtained from the TOC analyses, it can be suggested that the catalyst had shown high performance and a very good catalytic stability. As can be seen from Figure 4.38 and Figure 4.39, Co_3O_4-mpSiO$_2$ and Fe-d-SnO$_2$ also showed similar trends. Comparing Fe_3O_4-mpSiO$_2$, Co_3O_4-mpSiO$_2$ and Fe-d-SnO$_2$ making reference to the amounts of TOC removals achieved after the four consecutive runs, it was observed that the highest rate of mineralization was achieved when Fe_3O_4-mpSiO$_2$ was used in the experiment. On the other hand, the TOC removal values of the reusability test also showed that at the end of the four consecutive runs, higher amounts of PPA removal were achieved with Fe-d-SnO$_2$ than Co_3O_4-mpSiO$_2$. As a result it can be said that the catalytic performance of Fe-d-SnO$_2$ was better than that of Co_3O_4-mpSiO$_2$. So, it can be concluded that the least catalytic performance was observed when Co_3O_4-mpSiO$_2$ was used in the experiments as it produced the lowest amount of TOC removal values after each consecutive run. As can be seen from 4.38, the TOC removal values of PPA for all the four consecutive runs during the reusability test were very close to one another indicating high stability of the catalyst. Meanwhile, as can be seen from Figure 4.39, the four consecutive reusability runs of the Fe-d-SnO$_2$ catalyst are presented. After four runs of degradation experiment, a TOC removal value of ~72% was maintained throughout the runs which imply that the catalyst did not show any substantial loss of activity. A very close result is found in the literature (Ali Baig et al., 2021).

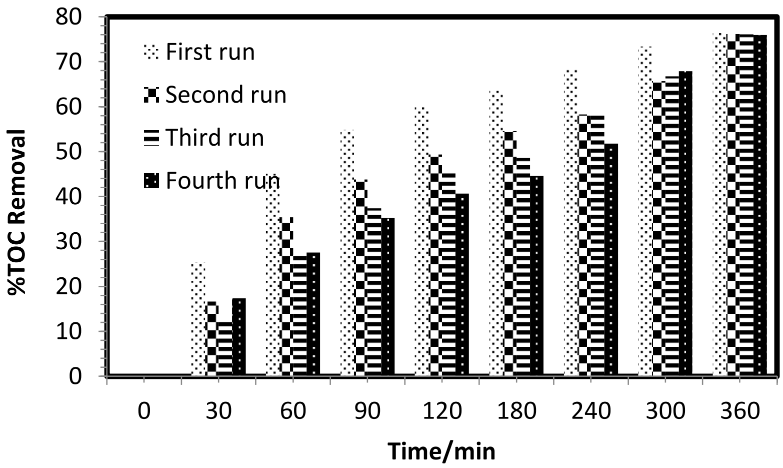

Figure 4.37. *The reusability and stability test on the mineralization of PPA during the HEF treatment using Fe_3O_4-mpSiO$_2$. $[PPA]_0$: 0.25 mM, m(Fe_3O_4-mpSiO$_2$): 0.571 g/L, $[Na_2SO_4]_0$: 0.05 M, I: 100 mA, Pt/CF, pH: 3.0, V: 0.175 L*

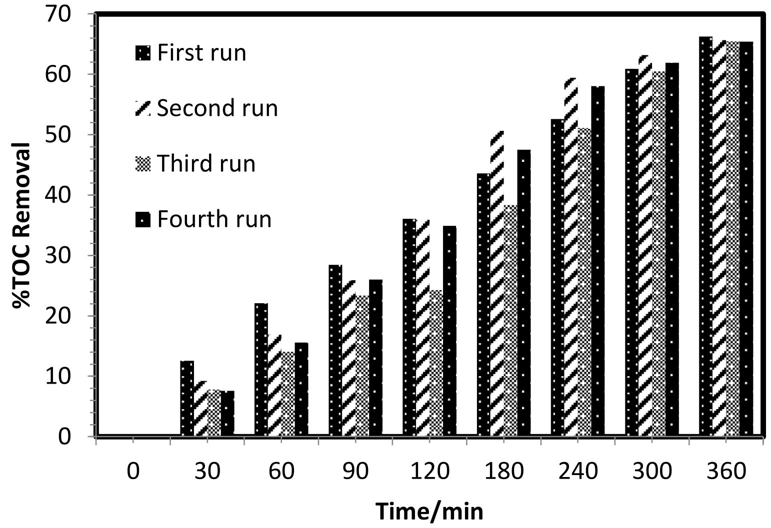

Figure 4.38. *The reusability and stability test on the mineralization of PPA during the HEF treatment using Co_3O_4-mpSiO$_2$. [PPA]$_0$: 0.25 mM, m(Co_3O_4-mpSiO$_2$): 0.571 g/L, [Na_2SO_4]$_0$: 0.05 M, I: 100 mA, Pt/CF, pH: 3.0, V: 0.175 L*

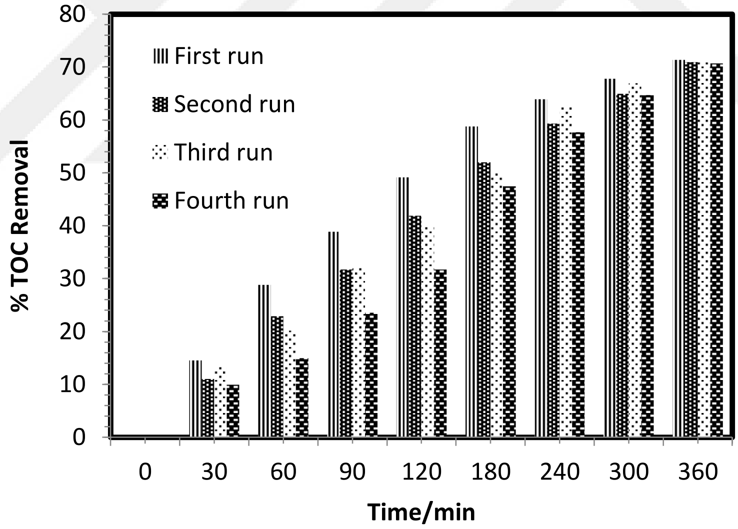

Figure 4.39. *The reusability and stability test on the mineralization of PPA during the HEF treatment using Fe-d- SnO_2. [PPA]$_0$: 0.25 mM, m(Fe-d-SnO_2): 0.571 g/L, [Na_2SO_4]$_0$: 0.05 M, I: 100 mA, Pt/CF, pH: 3.0, V: 0.175 L*

4.2.6. Identification of intermediates formed during the oxidation of pipemidic acid with hydroxyl radicals

In the EF process, hydroxyl radicals ($^{\bullet}OH$) considered as powerful oxidizing agents are produced. These oxidizing agents have the ability to non-selectively oxidize and subsequently transform organic pollutants into less harmful compounds with their further mineralization into CO_2, H_2O and inorganic ions. In line with the above information, a heterogeneous EF process was employed to identify the intermediates formed during the oxidation of PPA using chromatographic methods such as high performance liquid chromatography (HPLC) and ion chromatography (IC) to carefully identify short-chain carboxylic acids and inorganic ions, respectively.

4.2.6.1. Identification of short-chain carboxylic acids

During the electro-Fenton treatment, it is noteworthy to emphasize that the formation of short-chain carboxylic acids are due to the oxidative ring opening reactions of hydroxylated aromatic (or quinoid) intermediates (Özcan et al., 2009). In this thesis, the evolution of short-chain carboxylic acids in the homogeneous and heterogeneous electro-Fenton treatments was followed with an ion-exclusion chromatography.

The data obtained from the ion-exclusion chromatography indicated the formation of two dominant carboxylic acids, oxalic and oxamic acids with the corresponding retention times of 7.08 and 10.80 min, respectively. The evolution of these carboxylic acids during the homogeneous electro-Fenton process is given in Figure 4.40. As can be seen, at the initial stage of electrolyzes the formation rates of these carboxylic acids were very high, and they reached their maximal accumulation values in 90 min and then their concentrations were gradually decreased. Similar results were found in the literature (Özcan, Şahin, & Oturan, 2008).

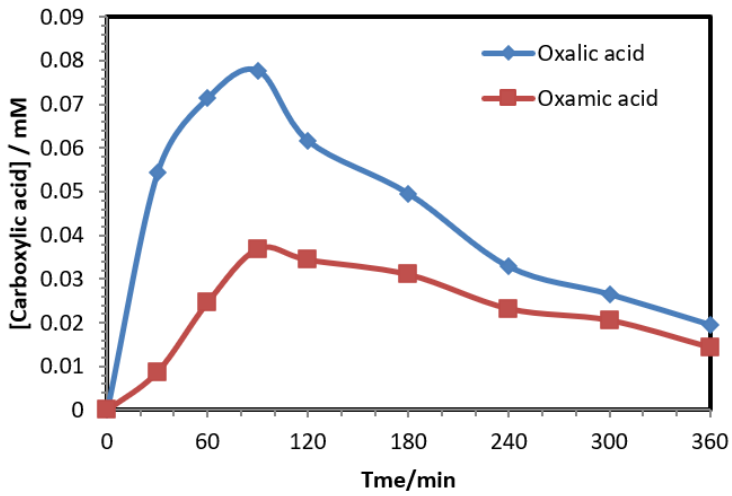

Figure 4.40. *Time-course of carboxylic acids (oxalic and oxamic acid) during the homogeneous electro-Fenton treatment of PPA using $Fe_2(SO_4).5H_2O$. $[PPA]_0$: 0.25 mM, $[Fe_2(SO_4).5H_2O]$: 0.01 mM, $[Na_2SO_4]_0$: 0.01 M, I: 100 mA, Pt/CF, pH: 3.0, V: 0.175 L*

Figure 4.41 shows the evolution of oxalic and oxamic acids during the heterogeneous electro-Fenton treatment of PPA using Fe_3O_4-mpSiO_2. As can be seen, the formation rates for both oxalic and oxamic acids are very fast at the initial stage of the electrolysis. However, they reached their maximal values at 120 min and subsequently there was a gradual decrease in concentration. Similar trend was observed as can be seen from Figure 4.42 and Figure 4.43 for Co_3O_4-mpSiO_2 and Fe-d-SnO_2, respectively.

From the above data, it can be observed that the concentration of oxalic and oxamic acids in the homogeneous electro-Fenton system were almost the same with that of Fe_3O_4-mpSiO_2 with evolution rates of ~ 0.08mM and 0.03mM for oxalic and oxamic acids in both systems. In the heterogeneous electro-Fenton system, the highest concentration of carboxylic acid evolution was obtained when Fe_3O_4-mpSiO_2 was used in the experiments.

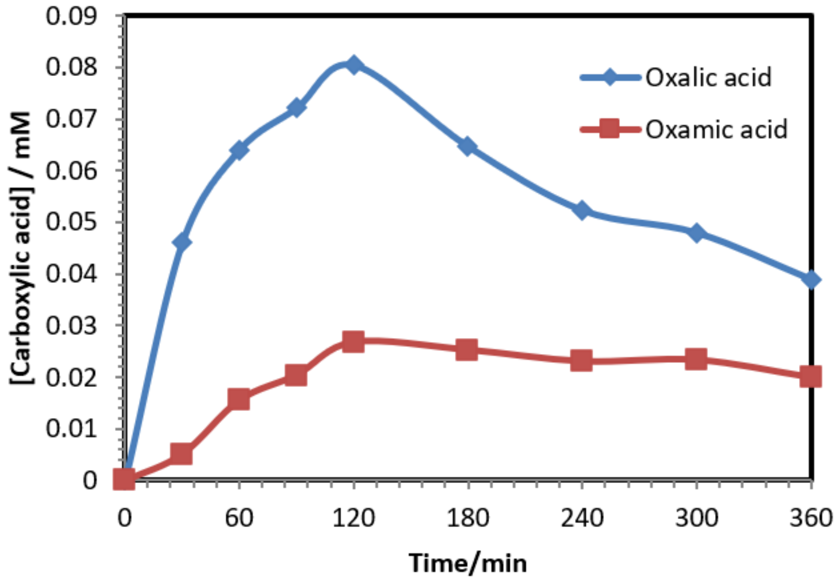

Figure 4.41. *Time-course of carboxylic acids (oxalic and oxamic acid) during the heterogeneous electro-Fenton treatment of PPA using Fe_3O_4-mpSiO_2. $[PPA]_0$: 0.25 mM, m(Fe_3O_4-mpSiO_2): 0.571 g/L, $[Na_2SO_4]_0$:0.01 M, I: 100 mA, Pt/CF, pH: 3.0, V: 0.175 L*

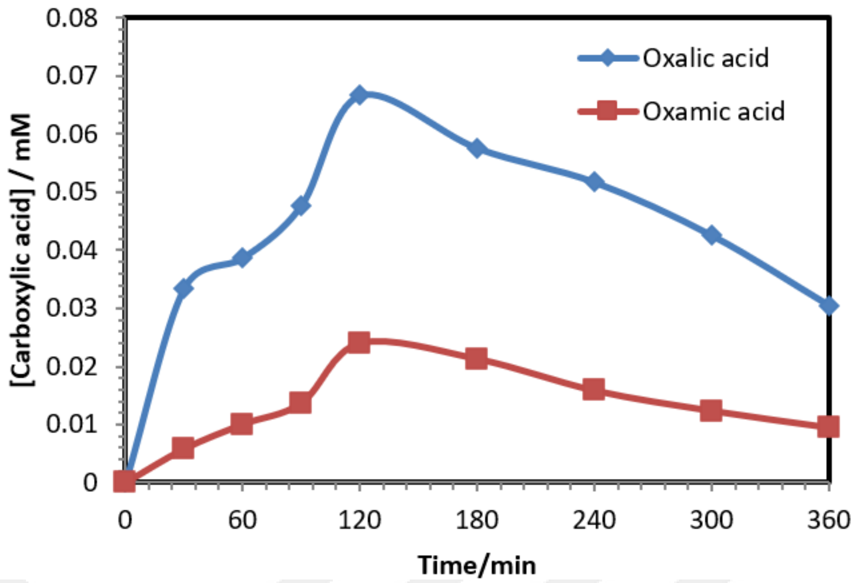

Figure 4.42. *Time-course of carboxylic acids (oxalic and oxamic acid) during the heterogeneous electro-Fenton treatment of PPA using Co_3O_4-mpSiO$_2$. [PPA]$_0$: 0.25 mM, m(Co_3O_4-mpSiO$_2$): 0.571 g/L, [Na_2SO_4]$_0$: 0.01 M, I: 100 mA, Pt/CF, pH: 3.0, V: 0.175 L*

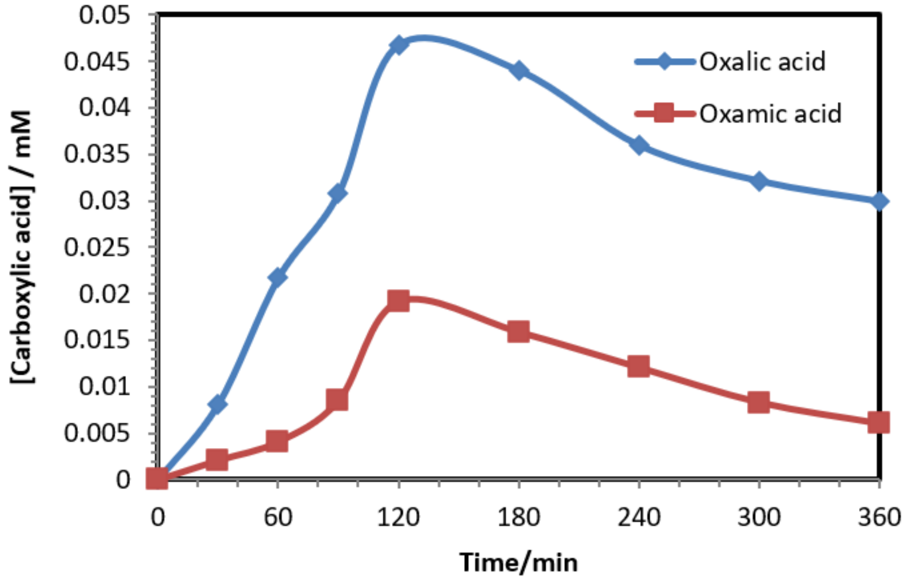

Figure 4.43. *Time-course of carboxylic acids (oxalic and oxamic acid) during the heterogeneous electro-Fenton treatment of PPA using Fe-d-SnO$_2$. [PPA]$_0$: 0.25 mM, m(Fe-d-SnO$_2$): 0.571 g/L, [Na_2SO_4]$_0$: 0.01 M,I:100 mA, Pt/CF, pH: 3.0, V: 0.175 L*

4.2.6.2. Identification of inorganic ions

The fate of the initial N atom of PPA during homogeneous EF and heterogeneous EF treatment using Pt/CF electrode combination at 100 mA was investigated. The initial and electrolyzed samples were followed up with ion chromatography system equipped with ion-exchange columns (Fig 3.5). In both systems, the chromatograms showed the release of NH_4^+ and NO_3^- ions. No other inorganic nitrogen ions such as NO_2^- were detected. It can also be observed that NH_4^+ ion was accumulated in larger extent than NO_3^- ion in both systems, which is in agreement with what was proposed in Reaction (3.1).

Figure 4.44 shows the identification and evolution of inorganic ions during the homogeneous electro-Fenton treatment of PPA. As can be seen, the total concentrations (1.241 mM) of ammonium and nitrate correspond to 99.28% of initial amounts (0.25 mM × 5 = 1.25 mM) of nitrogen atoms. Thus, contents of 0.936 mM NH_4^+ (74.88% of initial N) and 0.305 mM NO_3^- (24.4% of initial N) were accumulated after 360 min with Pt/CF electrode combination.

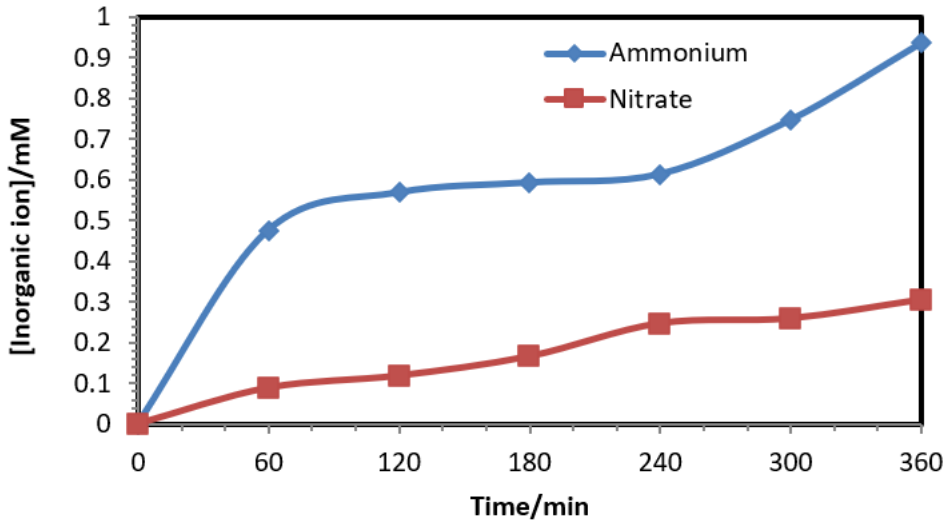

Figure 4.44. *Time-course of the concentration of inorganic ions during homogeneous treatment of PPA using $Fe_2(SO_4).5H_2O$. $[PPA]_0$: 0.25 mM, $[Fe_2(SO_4).5H_2O]$: 0.01 M, $[Na_2SO_4]_0$: 0.01 M, I: 100 mA, Pt/CF, pH: 3.0, V: 0.175 L*

In the heterogeneous electro-Fenton treatment, the efficiency of the synthesized solid-phase catalysts in the identification and evolution of inorganic ions was systematically examined. The ion-exchange chromatographic analysis of Fe_3O_4-mpSiO_2 is provided in Figure 4.45. As can be observed prominent amounts of ammonium (0.986 mM) and nitrate (0.257 mM) were accumulated in the electrolyzed solution after 360 min electrolysis. The total amounts (1.243 mM) of nitrate and ammonium correspond to 99.44% of initial amounts (0.25 mM × 5 = 1.25 mM) of nitrogen atoms. Similar trend was observed for Co_3O_4-mpSiO_2 and Fe-d-SnO_2 as can be seen in Figure 4.46 and Figure 4.47, respectively

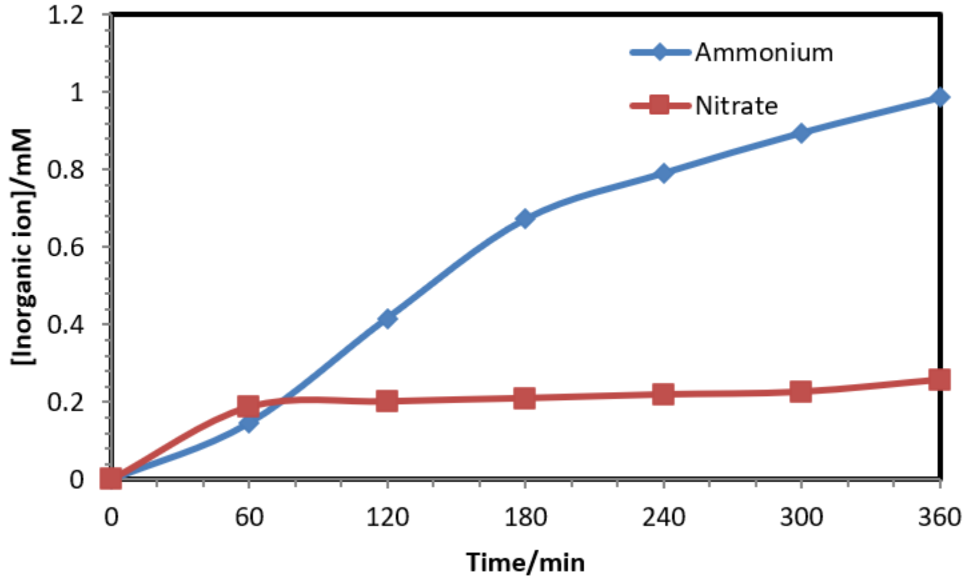

Figure 4.45. *Time-course of the inorganic ion concentration of PPA in the oxidation of PPA during HEF treatment using Fe_3O_4-mpSiO$_2$. [PPA]$_0$: 0.25 mM, m(Fe_3O_4-mpSiO$_2$): 0.571 g/L, [Na_2SO_4]$_0$: 0.01 M, I:100 mA, Pt/CF, pH: 3.0, V: 0.175 L*

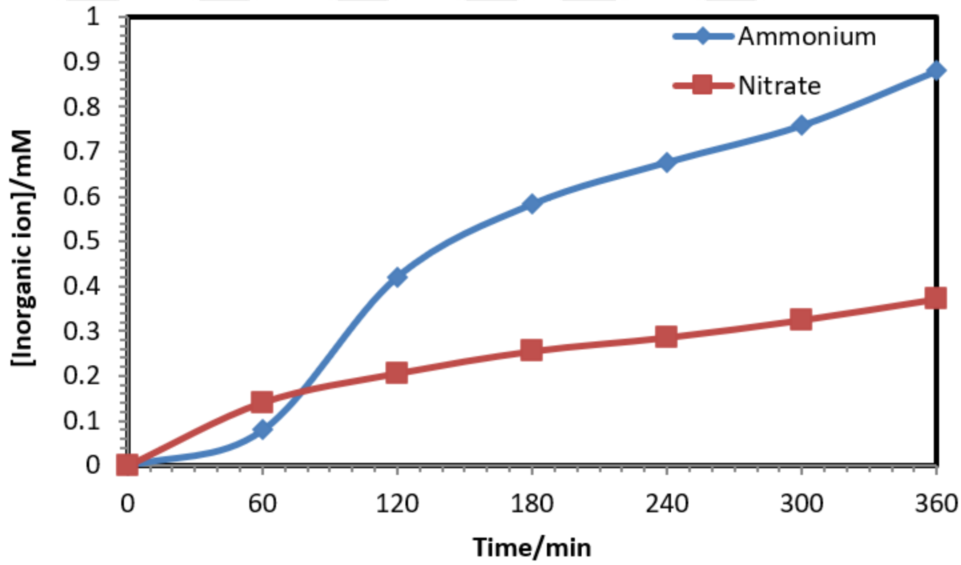

Figure 4.46. *Time-course of the concentration of inorganic ions during HEF treatment of PPA using Co_3O_4- mpSiO$_2$. [PPA]$_0$: 0.25 mM, m(Co_3O_4-mpSiO$_2$): 0.571 g/L, [Na_2SO_4]$_0$: 0.01 M, I: 100 mA, Pt/CF, pH: 3.0, V: 0.175 L*

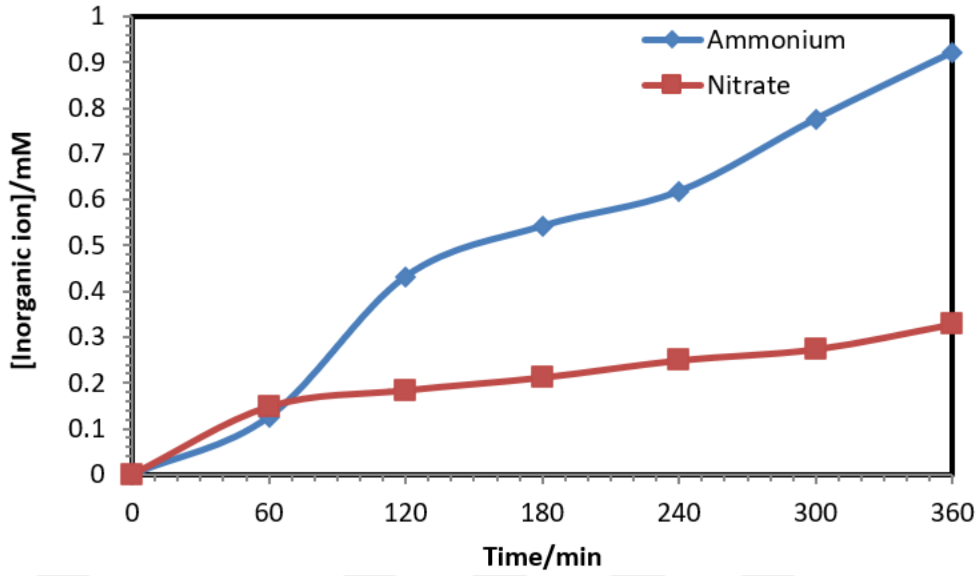

Figure 4.47. *Time-course of the concentration of inorganic ions during HEF treatment of PPA using Fe-d-SnO_2.$[PPA]_0$: 0.25 mM, m(Fe-d-SnO_2): 0.571 g/L, $[Na_2SO_4]_0$: 0.01 M, I: 100 mA, Pt/CF, pH: 3.0, V: 0.175 L*

Comparing the IC analyses of the synthesized solid-phase catalysts, Fe_3O_4-mpSiO_2, Co_3O_4-mpSiO_2 and Fe-d-SnO_2 as presented above showed that for all the catalysts, the concentration of ammonium ions was very much higher than the nitrate ions. Meanwhile, it is also observed that the ionic concentration of ammonium ion was highest when Fe_3O_4-mpSiO_2 was used in the experiment as compared to Co_3O_4-mpSiO_2 and Fe-d-SnO_2. The ionic concentration of NH_4^+ and NO_3^- in the homogeneous EF system was almost the same as in the case of heterogeneous EF system.

4.3. Comparing the Effectiveness of Homogeneous and Heterogeneous EF Processes in the Removal of PPA

In final step of the thesis, the effectiveness of homogeneous and heterogeneous EF processes in the removal of PPA was compared. During this evaluation, operational conditions such as 0.25 mM PPA, 100mA applied current, 50 mM Na_2SO_4, and pH 3.0 were used for both processes. In the case of homogeneous EF, 0.1mM $Fe_2(SO_4)_3.5H_2O$ was used as the soluble iron catalyst whereas 0.571 g/L of the solid-phase catalyst was used as the heterogeneous catalysts in the HEF treatment.

The synthesized three different solid-phase catalysts were sequentially compared with the homogeneous EF system. In the first step, the effect of adsorption of PPA on the catalysts surfaces was evaluated by performing TOC analysis. After that, the effect of electrochemical oxidation of PPA on electrode surfaces was also evaluated by performing experiments in the absence of catalysts at the same conditions. Next, homogeneous electro-Fenton treatment of PPA was performed by using Pt and BDD as anodes. Finally, heterogeneous electro-Fenton treatment of PPA was conducted at the same conditions. The results for the Fe_3O_4-mpSiO_2, Co_3O_4-mpSiO_2 and Fe-d-SnO_2 are shown in Figure 4.48, Figure 4.49 and Figure 4.50, respectively.

As can be seen in Figure 4.47, the adsorption of PPA on the surfaces of the catalyst had no meaningful effect on the removal of PPA from the experimental solutions as the amount of PPA present in the solution remained very high and constant throughout the experiment. In addition, it was further observed that when an experiment was performed using a non-catalyzed system, there was only a slight decrease in the amount of PPA from the solution indicating a very low rate of mineralization. On the other hand, when a Pt/CF electrode combination was used in the experiments, the rate of mineralization in both homogeneous and heterogeneous EF systems had increased and appeared closed to each other. Furthermore, when a BBD/CF electrode combination was used in the experiment, the rate of mineralization for homogeneous EF and heterogeneous EF systems also followed a similar trend, however, the amount of PPA removal from the reaction solution was remarkably higher especially in the heterogeneous system as compared to the Pt/CF electrode combination. Therefore, with these observations, it can be suggested that the use of Fe_3O_4-mpSiO_2 has strengthened the mineralization of PPA to attain its maximum value. Equally, the obtained result is an indication of the high catalytic competence of the newly prepared Fe_3O_4-mpSiO_2 as a heterogeneous catalyst in the degradation of PPA by an EF system. A similar pattern of mineralization of PPA was observed in the case of Co_3O_4-mpSiO_2 and Fe-d-SnO_2 as can be seen from Figure 4.48 and Figure 4.49, respectively.

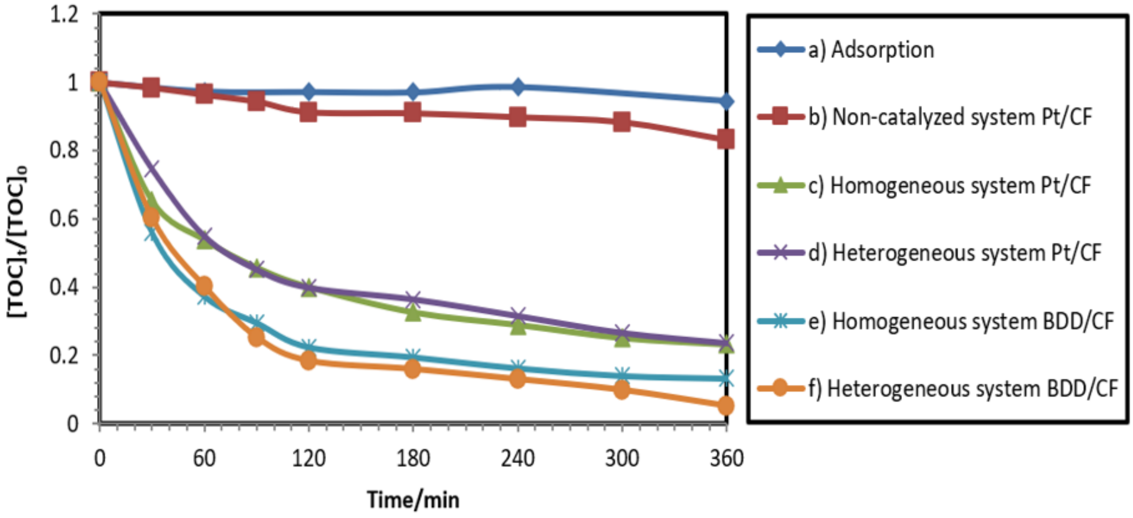

Figure 4.48. *TOC removal values of PPA with different methods in the absence and presence of Fe_3O_4-$mpSiO_2$.$[PPA]_0$: 0.25 mM, $[Na_2SO_4]_0$: 0.05 M, $[Fe^{3+}]$: 0.1 mM (c and e), m(Fe_3O_4-$mpSiO_2$): 0.571 g/L (d and f), I: 100 mA, pH: 3.0, V: 0.175 L*

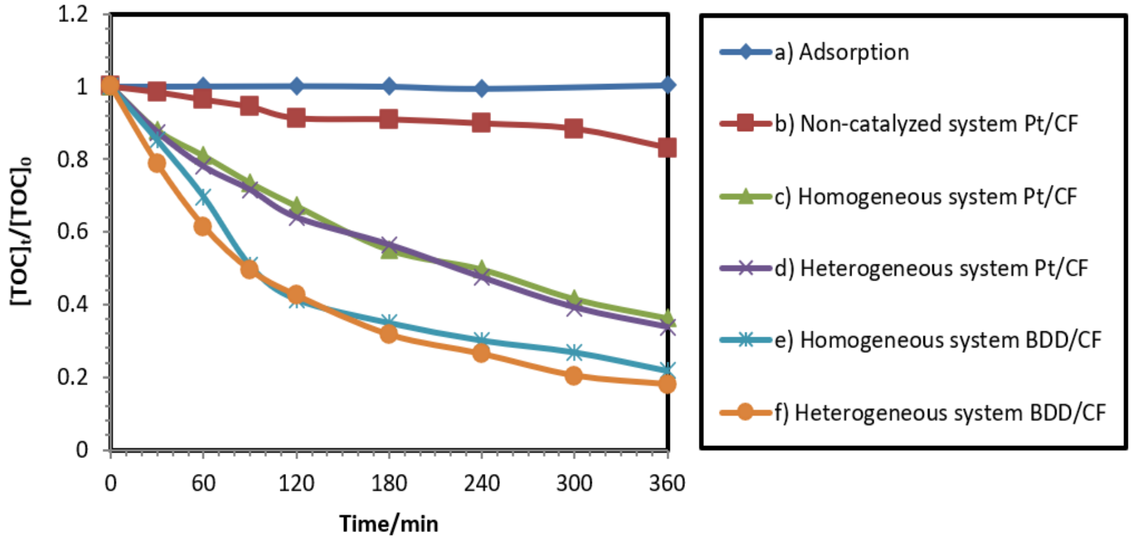

Figure 4.49. *TOC removal values of PPA with different methods in the absence and presence of Co_3O_4-$mpSiO_2$.$[PPA]_0$: 0.25 mM, $[Na_2SO_4]_0$: 0.05 M, $[Co^{3+}]$: 0.2 mM (c and e), m(Co_3O_4-$mpSiO_2$): 0.571 g/L (d and f), I: 100 mA, pH: 3.0, V: 0.175 L*

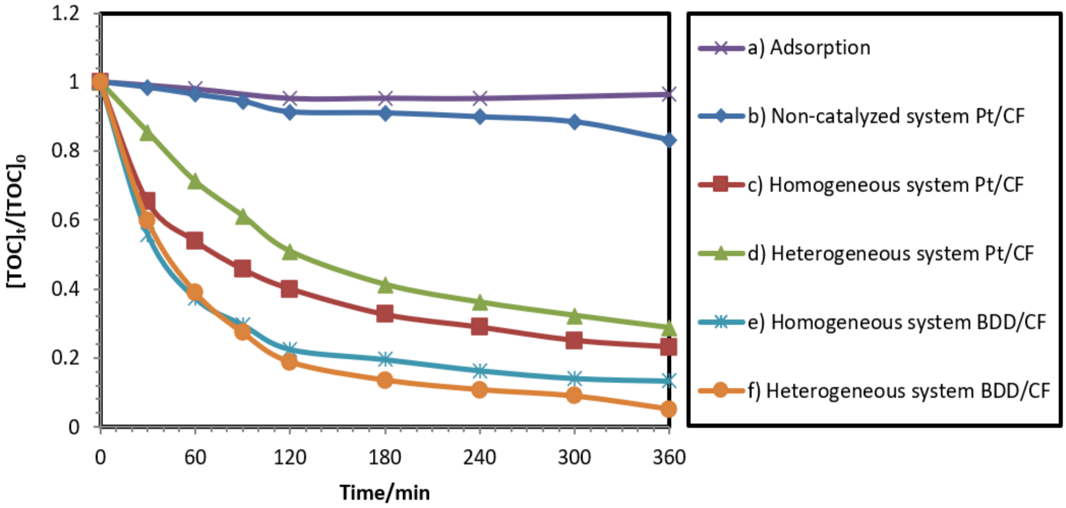

Figure 4.50. *TOC removal values of PPA with different methods in the absence and presence of Fe-d-SnO_2. $[PPA]_0$: 0.25 mM, $[Na_2SO_4]_0$: 0.05 M, $[Fe^{3+}]$: 0.1 mM (c and e), m(Fe-d-SnO_2): 0.571 g/L (d and f), I: 100 mA, pH: 3.0, V: 0.175 L*

5. CONCLUSIONS

In this thesis, the preparation and characterization of solid-phase catalysts have been aimed for the heterogeneous electro-Fenton treatment of pipemidic acid, a widely used antibiotic. The research was separated into three different main stages. In the first stage, the oxidation and mineralization of the model organic pollutant, pipemidic acid (PPA), was investigated using a homogeneous electro-Fenton process. In the EF system, different electrode materials can be used for the production of hydroxyl radicals. As can be seen in Figure 4.1, it can be said that the rate of destruction was faster in BDD/CF than Pt/CF electrode combination throughout the electrolysis. The degradation rate of PPA was slower and took longer electrolysis time when a Pt/CF electrode combination was used and this could be explained as Pt is considered to have strong interaction with the $^{\bullet}OH$ and this might eventually decrease the availability of $^{\bullet}OH$ for the pollutant degradation (Nair et al., 2021). The fast rate of degradation in BDD/CF electrode combination on the other hand can be attributed to the different sources of hydroxyl radical production during the treatment. Firstly, $^{\bullet}OH$ were produced from the Fenton's reaction (Eq. (2.1)). Secondly, from the oxidation of water on the BDD anode surface according to Eq. (4.1), $^{\bullet}OH$ was also produced. Cumulatively, these sources contributed to the increase in the degradation of PPA (Özcan et al., 2016). Moreover, the oxidation of PPA using different electrode combinations were also monitored using TOC analysis (Fig 4.2). At the end of the analysis, TOC removal values of 76% and 95.49% for Pt/CF and BDD/CF electrode combinations, respectively was yielded showing a significant decrease in the amount of organic pollutant present in the reaction solution. With this amounts of mineralization of PPA from the solution, it can be suggested that the oxidation power of the electro-Fenton system was very high towards the mineralization of PPA from water. Operational parameters such as applied current intensity and iron concentration were also investigated. In monitoring the effect of applied current intensity for both HPLC and TOC, it was observed that the rate of oxidation and mineralization increased with increase in applied current intensity which could be as a result of an increase of H_2O_2 production and an increase of the regeneration rate of Fe^{2+} at the cathode, leading to a higher amount of hydroxyl radicals produced (Annabi et al., 2016). The effect of the concentration of Fe^{3+} on the removal of the model organic pollutant was monitored at constant current intensity of 50 mA. As can be seen from Figure 4.6 and Figure 4.7 for HPLC and TOC, respectively, 0.1mM was the optimum iron concentration throughout the electrolysis. The rate constants of the reactions between PPA and $^{\bullet}OH$ radicals was determined by competition kinetics method. At the end of this evaluation, the second-order rate constant was calculated and found to be (1.18 ± 0.03) x10^9 $M^{-1}s^{-1}$.

After the first stage of the thesis, the research was focused on the synthesis, characterization and thereafter examining the efficiency of the solid-phase catalysts (Fe_3O_4-mpSiO_2, Co_3O_4-mpSiO_2 and Fe-d-SnO_2) on the removal of PPA by the HEF method. The mesoporous silica supported catalysts (Fe_3O_4-mpSiO_2, Co_3O_4-mpSiO_2) showed high content of magnetism after their synthesis. This property which is due to para-magnetism allowed them to be easily recovered and recycled with simple magnets after being electrolyzed. The synthesized catalysts were characterized using different methods namely: X-Ray Diffraction (XRD), Scanning Electron Microscopy (SEM), Energy Dispersive X-ray (EDX) and Brunauer, Emmett, Teller (BET). The diffraction peaks of Fe_3O_4-mpSiO_2 and Co_3O_4-mpSiO_2 were almost the same with that of Fe_3O_4 and Co_3O_4, respectively indicating the successful coating of Fe_3O_4 and Co_3O_4 on the surface of mpSiO_2. The XRD pattern of Fe-d-SnO_2 nanoparticles (Fig 4.12) showed some intense diffraction peaks at 2θ =26.64°, 34.10°, 37.89° and 52.20°. The SEM images of mpSiO_2 nanoparticles (Fig 4.13) were remarkably well-dispersed and composed of many smaller convex spherical particles. As can be seen from Figure 4.14 and Figure 4.16, the SEM images for Fe_3O_4 and Co_3O_4, respectively indicated well-agglomerated nanoparticles which could be due to large particle sizes, however, in the case of Fe_3O_4-mpSiO_2 (Fig 4.15) and Co_3O_4-mpSiO_2 (Fig 4.17), the SEM images show a low degree of agglomeration which can be attributed to the presence of mpSiO_2. In Fe-d-SnO_2, the SEM micrographs indicate the presence of some loosely aggregates of particles in Fe-d-SnO_2 powders (Fig 4.18). Different shapes were also observed, some of which appeared spherical. The EDX mapping images of the Fe_3O_4-mpSiO_2 revealed that the prepared nanocomposite catalyst consisted of only Fe, O, and Si elements (Fig 4.19). The EDX of Co_3O_4-mpSiO_2 (Fig 4.20) shows that the final product includes Co, O, and Si. Furthermore, the EDX spectrum of Fe-d-SnO_2 reveals the presence of elements such as Fe, O and Sn in accordance with the chemical composition of the as-prepared catalyst (Fig 4.21). The BET analysis of the synthesized solid-phase catalyst is presented in Table 4.1. It can be seen that the coating of Fe_3O_4 and Co_3O_4 on the surface of mpSiO_2 led to the reduced particle sizes of Fe_3O_4-mpSiO_2 and Co_3O_4-mpSiO_2, respectively thereby consequently increasing the surface areas. On the other hand, doping of SnO_2 with Fe^{3+}

has also caused the increase in the surface area of Fe-d- SnO_2 catalyst. Moreover, the rate of mineralization of PPA from the experiment solutions using the three synthesized solid-phase catalysts was studied in detail. As can be seen from Figure 4.22, Figure 4.23 and Figure 4.24 for Fe_3O_4-mpSiO_2, Co_3O_4-mpSiO_2 and Fe-d-SnO_2, respectively the highest rate of mineralization was achieved when 2.286 g/L was used in the experiments for all the catalysts. Briefly, it can be said that the rate of mineralization increased with increase in the amount of iron concentration. Also, from Figure 4.25, Figure 4.26 and Figure 4.27 for Fe_3O_4-mpSiO_2, Co_3O_4-mpSiO_2 and Fe-d-SnO_2, respectively it was shown that MCE values increase with increase in the amount of iron concentration for all the catalysts and as such 2.286 g/L was considered to have the highest MCE value. It was further observed that among the solid-phase catalysts, Fe_3O_4-mpSiO_2 has the highest rate of mineralization when used in the experiments. The effect of applied current on the mineralization of PPA using the three synthesized heterogeneous catalysts showed that the optimum applied current was achieved when 300 mA was used in the experiments as can be seen from Figure 4.28, Figure 4.29 and Figure 4.30. The effectiveness of the initial pH values is one of the parameters tested in the removal of PPA from water using a HEF treatment which was followed by TOC analysis. The experiments were performed without any pH adjustment at their natural pH values. The initial pH values were measured as 6.39, 6.41 and 6.76 for the PPA solution containing 0.1 g of Fe_3O_4-mpSiO_2, Co_3O_4-mpSiO_2 and Fe-d-SnO_2, respectively. Among the tested initial pH values, 6.39 have achieved the highest rate of mineralization. The reusability test results after four consecutive runs for Fe_3O_4-mpSiO_2, Co_3O_4-mpSiO_2 and Fe-d-SnO_2, are shown in Figure 4.37, Figure 4.38 and Figure 4.39, respectively. Fe_3O_4-mpSiO_2 has obtained the highest amounts of TOC removal values without showing any substantial loss in catalytic activity. A heterogeneous EF process was employed to identify the intermediates formed during the oxidation of PPA using chromatographic methods such as HPLC and IC to carefully identify short-chain carboxylic acids and inorganic ions, respectively. As can be seen from Figure 4.41, Figure 4.42 and Figure 4.43 for Fe_3O_4-mpSiO_2, Co_3O_4-mpSiO_2 and Fe-d-SnO_2, respectively, The ion-exclusion chromatograms showed the formation of two dominant carboxylic acids, oxalic and oxamic acids. Among these synthesized solid-phase catalysts, Fe_3O_4-mpSiO_2 has the highest amount of carboxylic acids evolution. IC analysis results indicated that for all the solid-phase catalysts, the concentration of NH_4^+ ions were higher than NO_3^-

ions. Additionally, it was observed that Fe_3O_4-mpSiO_2 had the highest concentration of NH_4^+ ions as compared to Co_3O_4-mpSiO_2 and Fe-d-SnO_2.

In final step of the thesis, the effectiveness of the synthesized three different solid-phase catalysts in the removal of PPA was sequentially compared with the homogeneous EF system. In the first step, the effect of adsorption of PPA on the catalyst surfaces was evaluated by performing TOC analysis. After that, the effect of electrochemical oxidation of PPA on electrode surfaces was also evaluated by performing experiments in the absence of catalysts at the same conditions. Next, homogeneous electro-Fenton treatment of PPA was performed by using Pt and BDD as anodes. Finally, heterogeneous electro-Fenton treatment of PPA was conducted at the same conditions. The results for the Fe_3O_4-mpSiO_2, Co_3O_4-mpSiO_2 and Fe-d-SnO_2 are shown in Figure 4.48, Figure 4.49 and Figure 4.50, respectively. The data obtained from the TOC analysis for all the catalysts indicated that the rate of mineralization were higher in the heterogeneous electro-Fenton system than the homogeneous electro-Fenton system particularly when a BBD/CF was used in the experiment.

In conclusion, the data obtained from the studies undertaken within the context of the thesis show that the thesis study has successfully achieved its intended purpose. It is also with strong conviction that the data obtained from these studies will serve as a basis for new studies in the field of analytical and environmental chemistry especially for those who might be interested in water and wastewater treatment.

REFERENCES

Agarwal, S., Tyagi, I., Gupta, V. K., Sohrabi, M., Mohammadi, S., Golikand, A. N., & Fakhri, A. (2017). Iron doped SnO2/Co3O4 nanocomposites synthesized by sol-gel and precipitation method for metronidazole antibiotic degradation. *Materials Science and Engineering C*, *70*, 178–183. https://doi.org/10.1016/j.msec.2016.08.062

Al-Khafaji, R. Q., & Mohammed, A. H. A. K. (2019). Optimization of Continuous Electro-Fenton and Photo electro-Fenton Processes to Treat Iraqi Oilfield Produced Water Using Surface Response Methodology. *IOP Conference Series: Materials Science and Engineering*, *518*(6), 0–11. https://doi.org/10.1088/1757-899X/518/6/062007

Al-Zubaidi, D. K., & Pak, K. S. (2020). Degradation of parachlorophenol in synthetic wastewater using batch electro-fenton process. *Materials Today: Proceedings*, *20*, 414–419. https://doi.org/10.1016/j.matpr.2019.09.157

Ali Baig, A. B., Rathinam, V., & Ramya, V. (2021). Synthesis and Investigation of Fe doped SnO2 Nanoparticles for Improved Photocatalytic Activity under Visible Light and Antibacterial performances. *Materials Technology*, *36*(10), 623–635. https://doi.org/10.1080/10667857.2020.1786781

Ammar, S., Oturan, M. A., Labiadh, L., Guersalli, A., Abdelhedi, R., Oturan, N., & Brillas, E. (2015). Degradation of tyrosol by a novel electro-Fenton process using pyrite as heterogeneous source of iron catalyst. *Water Research*, *74*, 77–87. https://doi.org/10.1016/j.watres.2015.02.006

Anh, H. Q., Le, T. P. Q., Da Le, N., Lu, X. X., Duong, T. T., Garnier, J., Rochelle-Newall, E., Zhang, S., Oh, N. H., Oeurng, C., Ekkawatpanit, C., Nguyen, T. D., Nguyen, Q. T., Nguyen, T. D., Nguyen, T. N., Tran, T. L., Kunisue, T., Tanoue, R., Takahashi, S., … Nguyen, T. A. H. (2021). Antibiotics in surface water of East and Southeast Asian countries: A focused review on contamination status, pollution sources, potential risks, and future perspectives. *Science of the Total Environment*, *764*. https://doi.org/10.1016/j.scitotenv.2020.142865

Annabi, C., Fourcade, F., Soutrel, I., Geneste, F., Floner, D., Bellakhal, N., & Amrane, A. (2016). Degradation of enoxacin antibiotic by the electro-Fenton process:

Optimization, biodegradability improvement and degradation mechanism. *Journal of Environmental Management*, *165*, 96–105. https://doi.org/10.1016/j.jenvman.2015.09.018

Asgharzadeh, F., Moradi, M., Jonidi Jafari, A., Esrafili, A., Tahergorabi, M., & Rezaei kalantari, R. (2019). Enhanced electro kinetic- pseudo-Fenton degradation of pyrene-contaminated soil using Fe3O4 magnetic nanoparticles: A data set. *Data in Brief*, *24*, 4–11. https://doi.org/10.1016/j.dib.2018.11.068

Atique Ullah, A. K. M., Amin, F. B., & Hossain, A. (2020). Tailoring surface morphology and magnetic property by precipitants concentrations dependent synthesis of Co3O4 nanoparticles. *Ceramics International*, *46*(17), 27892–27896. https://doi.org/10.1016/j.ceramint.2020.07.167

Babuponnusami, A., & Muthukumar, K. (2014). A review on Fenton and improvements to the Fenton process for wastewater treatment. *Journal of Environmental Chemical Engineering*, *2*(1), 557–572. https://doi.org/10.1016/j.jece.2013.10.011

Ball, P. (2000). Quinolone generations: Natural history or natural selection? *Journal of Antimicrobial Chemotherapy*, *46*(TOPIC T1), 17–24. https://doi.org/10.1093/oxfordjournals.jac.a020889

Barhoumi, N., Olvera-Vargas, H., Oturan, N., Huguenot, D., Gadri, A., Ammar, S., Brillas, E., & Oturan, M. A. (2017). Kinetics of oxidative degradation/mineralization pathways of the antibiotic tetracycline by the novel heterogeneous electro-Fenton process with solid catalyst chalcopyrite. *Applied Catalysis B: Environmental*, *209*, 637–647. https://doi.org/10.1016/j.apcatb.2017.03.034

Becker, D., Varela Della Giustina, S., Rodriguez-Mozaz, S., Schoevaart, R., Barceló, D., de Cazes, M., Belleville, M. P., Sanchez-Marcano, J., de Gunzburg, J., Couillerot, O., Völker, J., Oehlmann, J., & Wagner, M. (2016). Removal of antibiotics in wastewater by enzymatic treatment with fungal laccase – Degradation of compounds does not always eliminate toxicity. *Bioresource Technology*, *219*, 500–509. https://doi.org/10.1016/j.biortech.2016.08.004

Bello, M. M., Abdul Raman, A. A., & Asghar, A. (2019). A review on approaches for addressing the limitations of Fenton oxidation for recalcitrant wastewater treatment. *Process Safety and Environmental Protection*, *126*, 119–140.

https://doi.org/10.1016/j.psep.2019.03.028

Bilal, M., Ashraf, S. S., Barceló, D., & Iqbal, H. M. N. (2019). Biocatalytic degradation/redefining "removal" fate of pharmaceutically active compounds and antibiotics in the aquatic environment. *Science of the Total Environment*, *691*, 1190–1211. https://doi.org/10.1016/j.scitotenv.2019.07.224

Biton Seror, S., Shamir, D., Albo, Y., Kornweitz, H., & Burg, A. (2022). Elucidation of a mechanism for the heterogeneous electro-fenton process and its application in the green treatment of azo dyes. *Chemosphere*, *286*(P3), 131832. https://doi.org/10.1016/j.chemosphere.2021.131832

Brillas, E. (2022). Progress of homogeneous and heterogeneous electro-Fenton treatments of antibiotics in synthetic and real wastewaters. A critical review on the period 2017–2021. *Science of the Total Environment*, *819*, 153102. https://doi.org/10.1016/j.scitotenv.2022.153102

Bulánek, R., Hrdina, R., & Hassan, A. F. (2019). Preparation of polyvinylpyrrolidone modified nanomagnetite for degradation of nicotine by heterogeneous Fenton process. *Journal of Environmental Chemical Engineering*, *7*(2), 102988. https://doi.org/10.1016/j.jece.2019.102988

Cai, H., Li, X., Ma, D., Feng, Q., Wang, D., Liu, Z., Wei, X., Chen, K., Lin, H., Qin, S., & Lu, F. (2021). Stable Fe3O4 submicrospheres with SiO2 coating for heterogeneous Fenton-like reaction at alkaline condition. *Science of the Total Environment*, *764*, 144200. https://doi.org/10.1016/j.scitotenv.2020.144200

Chen, F., Xie, S., Huang, X., & Qiu, X. (2017). Ionothermal synthesis of Fe 3 O 4 magnetic nanoparticles as efficient heterogeneous Fenton-like catalysts for degradation of organic pollutants with H 2 O 2. *Journal of Hazardous Materials*, *322*, 152–162. https://doi.org/10.1016/j.jhazmat.2016.02.073

Cruz, D. R. S., de Jesus, G. K., Santos, C. A., Silva, W. R., Wisniewski, A., Cunha, G. C., & Romão, L. P. C. (2021). Magnetic nanostructured material as heterogeneous catalyst for degradation of AB210 dye in tannery wastewater by electro-Fenton process. *Chemosphere*, *280*(January). https://doi.org/10.1016/j.chemosphere.2021.130675

Dadashi, J., Ali Ghasemzadeh, M., Alipour, S., & Zamani, F. (2022). A review on catalytic reduction/degradation of organic pollution through silver-based hydrogels. *Arabian Journal of Chemistry*, *15*(9), 104023. https://doi.org/10.1016/j.arabjc.2022.104023

de Souza Santos, L. V., Meireles, A. M., & Lange, L. C. (2015). Degradation of antibiotics norfloxacin by Fenton, UV and UV/H2O2. *Journal of Environmental Management*, *154*, 8–12. https://doi.org/10.1016/j.jenvman.2015.02.021

Ding, J., Sarrigani, G. V., Qu, J., Ebrahimi, A., Zhong, X., Hou, W. C., Cairney, J. M., Huang, J., Wiley, D. E., & Wang, D. K. (2021). Designing Co3O4/silica catalysts and intensified ultrafiltration membrane-catalysis process for wastewater treatment. *Chemical Engineering Journal*, *419*(December 2020), 129465. https://doi.org/10.1016/j.cej.2021.129465

Divyapriya, G., Nambi, I. M., & Senthilnathan, J. (2016). Nanocatalysts in fenton based advanced oxidation process for water and wastewater treatment. *Journal of Bionanoscience*, *10*(5), 356–368. https://doi.org/10.1166/jbns.2016.1387

Duhan, M., Kumar, N., Gupta, A., Singh, A., & Kaur, H. (2020). Enhanced room temperature ferromagnetism in Cr and Fe co-doped SnO2 nanoparticles synthesized by sol-gel method. *Vacuum*, *181*(July), 109635. https://doi.org/10.1016/j.vacuum.2020.109635

Dung, N. T., Duong, L. T., Hoa, N. T., Thao, V. D., Ngan, L. V., & Huy, N. N. (2022). A comprehensive study on the heterogeneous electro-Fenton degradation of tartrazine in water using CoFe2O4/carbon felt cathode. *Chemosphere*, *287*(P2), 132141. https://doi.org/10.1016/j.chemosphere.2021.132141

Ebimieowei, E., & Ibemologi, A. (2016). Antibiotics: Classification and mechanisms of action with emphasis on molecular perspectives. *International Journal of Applied Microbiology and Biotechnology Rsearch*, *4*(September 2017), 90–101.

Efthimiadou, E. K., Sanakis, Y., Katsaros, N., Karaliota, A., & Psomas, G. (2007). Transition metal complexes with the quinolone antibacterial agent pipemidic acid: Synthesis, characterization and biological activity. *Polyhedron*, *26*(5), 1148–1158. https://doi.org/10.1016/j.poly.2006.10.017

Farhadian, N., Liu, S., Asadi, A., Shahlaei, M., & Moradi, S. (2021). Enhanced heterogeneous Fenton oxidation of organic pollutant via Fe-containing mesoporous silica composites: A review. *Journal of Molecular Liquids*, *321*, 114896. https://doi.org/10.1016/j.molliq.2020.114896

Feng, J., Yang, J., Shen, Y., Deng, W., Chen, W., Ma, Y., Chen, Z., & Dong, S. (2021). Mesoporous silica nanoparticles prepared via a one-pot method for controlled release of abamectin: Properties and applications. *Microporous and Mesoporous Materials*, *311*(October 2020), 110688. https://doi.org/10.1016/j.micromeso.2020.110688

Frontistis, Z., Mantzavinos, D., & Meriç, S. (2018). Degradation of antibiotic ampicillin on boron-doped diamond anode using the combined electrochemical oxidation - Sodium persulfate process. *Journal of Environmental Management*, *223*(June), 878–887. https://doi.org/10.1016/j.jenvman.2018.06.099

Ganiyu, S. O., Huong Le, T. X., Bechelany, M., Oturan, N., Papirio, S., Esposito, G., van Hullebusch, E., Cretin, M., & Oturan, M. A. (2018). Electrochemical mineralization of sulfamethoxazole over wide pH range using FeIIFeIII LDH modified carbon felt cathode: Degradation pathway, toxicity and reusability of the modified cathode. *Chemical Engineering Journal*, *350*(April), 844–855. https://doi.org/10.1016/j.cej.2018.04.141

Garrido-Ramírez, E. G., Marco, J. F., Escalona, N., & Ureta-Zañartu, M. S. (2016). Preparation and characterization of bimetallic Fe-Cu allophane nanoclays and their activity in the phenol oxidation by heterogeneous electro-Fenton reaction. *Microporous and Mesoporous Materials*, *225*, 303–311. https://doi.org/10.1016/j.micromeso.2016.01.013

Garrido-Ramírez, E. G., Mora, M. L., Marco, J. F., & Ureta-Zañartu, M. S. (2013). Characterization of nanostructured allophane clays and their use as support of iron species in a heterogeneous electro-Fenton system. *Applied Clay Science*, *86*, 153–161. https://doi.org/10.1016/j.clay.2013.10.001

Ghanbari, D., Salavati-Niasari, M., & Ghasemi-Kooch, M. (2014). A sonochemical method for synthesis of Fe3O4 nanoparticles and thermal stable PVA-based magnetic nanocomposite. *Journal of Industrial and Engineering Chemistry*, *20*(6), 3970–3974. https://doi.org/10.1016/j.jiec.2013.12.098

Ghasemi, M., Khataee, A., Gholami, P., & Cheshmeh Soltani, R. D. (2019). Templatefree microspheres decorated with Cu-Fe-NLDH for catalytic removal of gentamicin in heterogeneous electro-Fenton process. *Journal of Environmental Management, 248*(January), 109236. https://doi.org/10.1016/j.jenvman.2019.07.007

Görmez, F., Görmez, Ö., Gözmen, B., & Kalderis, D. (2019). Degradation of chloramphenicol and metronidazole by electro-Fenton process using graphene oxide-Fe3O4 as heterogeneous catalyst. *Journal of Environmental Chemical Engineering*, *7*(2), 102990. https://doi.org/10.1016/j.jece.2019.102990

Görmez, Ö., Görmez, F., & Gözmen, B. (2021). Comparison of the heterogeneous GO-FePO4/electro-Fenton against the homogeneous Fe(II) ion and Fe(III)-oxalate complex/electro-Fenton for the degradation of metronidazole. *Journal of Water Process Engineering*, *43*(May), 1–11. https://doi.org/10.1016/j.jwpe.2021.102265

Goudarzi, M., & Salavati-Niasari, M. (2019). Synthesis, characterization and evaluation of Co3O4 nanoparticles toxicological effect; synthesized by cochineal dye via environment friendly approach. *Journal of Alloys and Compounds*, *784*, 676–685. https://doi.org/10.1016/j.jallcom.2019.01.028

Gulati, A., Malik, J., Mandeep, & Kakkar, R. (2020). Peanut shell biotemplate to fabricate porous magnetic Co3O4 coral reef and its catalytic properties for p-nitrophenol reduction and oxidative dye degradation. *Colloids and Surfaces A: Physicochemical and Engineering Aspects*, *604*(May), 125328. https://doi.org/10.1016/j.colsurfa.2020.125328

Gümüş, D., & Akbal, F. (2016). Comparison of Fenton and electro-Fenton processes for oxidation of phenol. *Process Safety and Environmental Protection*, *103*(3), 252–258. https://doi.org/10.1016/j.psep.2016.07.008

Haber, F., & Weiss, J. (1934). The catalytic compensation of hydrogen peroxide by iron salts. *Proc R Soc London*, *147*, 332–351.

Hammouda, S. Ben, Adhoum, N., & Monser, L. (2015). Synthesis of magnetic alginate beads based on Fe3O4 nanoparticles for the removal of 3-methylindole from aqueous solution using Fenton process. *Journal of Hazardous Materials*, *294*, 128–136. https://doi.org/10.1016/j.jhazmat.2015.03.068

Hammouda, S. Ben, Fourcade, F., Assadi, A., Soutrel, I., Adhoum, N., Amrane, A., & Monser, L. (2016). Effective heterogeneous electro-Fenton process for the degradation of a malodorous compound, indole, using iron loaded alginate beads as a reusable catalyst. *Applied Catalysis B: Environmental*, *182*, 47–58. https://doi.org/10.1016/j.apcatb.2015.09.007

Hazra, M., Joshi, H., Williams, J. B., & Watts, J. E. M. (2022). Antibiotics and antibiotic resistant bacteria/genes in urban wastewater: A comparison of their fate in conventional treatment systems and constructed wetlands. *Chemosphere*, *303*(P2), 135148. https://doi.org/10.1016/j.chemosphere.2022.135148

Hu, L., Zhang, G., Liu, M., Wang, Q., Dong, S., & Wang, P. (2019). Application of nickel foam-supported Co3O4-Bi2O3 as a heterogeneous catalyst for BPA removal by peroxymonosulfate activation. *Science of the Total Environment*, *647*, 352–361. https://doi.org/10.1016/j.scitotenv.2018.08.003

Huang, D., Hu, C., Zeng, G., Cheng, M., Xu, P., Gong, X., Wang, R., & Xue, W. (2017). Combination of Fenton processes and biotreatment for wastewater treatment and soil remediation. *Science of the Total Environment*, *574*, 1599–1610. https://doi.org/10.1016/j.scitotenv.2016.08.199

Huang, Q., Zhang, J., He, Z., Shi, P., Qin, X., & Yao, W. (2017). Direct fabrication of lamellar self-supporting Co3O4/N/C peroxymonosulfate activation catalysts for effective aniline degradation. *Chemical Engineering Journal*, *313*, 1088–1098. https://doi.org/10.1016/j.cej.2016.11.002

Huong Le, T. X., Drobek, M., Bechelany, M., Motuzas, J., Julbe, A., & Cretin, M. (2019). Application of Fe-MFI zeolite catalyst in heterogeneous electro-Fenton process for water pollutants abatement. *Microporous and Mesoporous Materials*, *278*(October 2018), 64–69. https://doi.org/10.1016/j.micromeso.2018.11.021

Iglesias, O., de Dios, M. A. F., Tavares, T., Sanromán, M. A., & Pazos, M. (2015). Heterogeneous electro-Fenton treatment: Preparation, characterization and performance in groundwater pesticide removal. *Journal of Industrial and Engineering Chemistry*, *27*, 276–282. https://doi.org/10.1016/j.jiec.2014.12.044

Itteboina, R., & Sau, T. K. (2019). Sol-gel synthesis and characterizations of morphology-controlled Co 3 O 4 particles. *Materials Today: Proceedings*, *9*, 458–467. https://doi.org/10.1016/j.matpr.2019.02.176

Jaafarzadeh, N., Ghanbari, F., Ahmadi, M., & Omidinasab, M. (2017). Efficient integrated processes for pulp and paper wastewater treatment and phytotoxicity reduction: Permanganate, electro-Fenton and Co3O4/UV/peroxymonosulfate. *Chemical Engineering Journal*, *308*, 142–150. https://doi.org/10.1016/j.cej.2016.09.015

Jabbar, Z. H., Ammar, S. H., & Esmail Ebrahim, S. (2021). Enhanced visible-light photocatalytic bacterial inhibition using recyclable magnetic heterogeneous nanocomposites (Fe3O4@SiO2@Ag2WO4@Ag2S) in core/shell structure. *Environmental Nanotechnology, Monitoring and Management*, *16*(October), 100601. https://doi.org/10.1016/j.enmm.2021.100601

Jia, A., Wan, Y., Xiao, Y., & Hu, J. (2012). Occurrence and fate of quinolone and fluoroquinolone antibiotics in a municipal sewage treatment plant. *Water Research*, *46*(2), 387–394. https://doi.org/10.1016/j.watres.2011.10.055

Jiao, Y., Ma, L., Tian, Y., & Zhou, M. (2020). A flow-through electro-Fenton process using modified activated carbon fiber cathode for orange II removal. *Chemosphere*, *252*, 126483. https://doi.org/10.1016/j.chemosphere.2020.126483

Kalantary, R. R., Farzadkia, M., Kermani, M., & Rahmatinia, M. (2018). Heterogeneous electro-Fenton process by Nano-Fe3O4 for catalytic degradation of amoxicillin: Process optimization using response surface methodology. *Journal of Environmental Chemical Engineering*, *6*(4), 4644–4652. https://doi.org/10.1016/j.jece.2018.06.043

Kavitha, V., & Palanivelu, K. (2005). Degradation of nitrophenols by Fenton and photo-Fenton processes. *Journal of Photochemistry and Photobiology A: Chemistry*, *170*(1), 83–95. https://doi.org/10.1016/j.jphotochem.2004.08.003

Kim, K., Qiu, P., Cui, M., & Khim, J. (2016). Development and application of Fe3O4-Pd nanospheres as catalyst for electrochemical-heterogeneous Fenton process. *Chemical Engineering Journal*, *284*, 1165–1173. https://doi.org/10.1016/j.cej.2015.09.035

Kraemer, S. A., Ramachandran, A., & Perron, G. G. (2019). Antibiotic pollution in the environment: From microbial ecology to public policy. *Microorganisms*, *7*(6), 1–24. https://doi.org/10.3390/microorganisms7060180

Labiadh, L., Ammar, S., & Kamali, A. R. (2019). Oxidation/mineralization of AO7 by electro-Fenton process using chalcopyrite as the heterogeneous source of iron and copper catalysts with enhanced degradation activity and reusability. *Journal of Electroanalytical Chemistry*, *853*(September), 113532. https://doi.org/10.1016/j.jelechem.2019.113532

Lei, H., Li, H., Li, Z., Li, Z., Chen, K., Zhang, X., & Wang, H. (2010). Electro-Fenton degradation of cationic red X-GRL using an activated carbon fiber cathode. *Process Safety and Environmental Protection*, *88*(6), 431–438. https://doi.org/10.1016/j.psep.2010.06.005

Leng, L., Huang, H., Li, H., Li, J., & Zhou, W. (2019). Biochar stability assessment methods: A review. *Science of the Total Environment*, *647*, 210–222. https://doi.org/10.1016/j.scitotenv.2018.07.402

Li, J., Luan, Z., Yu, L., & Ji, Z. (2012). Pretreatment of acrylic fiber manufacturing wastewater by the Fenton process. *Desalination*, *284*, 62–65. https://doi.org/10.1016/j.desal.2011.08.037

Li, L., Hu, H., Teng, X., Yu, Y., Zhu, Y., & Su, X. (2018). Electrogeneration of H2O2 using a porous hydrophobic acetylene black cathode for electro-Fenton process. *Chemical Engineering and Processing - Process Intensification*, *133*(2), 34–39. https://doi.org/10.1016/j.cep.2018.09.013

Li, M. T., Sun, J. W., Sha, J. Q., Wu, H. Bin, Zhang, E. L., & Zheng, T. Y. (2013). An unprecedented Ag-pipemidic acid complex with helical structure: Synthesis, structure and interaction with CT-DNA. *Journal of Molecular Structure*, *1045*, 29–34. https://doi.org/10.1016/j.molstruc.2013.04.028

Li, Q., Li, H. qiang, Rao, Q., & Yang, P. (2021). MgAl-LDH@Fe3O4 based heterogeneous electro-Fenton process for the concentrated liquor of gas field wastewater treatment: Optimization, mechanism, and stability. *Journal of Environmental Chemical Engineering*, *9*(6), 106407. https://doi.org/10.1016/j.jece.2021.106407

Li, Y., Liu, L., Wang, Z., Zhou, L., Lan, Y., & Chen, C. (2021). Simultaneous oxidation of 4-aminophenylarsonic acid and adsorption of the produced inorganic arsenic by a combination of Co3O4-La2CO5@RSBC with peroxymonosulfate. *Chemical Engineering Journal*, *413*(July 2020), 127417.

https://doi.org/10.1016/j.cej.2020.127417

Lima, V. N., Rodrigues, C. S. D., Sampaio, E. F. S., & Madeira, L. M. (2020). Insights into real industrial wastewater treatment by Fenton's oxidation in gas bubbling reactors. *Journal of Environmental Management*, *265*(January), 110501. https://doi.org/10.1016/j.jenvman.2020.110501

Liu, W. J., Wang, H., Lee, J., Kwon, E., Thanh, B. X., You, S., Park, Y. K., Tong, S., & Lin, K. Y. A. (2021). Investigating crystal plane effect of Co3O4 with various morphologies on catalytic activation of monopersulfate for degradation of phenol in water. *Separation and Purification Technology*, *276*(July), 119368. https://doi.org/10.1016/j.seppur.2021.119368

Liu, Z., Cheng, L., Zeng, J., Hu, X., Zhangxue, S., Yuan, S., Bo, Q., Zhang, B., & Jiang, Y. (2020). Synthesis, characterization and catalytic performance of nanocrystalline Co3O4 towards propane combustion: Effects of small molecular carboxylic acids. *Journal of Solid State Chemistry*, *292*(September), 121712. https://doi.org/10.1016/j.jssc.2020.121712

Magdalane, C. M., Kaviyarasu, K., Arularasu, M. V., Kanimozhi, K., & Ramalingam, G. (2019). Structural and morphological properties of Co3O4 nanostructures: Investigation of low temperature oxidation for photocatalytic application for waste water treatment. *Surfaces and Interfaces*, *17*(June), 100369. https://doi.org/10.1016/j.surfin.2019.100369

Mahtab, M. S., Farooqi, I. H., & Khursheed, A. (2021). Sustainable approaches to the Fenton process for wastewater treatment: A review. *Materials Today: Proceedings*, *47*, 1480–1484. https://doi.org/10.1016/j.matpr.2021.04.215

Malefane, M. E., Feleni, U., Mafa, P. J., & Kuvarega, A. T. (2020). Fabrication of direct Z-scheme Co3O4/BiOI for ibuprofen and trimethoprim degradation under visible light irradiation. *Applied Surface Science*, *514*(November 2019), 145940. https://doi.org/10.1016/j.apsusc.2020.145940

Matyszczak, G., Krzyczkowska, K., & Fidler, A. (2020). A novel, two-electron catalysts for the electro-Fenton process. *Journal of Water Process Engineering*, *36*(November 2019), 101242. https://doi.org/10.1016/j.jwpe.2020.101242

Mbaye, M., Diaw, P. A., Mbaye, O. M. A., Oturan, N., Gaye Seye, M. D., Trellu, C., Coly, A., Tine, A., Aaron, J. J., & Oturan, M. A. (2022). Rapid removal of fungicide thiram in aqueous medium by electro-Fenton process with Pt and BDD anodes. *Separation and Purification Technology*, *281*(June 2021). https://doi.org/10.1016/j.seppur.2021.119837

Millanao, A. R., Mora, A. Y., Villagra, N. A., Bucarey, S. A., & Hidalgo, A. A. (2021). Biological effects of quinolones: A family of broad-spectrum antimicrobial agents. In *Molecules* (Vol. 26, Issue 23). https://doi.org/10.3390/molecules26237153

Monteil, H., Péchaud, Y., Oturan, N., & Oturan, M. A. (2019). A review on efficiency and cost effectiveness of electro- and bio-electro-Fenton processes: Application to the treatment of pharmaceutical pollutants in water. *Chemical Engineering Journal*, *376*(August 2018), 119577. https://doi.org/10.1016/j.cej.2018.07.179

Moreira, F. C., Boaventura, R. A. R., Brillas, E., & Vilar, V. J. P. (2017). Electrochemical advanced oxidation processes: A review on their application to synthetic and real wastewaters. *Applied Catalysis B: Environmental*, *202*, 217–261. https://doi.org/10.1016/j.apcatb.2016.08.037

Nair, K. M., Kumaravel, V., & Pillai, S. C. (2021). Carbonaceous cathode materials for electro-Fenton technology: Mechanism, kinetics, recent advances, opportunities and challenges. *Chemosphere*, *269*, 129325. https://doi.org/10.1016/j.chemosphere.2020.129325

Nasr-Esfahani, M., Hoseini, S. J., Montazerozohori, M., Mehrabi, R., & Nasrabadi, H. (2014). Magnetic Fe3O4 nanoparticles: Efficient and recoverable nanocatalyst for the synthesis of polyhydroquinolines and Hantzsch 1,4-dihydropyridines under solvent-free conditions. *Journal of Molecular Catalysis A: Chemical*, *382*, 99–105. https://doi.org/10.1016/j.molcata.2013.11.010

Nidheesh, P. V, & Olvera-vargas, H. (2017). *Heterogeneous Electro-Fenton Process : Principles and Applications Heterogeneous Electro-Fenton Process : Principles and Applications*. *August*. https://doi.org/10.1007/698

Olvera-Vargas, H., Rouch, J. C., Coetsier, C., Cretin, M., & Causserand, C. (2018). Dynamic cross-flow electro-Fenton process coupled to anodic oxidation for wastewater treatment: Application to the degradation of acetaminophen. *Separation and Purification Technology*, *203*(January), 143–151.

https://doi.org/10.1016/j.seppur.2018.03.063

Oturan, M. A. (2021). Outstanding performances of the BDD film anode in electro-Fenton process: Applications and comparative performance. *Current Opinion in Solid State and Materials Science*, *25*(3), 100925. https://doi.org/10.1016/j.cossms.2021.100925

Oturan, M. A., Oturan, N., Lahitte, C., & Trevin, S. (2001). Production of hydroxyl radicals by electrochemically assisted Fenton's reagent: Application to the mineralization of an organic micropollutant, pentachlorophenol. *Journal of Electroanalytical Chemistry*, *507*(1–2), 96–102. https://doi.org/10.1016/S0022-0728(01)00369-2

Oturan, N., Hamza, M., Ammar, S., Abdelhédi, R., & Oturan, M. A. (2011). Oxidation/mineralization of 2-Nitrophenol in aqueous medium by electrochemical advanced oxidation processes using Pt/carbon-felt and BDD/carbon-felt cells. *Journal of Electroanalytical Chemistry*, *661*(1), 66–71. https://doi.org/10.1016/j.jelechem.2011.07.017

Ouiriemmi, I., Karrab, A., Oturan, N., Pazos, M., Rozales, E., Gadri, A., Sanromán, M. Á., Ammar, S., & Oturan, M. A. (2017). Heterogeneous electro-Fenton using natural pyrite as solid catalyst for oxidative degradation of vanillic acid. *Journal of Electroanalytical Chemistry*, *797*(May), 69–77. https://doi.org/10.1016/j.jelechem.2017.05.028

Özcan, A., Atılır Özcan, A., & Demirci, Y. (2016). Evaluation of mineralization kinetics and pathway of norfloxacin removal from water by electro-Fenton treatment. *Chemical Engineering Journal*, *304*, 518–526. https://doi.org/10.1016/j.cej.2016.06.105

Özcan, A., Atılır Özcan, A., Demirci, Y., & Şener, E. (2017). Preparation of Fe2O3 modified kaolin and application in heterogeneous electro-catalytic oxidation of enoxacin. *Applied Catalysis B: Environmental*, *200*, 361–371. https://doi.org/10.1016/j.apcatb.2016.07.018

Özcan, A., Şahin, Y., Koparal, A. S., & Oturan, M. A. (2008). Propham mineralization in aqueous medium by anodic oxidation using boron-doped diamond anode: Influence of experimental parameters on degradation kinetics and mineralization efficiency.

Water Research, *42*(12), 2889–2898. https://doi.org/10.1016/j.watres.2008.02.027

Özcan, A., Şahin, Y., Koparal, A. S., & Oturan, M. A. (2009). A comparative study on the efficiency of electro-Fenton process in the removal of propham from water. *Applied Catalysis B: Environmental*, *89*(3–4), 620–626. https://doi.org/10.1016/j.apcatb.2009.01.022

Özcan, A., Şahin, Y., & Oturan, M. A. (2008). Removal of propham from water by using electro-Fenton technology: Kinetics and mechanism. *Chemosphere*, *73*(5), 737–744. https://doi.org/10.1016/j.chemosphere.2008.06.027

Pagani, A. P., & Ibañez, G. A. (2019). Analytical approach for the simultaneous determination of quinolones in edible animal products. Modeling pH–modulated fluorescence excitation–emission matrices four–way arrays. *Talanta*, *192*(June 2018), 52–60. https://doi.org/10.1016/j.talanta.2018.09.015

Pan, G., & Sun, Z. (2021). Cu-doped g-C3N4 catalyst with stable Cu0 and Cu+ for enhanced amoxicillin degradation by heterogeneous electro-Fenton process at neutral pH. *Chemosphere*, *283*(June), 131257. https://doi.org/10.1016/j.chemosphere.2021.131257

Panizza, M., & Oturan, M. A. (2011). Degradation of Alizarin Red by electro-Fenton process using a graphite-felt cathode. *Electrochimica Acta*, *56*(20), 7084–7087. https://doi.org/10.1016/j.electacta.2011.05.105

Pham, T. D. M., Ziora, Z. M., & Blaskovich, M. A. T. (2019). Quinolone antibiotics. *MedChemComm*, *10*(10), 1719–1739. https://doi.org/10.1039/c9md00120d

Pimentel, M., Oturan, N., Dezotti, M., & Oturan, M. A. (2008). Phenol degradation by advanced electrochemical oxidation process electro-Fenton using a carbon felt cathode. *Applied Catalysis B: Environmental*, *83*(1–2), 140–149. https://doi.org/10.1016/j.apcatb.2008.02.011

Poza-Nogueiras, V., Moratalla, Á., Pazos, M., Sanromán, Á., Sáez, C., & Rodrigo, M. A. (2021). Towards a more realistic heterogeneous electro-Fenton. *Journal of Electroanalytical Chemistry*, *895*(June). https://doi.org/10.1016/j.jelechem.2021.115475

Poza-Nogueiras, V., Rosales, E., Pazos, M., & Sanromán, M. Á. (2018). Current advances and trends in electro-Fenton process using heterogeneous catalysts – A review.

Chemosphere, *201*, 399–416. https://doi.org/10.1016/j.chemosphere.2018.03.002

Prakash, N., Balaji, R., Govindaraju, S., Steffi, A. P., Santhanalakshmi, N., Mohanraj, K., Selvarajan, E., Chandrasekar, N., & Samuel, M. S. (2022). Influence of 2D template-assisted (SBA-15) metal oxide Co3O4 for pseudocapacitive and dye degradation application. *Environmental Research*, *204*(PD), 112383. https://doi.org/10.1016/j.envres.2021.112383

Pushpalatha, M., & Krishna, M. B. (2017). Electro-Fenton Process for Waste Water Treatment A Review. *International Journal of Advance Research*, *3*(1), 439–451. www.ijariit.com

Qiao, M., Ying, G. G., Singer, A. C., & Zhu, Y. G. (2018). Review of antibiotic resistance in China and its environment. *Environment International*, *110*(October 2017), 160–172. https://doi.org/10.1016/j.envint.2017.10.016

Rahmatinia, Z., & Rahmatinia, M. (2018). Removal of the metronidazole from aqueous solution by heterogeneous electro-Fenton process using nano-Fe3O4. *Data in Brief*, *19*, 2139–2145. https://doi.org/10.1016/j.dib.2018.06.118

Rajput, S., Pittman, C. U., & Mohan, D. (2016). Magnetic magnetite (Fe3O4) nanoparticle synthesis and applications for lead (Pb2+) and chromium (Cr6+) removal from water. *Journal of Colloid and Interface Science*, *468*, 334–346. https://doi.org/10.1016/j.jcis.2015.12.008

Rezaei, A., Rezaei, M. R., & Sayadi, M. H. (2021). 3D network structure graphene hydrogel-Fe3O4@SnO2/Ag via an adsorption/photocatalysis synergy for removal of 2,4 dichlorophenol. *Journal of the Taiwan Institute of Chemical Engineers*, *121*, 154–167. https://doi.org/10.1016/j.jtice.2021.03.048

Ribeiro, J. P., Marques, C. C., Portugal, I., & Nunes, M. I. (2020). Fenton processes for AOX removal from a kraft pulp bleaching industrial wastewater: Optimisation of operating conditions and cost assessment. *Journal of Environmental Chemical Engineering*, *8*(4), 104032. https://doi.org/10.1016/j.jece.2020.104032

Ribeiro, J. P., & Nunes, M. I. (2021). Recent trends and developments in Fenton processes for industrial wastewater treatment – A critical review. *Environmental Research*, *197*(July 2020). https://doi.org/10.1016/j.envres.2021.110957

Rodriguez-Mozaz, S., Vaz-Moreira, I., Varela Della Giustina, S., Llorca, M., Barceló, D., Schubert, S., Berendonk, T. U., Michael-Kordatou, I., Fatta-Kassinos, D., Martinez, J. L., Elpers, C., Henriques, I., Jaeger, T., Schwartz, T., Paulshus, E., O'Sullivan, K., Pärnänen, K. M. M., Virta, M., Do, T. T., … Manaia, C. M. (2020). Antibiotic residues in final effluents of European wastewater treatment plants and their impact on the aquatic environment. *Environment International*, *140*(March), 105733. https://doi.org/10.1016/j.envint.2020.105733

Rodríguez-Narvaez, O. M., Rajapaksha, R. D., Ranasinghe, M. I., Bai, X., Peralta-Hernández, J. M., & Bandala, E. R. (2020). Peroxymonosulfate decomposition by homogeneous and heterogeneous Co: Kinetics and application for the degradation of acetaminophen. *Journal of Environmental Sciences (China)*, *93*, 30–40. https://doi.org/10.1016/j.jes.2020.03.002

Saeed, M., Muneer, M., Mumtaz, N., Siddique, M., Akram, N., & Hamayun, M. (2018). Ag-Co3O4: Synthesis, characterization and evaluation of its photo-catalytic activity towards degradation of rhodamine B dye in aqueous medium. *Chinese Journal of Chemical Engineering*, *26*(6), 1264–1269. https://doi.org/10.1016/j.cjche.2018.02.024

Sánchez-Sánchez, C. M., Expósito, E., Casado, J., & Montiel, V. (2007). Goethite as a more effective iron dosage source for mineralization of organic pollutants by electro-Fenton process. *Electrochemistry Communications*, *9*(1), 19–24. https://doi.org/10.1016/j.elecom.2006.08.023

Sha, J. Q., Li, X., Zhou, Y. H., Yan, P. F., Li, G. M., & Wang, C. (2011). The introduction of antibacterial drug pipemidic acid into the POM field: Syntheses, characterization and antitumor activity. *Solid State Sciences*, *13*(11), 1972–1977. https://doi.org/10.1016/j.solidstatesciences.2011.08.027

Shamim, S., Hornyak, G. L., Crespy, D., Kyaw, H., & Bora, T. (2022). Morphology and visible photoluminescence modulation in dye-free mesoporous silica nanoparticles using a simple calcination step. *Materials Research Bulletin*, *152*(July 2021), 111842. https://doi.org/10.1016/j.materresbull.2022.111842

Shukla, P., Sun, H., Wang, S., Ang, H. M., & Tadé, M. O. (2011). Nanosized Co3O4/SiO2 for heterogeneous oxidation of phenolic contaminants in waste water. *Separation and Purification Technology*, *77*(2), 230–236. https://doi.org/10.1016/j.seppur.2010.12.011

Sopaj, F., Oturan, N., Pinson, J., Podvorica, F., & Oturan, M. A. (2016). Effect of the anode materials on the efficiency of the electro-Fenton process for the mineralization of the antibiotic sulfamethazine. *Applied Catalysis B: Environmental*, *199*, 331–341. https://doi.org/10.1016/j.apcatb.2016.06.035

Sun, S. P., & Lemley, A. T. (2011). P-Nitrophenol degradation by a heterogeneous Fenton-like reaction on nano-magnetite: Process optimization, kinetics, and degradation pathways. *Journal of Molecular Catalysis A: Chemical*, *349*(1–2), 71–79. https://doi.org/10.1016/j.molcata.2011.08.022

Szymańska, B., Skrzypek, D., Kovala-Demertzi, D., Staninska, M., & Demertzis, M. A. (2006). Synthesis and spectroscopic study of copper(II) and manganese(II) complexes with pipemidic acid. *Spectrochimica Acta - Part A: Molecular and Biomolecular Spectroscopy*, *63*(3), 518–523. https://doi.org/10.1016/j.saa.2005.05.038

Thokchom, B., Qiu, P., Cui, M., Park, B., Pandit, A. B., & Khim, J. (2017). Magnetic Pd@Fe3O4 composite nanostructure as recoverable catalyst for sonoelectrohybrid degradation of Ibuprofen. *Ultrasonics Sonochemistry*, *34*, 262–272. https://doi.org/10.1016/j.ultsonch.2016.05.030

Titchou, F. E., Zazou, H., Afanga, H., El Gaayda, J., Ait Akbour, R., Hamdani, M., & Oturan, M. A. (2021). Electro-Fenton process for the removal of Direct Red 23 using BDD anode in chloride and sulfate media. *Journal of Electroanalytical Chemistry*, *897*(June), 115560. https://doi.org/10.1016/j.jelechem.2021.115560

Toor, U. A., Duong, T. T., Ko, S. Y., Hussain, F., & Oh, S. E. (2020). Optimization of Fenton process for removing TOC and color from swine wastewater using response surface method (RSM). *Journal of Environmental Management*, *279*(December 2020), 111625. https://doi.org/10.1016/j.jenvman.2020.111625

Wang, C., Jia, S., Zhang, Y., Nian, Y., Wang, Y., Han, Y., Liu, Y., Ren, H., Wu, S., Yao, K., & Han, X. (2020). Catalytic reactivity of Co3O4 with different facets in the hydrogen abstraction of phenol by persulfate. *Applied Catalysis B: Environmental*, *270*(March), 118819. https://doi.org/10.1016/j.apcatb.2020.118819

Wang, C. T., Hu, J. L., Chou, W. L., & Kuo, Y. M. (2008). Removal of color from real dyeing wastewater by Electro-Fenton technology using a three-dimensional graphite cathode. *Journal of Hazardous Materials*, *152*(2), 601–606. https://doi.org/10.1016/j.jhazmat.2007.07.023

Wang, H., & Wang, J. (2007). Electrochemical degradation of 4-chlorophenol using a novel Pd/C gas-diffusion electrode. *Applied Catalysis B: Environmental*, *77*(1–2), 58–65. https://doi.org/10.1016/j.apcatb.2007.07.004

Wang, J., & Tang, J. (2021a). Fe-based Fenton-like catalysts for water treatment: Catalytic mechanisms and applications. *Journal of Molecular Liquids*, *332*, 115755. https://doi.org/10.1016/j.molliq.2021.115755

Wang, J., & Tang, J. (2021b). Fe-based Fenton-like catalysts for water treatment: Preparation, characterization and modification. *Chemosphere*, *276*, 130177. https://doi.org/10.1016/j.chemosphere.2021.130177

Wang, Y., Zhou, L., Duan, X., Sun, H., Tin, E. L., Jin, W., & Wang, S. (2015). Photochemical degradation of phenol solutions on Co3O4 nanorods with sulfate radicals. *Catalysis Today*, *258*, 576–584. https://doi.org/10.1016/j.cattod.2014.12.020

Warang, T., Patel, N., Fernandes, R., Bazzanella, N., & Miotello, A. (2013). Co3O4 nanoparticles assembled coatings synthesized by different techniques for photo-degradation of methylene blue dye. *Applied Catalysis B: Environmental*, *132–133*, 204–211. https://doi.org/10.1016/j.apcatb.2012.11.040

Wu, H., & Wang, S. (2012). Impacts of operating parameters on oxidation-reduction potential and pretreatment efficacy in the pretreatment of printing and dyeing wastewater by Fenton process. *Journal of Hazardous Materials*, *243*, 86–94. https://doi.org/10.1016/j.jhazmat.2012.10.030

Xian, G., Zhang, G., Chang, H., Zhang, Y., Zou, Z., & Li, X. (2019). Heterogeneous activation of persulfate by Co3O4-CeO2 catalyst for diclofenac removal. *Journal of Environmental Management*, *234*(December 2018), 265–272. https://doi.org/10.1016/j.jenvman.2019.01.013

Xu, H., Zhang, Y., Li, J., Hao, Q., Li, X., & Liu, F. (2020). Heterogeneous activation of peroxymonosulfate by a biochar-supported Co3O4 composite for efficient degradation of chloramphenicols. *Environmental Pollution*, *257*, 113610. https://doi.org/10.1016/j.envpol.2019.113610

Yang, Q., Choi, H., Chen, Y., & Dionysiou, D. D. (2008). Heterogeneous activation of peroxymonosulfate by supported cobalt catalysts for the degradation of 2,4-dichlorophenol in water: The effect of support, cobalt precursor, and UV radiation. *Applied Catalysis B: Environmental*, *77*(3–4), 300–307. https://doi.org/10.1016/j.apcatb.2007.07.020

Ye, G., Lu, J., Qian, L., Xie, L., Zhou, H., & Zhu, C. (2021). Synthesis of manganese ore/Co3O4 composites by sol–gel method for the catalytic oxidation of gaseous chlorobenzene. *Journal of Saudi Chemical Society*, *25*(5), 101229. https://doi.org/10.1016/j.jscs.2021.101229

Zhang, B., Hou, Y., Yu, Z., Liu, Y., Huang, J., Qian, L., & Xiong, J. (2019). Three-dimensional electro-Fenton degradation of Rhodamine B with efficient Fe-Cu/kaolin particle electrodes: Electrodes optimization, kinetics, influencing factors and mechanism. *Separation and Purification Technology*, *210*(August 2018), 60–68. https://doi.org/10.1016/j.seppur.2018.07.084

Zhang, C., Zhou, M., Ren, G., Yu, X., Ma, L., Yang, J., & Yu, F. (2015). Heterogeneous electro-Fenton using modified iron-carbon as catalyst for 2,4-dichlorophenol degradation: Influence factors, mechanism and degradation pathway. *Water Research*, *70*, 414–424. https://doi.org/10.1016/j.watres.2014.12.022

Zhang, M. hui, Dong, H., Zhao, L., Wang, D. xi, & Meng, D. (2019). A review on Fenton process for organic wastewater treatment based on optimization perspective. *Science of the Total Environment*, *670*, 110–121. https://doi.org/10.1016/j.scitotenv.2019.03.180

Zhang, M. zhi, Zhou, Z. ming, Xu, J., Wang, W. li, Pu, S. huan, Hu, W. ye, Luo, P., Tian, Z. qun, Gong, Z. bin, & Liu, G. kun. (2022). Qualitative analysis of trace quinolone antibiotics by SERS with fine structure dependent sensitivity. *Spectrochimica Acta - Part A: Molecular and Biomolecular Spectroscopy*, *278*, 121365. https://doi.org/10.1016/j.saa.2022.121365

Zhang, W., Xi, J., Li, Z., Zhou, H., Liu, L., Wu, Z., & Qiu, X. (2013). Electrochemical activation of graphite felt electrode for VO 2+/VO2+ redox couple application. *Electrochimica Acta*, *89*, 429–435. https://doi.org/10.1016/j.electacta.2012.11.072

Zhang, Y., Hua, S., Sun, X., Liu, Z., Dang, Y., Zhang, L., & Zhou, Y. (2021). A novel electrochemical cathode based on sea urchin-like NiO/Co3O4 composite inducing efficient Fenton-like process for levofloxacin degradation. *Applied Catalysis A: General*, *628*(June), 118403. https://doi.org/10.1016/j.apcata.2021.118403

Zhao, X., Wen, T., Zhang, J., Ye, J., Ma, Z., Yuan, H., Ye, X., & Wang, Y. (2017). Fe-Doped SnO2 catalysts with both BA and la sites: Facile preparation and biomass carbohydrates conversion to methyl lactate MLA. *RSC Advances*, *7*(35), 21678–21685. https://doi.org/10.1039/c7ra01655g

Zou, M., Tian, W., Zhao, J., Chu, M., & Song, T. (2022). Quinolone antibiotics in sewage treatment plants with activated sludge treatment processes: A review on source, concentration and removal. *Process Safety and Environmental Protection*, *160*, 116–129. https://doi.org/10.1016/j.psep.2022.02.013

CURRICULUM VITAE

ORCID ID: 0000-0002-5420-9606

Name Surname: Abdoukarim SISOHO

Foreign Language: Turkish

Educational Background:

2010: Gambia Senior Secondary School

2014: University of the Gambia

2022: Eskisehir Technical University

Work Experience:

2015: Chemistry teacher: Charles Jow Memorial Academy

2016: Petroleum Officer: Ministry of Petroleum and Energy

2017 to date: Senior Technician/Analyst: Medicines Control Agency, The Gambia